Doctoral Dissertation

博士論文

Efficient Generative Methods for Assisting Aesthetic Design in Conceptual Stage

（コンセプト段階での意匠設計支援のための効率的なジェネラティブデザイン手法）

Dogan Kemal Mert

（ドアン ケマル メルト）

学籍番号 37-167264

The University of Tokyo

August 2019

Abstract

Common product design processes usually start with problem definition, then generate and evaluate solutions for the defined problem, and finally detail and test the promising solutions until deciding on a final design. The conceptual design is an early stage of the design process, where possible solutions to the design problem are generated in abstract forms. The solutions are evaluated based on engineering and industrial design requirements, which a product must satisfy. To reach aesthetically plausible shapes for target customers without compromising engineering requirements or causing extra costs, many design samples usually need to be generated until finding an optimal solution if there is not any guidance for designers to use in addition to their limited imagination. In the first part of this thesis, design parameters are screened to find important ones for an aesthetic objective. Therefore, the desired design solutions can efficiently be created as there will be a smaller number of design parameters to work with. In the second part, a generative sampling method is proposed to derive many samples from a single exemplary design using computer power with minimum possible user effort. Using this method, the initial idea can be varied quickly, which is useful for those who need to create and examine many design solutions to find better alternative or get inspiration from them.

The first approach uses a design concept from an earlier study called adjective-based design in which adjectives are used to describe product designs that are represented by geometric design parameters. In this earlier study, human preferences are collected by a survey method and converted into mathematical models, where variables are the design parameters, using a machine learning method to be used for quantitative judgments of aesthetics for a new generated design. Nevertheless, some design parameters were absent in the mathematical models although they were in the learning process due to nonexistent or weak correlations between them and participant responses. Getting rid of such irrelevant parameters, the reliability of the models can be enhanced as well as increasing sampling efficiency thanks to the knowledge of the relevant parameters to the objectives. In Chapter 2, the survey method is supported by visual evaluations using eye tracking technology so that the design parameters can be screened based on their attractiveness to the participants. The main advantage of eye tracking in a survey is that the collected human perception data is more likely to be accurate and objective compared to the conventional surveys since the evaluation is based on survey participants' attention rather than applying solely questionnaires that

cannot tell much about reasons of participants' choices. Eye tracking tools such as area of interest (AOI), gaze plot, and heat map are used to evaluate the attractiveness of the design parameters. Finally, a regression analysis method is used to find relations between attractive design parameters and the adjectives based on the gaze data.

Aesthetic design ideas are mostly developed by sketches on paper rather than using the generative power of computer environments due to time taking requirements. The second approach is a generative sampling method that derives design samples from an example design by auto constraining and using some conditions extracted from its profile curve to minimize the efforts needed from users. As a first step, a composite profile curve of an example design is defined using a number of control points that should be enough to represent each shape feature by a cubic Bézier curve segment. Primitive shapes such as triangles and circles are then constructed for each segment and used as constraints to prevent generating infeasible shapes. Moreover, profile similarities are computed using the triangles based on their anisotropy ratios to preserve key shape features of the original profile and modified Hausdorff distances between the control points to make sure the modification is made sufficiently while a new profile is generated for the sake of diversity. A customized sampling algorithm that fulfills the segment constraints and the similarity requirements is executed several times synchronously via parallel programming to create numerous samples. Using the settings related to similarity, it is possible to derive samples sticking to an initial idea to explore its better version or more creative results that they could not be imagined even by designers. The proposed method is carried on with a software that offers simplicity automating required steps to generate samples. An additional tool is also provided in this software with which weights can be adjusted for each control point to guide the sampling process and the chosen samples with their choices can be recorded to be analyzed later. This system also includes a sample management interface where additional geometric constraints can be defined to filter out undesired samples respect to these constraints.

To sum up, two approaches are studied to increase the efficiency of generating aesthetic ideas. The first approach aims to identify important design parameters for specific aesthetic objectives based on customer feelings so that new designs can be generated with fewer parameters that have direct influences on the target aesthetic objectives. The second approach is for generating many design samples with as minimum as possible effort, time and experience requirements for various profile curves. Finally, problem-specific geometric constraints can be utilized through the sample management system to filter out undesired solutions from the generated samples.

Contents

List of Figures

List of Tables

Chapter 1

Introduction

1.1 Aesthetic Design in Conceptual Stage of Products

Product design is usually an outcome of a design process consists of several stages conducted collaboratively by a group of people from different disciplines. Throughout the years, different process models were suggested [1, 2, 3, 4, 5, 6, 7, 8, 9, 10], these and more were also compared and analyzed in literature [11, 12, 13, 14]. Despite the differences between these process models, Howard et al. [14] offered six common stages illustrated in Fig.1.1 comparing various process models. The initial stages *establishing a need* and *analysis of task* are complementary in which a design problem is recognized, requirements are defined mostly based on feedback from market and analyzed in detail to clarify the design task. The *conceptual design stage* is where possible design solutions are produced in abstract form and evaluated to decide on optimal solutions that meet the defined requirements. The selected conceptual solutions are structured and further tested in *embodiment stage*. The *detailed design stage* gives final details that are needed in manufacturing processes. Finally, post design processes such as installation, manufacturing, and commercialization are carried out in the *implementation* stage.

The aesthetic is an important dimension that needs to be considered in the conceptual stage for a product that must be differentiated from the stable competitors in the market that already meet the performance and quality requirements of target customers [15, 16, 17, 18]. In addition, the aesthetic dimension including size property can solely increase product variations or improve an existing design to elevate its value [19]. Engineering and industrial designers are often collaborated to generate and evaluate design solutions by different strategies [7, 20, 21]. One way to collaborate is creating an outer form of the shape, which is expected from industrial designers, and engineering designers should fit their requirements in this form. In another way, engineering design is first generated and industrial design must be shaped under some constraints without compromising the inner form created by the engineering designers; in other words, "gift wrap" is provided to the engineering design [7]. Either way, many design solutions need to be generated and narrowed down to the final design that must satisfy both industrial and engineering design requirements. The process models usually iteratively generate, evaluate and select the ideas until a superior solution has been found; but, each additional cycle multiplies the cost and time. The conceptual stage plays a crucial role in lowering the number of cycles by forwarding promising solutions before investing too much on redundant ideas.
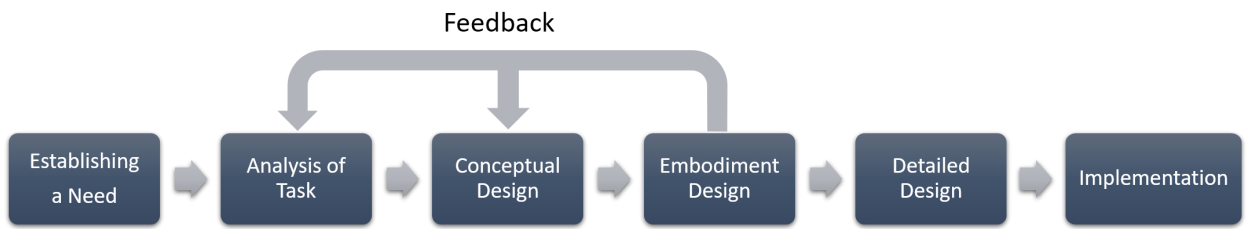
Figure 1.1: A product design process [14].

1.2 Basic Motivation and Approaches

When it comes to the product aesthetics, it is hard to generate solutions and decide on a better one that appeals majority of the target customers due to its subjectivity. At this point, potential customers' evaluations are preferably involved in the forming and selection process of the product appearance. Furthermore, no matter if the design goal is improving an outdated product or creating something totally new, industrial designers usually collect many design images and draws many sketches to develop their own ideas on the way to the best of possible solutions. However, there are several restrictions that make producing the ideas difficult such as cost, time and engineering design constraints aside from the aesthetics. In this thesis two different approaches are proposed to gain efficiency to the design process as follows:

- **Identifying important design parameters:** First proposed approach is a human-orientated design method that establishes relationships between the parameters and aesthetic related objectives based on the eye movements of human. With awareness of important parameters for customers' specific feelings, appealing designs more likely to be generated in a straightforward manner. In addition, under strict constraints of engineering design, working with fewer parameters may be useful for industrial designers such that wasting time with redundant shape modifications could be avoided.

- **Generating and managing concept solutions:** The ideal conceptual design stage should generate and evaluate as many as possible solutions to explore the design space fully; thus, to find the best possible solution [7]. A generative design method is also proposed and implemented with a software that can generate many samples efficiently around an initial idea to find out its better version or a new idea that is not imagined by the designers. The software is also supported by a management system that allows designers to organize and define geometrical constraints to narrow down the generated design solutions.

Following sections further introduce these topics and give insights about the proposed ap-

proaches.

1.2.1 Human-oriented Design

1.2.1.1 Background

Aesthetic is a qualitative measure that is hard to evaluate until the product meets with the customers for the first time. There are many studies [22, 23, 24, 25, 26] proposed to solve such difficulty usually by converting human preferences into quantitative measures. One way to do that is gathering subjective evaluations of potential customers using survey methods and applying statistical analysis to find relationships between design parameters and the collected opinions regarding aesthetics. The relations are represented in mathematical forms, which are then used for quantitative evaluation of newly generated design samples. Adjectives such as cute and strong are often used in the survey methods as representative keywords to describe the designs so that the evaluations are more meaningful and easier for the survey participants, who do not have any background about the product design.

The proposal of Chapter 2 has been inspired by the study of Dogan and Gunpinar [27], which is an adjective-based design method for yacht hulls. In their method, hull adjectives are first learned from the survey participants and yacht hull designs are matched with these adjectives using a series of surveys. The hulls are generated with a novel design framework [28], which uses a simple parametric representation of the design (see Fig. 2.4). In the end, the relationships between the design parameters and the adjectives of the hull designs are found using neural networks. The relationships are formed as mathematical models of the adjectives, in which variables are the design parameters, to be used in prediction of the adjectives of new samples or to retrieve a hull design that satisfies a queried adjective from an existing database. However, some design parameters were not involved in the mathematical models of the adjectives. This indicates the existence of irrelevant parameters for the given adjectives from the viewpoint of the participants. The parameters should be identified based on their relevance to the defined objectives to establish more solid relationships between the parameters and aesthetic objectives.

Conventional surveys with multiple-choice questions are not reliable for the aesthetic researches since the target customers are usually not design experts and do not see the design parameters as the designers do. Besides, the aesthetic is more about feelings that are hard to express by words. Therefore, it is trivial to ask the relevance of design parameters to the survey participants for their subjective choices. Instead, an eye tracking device is used during the surveys to monitor the gaze behavior of the participants while they match the adjectives with the displayed design samples. In

this way, the participants' attention on shape features until they select an adjective can be examined simply observing the areas they looked at. Furthermore, the decision-making progress of the subjects during the survey can be visualized and converted into quantitative measures using some eye tracking tools such as area of interest (AOI), gaze plot and heat map (see Fig. 2.1). Thus, the results are more reliable and make possible more realistic interpretation of the participants' intentions for the researchers. The proposed study in Chapter 2 uses the eye tracking method to find attractive design parameters to the participants and relates these parameters with the participant responses through the gaze data.

1.2.1.2 Eye tracking aided survey for human-oriented product design

An eye tracking device is used to collect the gaze data processing eye images with light reflections caused by a near-infrared light source and map this data on given stimuli. The data includes several quantitative measures such as locations of the gaze points of the survey participants at a time and time spent at these locations. Such measures are used to understand the most and least attractive shape features based on attention of the participants. The gaze data is analyzed utilizing the eye tracking tools (Fig. 2.1). Gaze plot is one of the tools that visualizes gaze fixations, which are the accumulations of gaze points, by circles indicating where the participants are looking at; and saccades between the gaze fixations by straight lines. The collection of the gaze fixations and the saccades is called scan path, which is visual of the eye movements according to time sequence. AOI is used to enclose specific areas to be examined individually with the gaze points inside these areas. Besides, the scan path of the participants can be observed as gaze transitions between the AOIs. The heat map displays the gaze point accumulations with a color scale such that red indicates more attractive areas comparing to green areas; since the more users look, the more gaze points are gathered at the corresponding areas.

In this dissertation, as it is made in the adjective-based design method [27], the adjectives are again matched with the hull design images, but this time the survey and its analysis are supported by the eye tracking technology. This survey is called as eye tracking aided survey (ETAS) and its approach is illustrated in Fig. 1.2, where a participant selects appropriate adjectives from the list for the displayed design and the gaze points are recorded via an eye tracking device at the same time. The survey aims to find relationships between the design parameters and the adjectives through the gaze data. If the gaze fixations of the participants accumulate in specific areas that are associated with design parameters, AOIs are defined surrounding each of these areas and the parameters are evaluated based on time duration inside these AOIs. On the other hand, if the

participants transit their fixations between specific areas, the transition counts are used to evaluate the relevant parameter. The gaze points are expected to accumulate locally if a parameter has a local impact on the appearance of the hull in the image and analyzed accordingly. However, as there is not any certain work that reveals the search behaviors of the participants for geometric design parameters, if their impacts on the hull appearance are not local, how they are gazing over these parameters is unknown. That is why an additional survey called template learning survey (TLS), where the questions are specific to the parameters, is used to examine gaze points of the parameters to decide on their evaluation methods. Besides, the information such as locations and sizes of areas where the gaze points are found is used as a template for the relevant parameter. The gaze data collected via ETAS is then evaluated using the eye tracking tools and the templates to determine attractive parameters for the participants. A regression analysis method is finally conducted to relate the attractive parameters with each adjective. Herewith, designers could modify or generate their designs by focusing only the relevant parameters of the target adjective, which is a more efficient and direct method to achieve target than working with all design parameters including irrelevant ones.
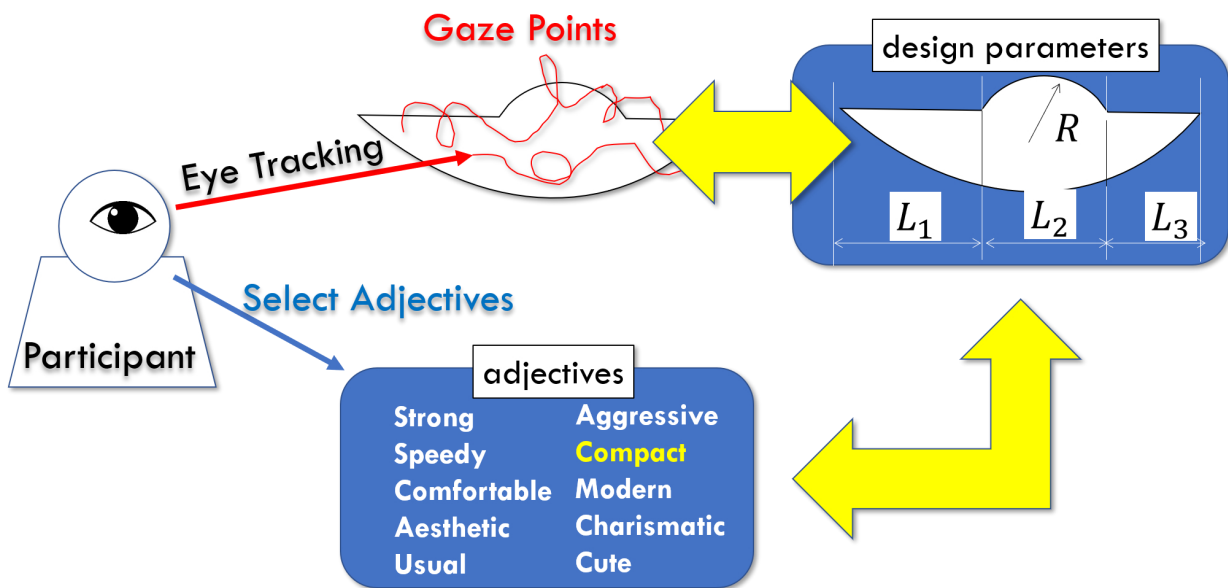
Figure 1.2: Eye tracking aided survey (ETAS) approach overview.

1.2.2 Generative Design

1.2.2.1 Background

Generative design methods [29] aim to minimize efforts needed to create numerous design samples that satisfy a predefined set of objectives. To do this, design parameters are first determined for target design and then modified to generate new samples [30, 31, 32]. A generative design supported with computer power can create a design space with an infinite number of design samples, which are either feasible or infeasible. The degree of freedom in the design space is depended on the number of design parameters; thus, these parameters should provide optimal conditions to avoid complexity while enough degree of freedom is still available to obtain desired samples. In addition to the need of constraints to avoid infeasible regions, appropriate upper and lower bounds for the parameters are also usually required to define a region in the space, where the candidate design solutions are existing.

Developing many design ideas in the conceptual design stage is usual step before deciding on an optimal one that satisfies several criteria such as engineering constraints, costs and aesthetics. Computer driven generative systems can generate many samples that may not be imagined by designers and can even make evaluation of some functional behaviors possible in the beginning of the design process. However, the designers usually collect design images or draw 2D sketches on papers to develop aesthetic ideas instead of using computers to produce digital designs. This is because meeting initial requirements like defining design parameters, appropriate constraints, and narrowing down the design space to the finite sub regions is usually impractical or exceeds their abilities. Furthermore, available generative systems are usually designed for specific purposes that are not suitable at all or need to be modified to make use of it for the purpose at that moment. Although there are several proposed generative methods, they usually bring additional burdens to the designers such as creating an initial set of designs [33], specific properties of initial design like being mesh model [34] or parametric model [30]. This thesis also proposes a generative design method in which an example product profile curve is modified for generating its alternatives. The method is implemented by a developed software, which is designed to minimize the initial requirements but to maximize the effectiveness of user involvement for guiding the sampling progress by weighting the modification amounts when needed. The target users of the proposed software are designers, who want to quickly derive alternative versions of their initial aesthetic idea to find better one; and customers, who want to explore their specific design based on an existing design to be used for better communication with a designer to realize it. The constraining is made using primitive shapes such as triangles and circles that are applicable to the various profiles and can

be visualized through the interface that makes simpler to comprehend even for non-experts. In addition, the sampling region is defined based on automatically recognized conditions in the defined profile curve such as continuity between its segments and curve degrees of these segments; and similarity thresholds defined by users. The generative system also includes a sample management system to narrow down the number of generated samples based on similarities of generated samples and user-defined geometric constraints.

1.2.2.2 Generative sampling system

An example based generative design method (see Fig. 1.3) is proposed to quickly generate many samples from an example profile, which is defined and constrained within a system based on control points that user provides. The profile curve is a composite Bézier curve, for which four control points are supplied for each segment either by importing from external sources or mouse clicks on a product image using the proposed software. To refrain generating irregular shapes, the constraints are constructed using the control points as primitive shapes such as triangle, circle, and ellipse that are able to be visualized and comprehensible for the inexperienced users. The triangles are further used in computing shape similarities such that anisotropy ratio [35] between corresponding triangles of the example and a generated profile is computed, and the sum of all triangles' anisotropy ratios is used as shape similarity. The shape similarity is constrained using a threshold set by the user that prevents generating too dissimilar samples from the exemplary design than the user is looking for. The diversity of the samples are also controlled with another similarity measure called modified Hausdorff distance (MHD) [36], such that there is not any sample couple exists within the set of generated samples that are close to each other more than allowed by another user-defined similarity threshold. In order to apply both regularity and similarity constraints together efficiently, a customized sample algorithm called chain sampling is used in which samples are generated one by one to be the next generated is far enough from the previously generated samples to satisfy diversity requirement and must satisfy the rest of the constraints. As the number of samples increases, the newly generated sample must be compared with more and more samples. Thus, to avoid performance problems, the chain algorithm is kept in small sizes and executed synchronously using a parallel algorithm for creating larger sample sets.

Proposed software has an optional tool that allows adjusting modification weights such that a shape feature can be preserved given less weights to the relevant control points or made more prominent its modification assigning more weights. In that way, users can control the direction of the sampling to be in the defined region; in other words, users can somehow decide on which

shape features of exemplar profile will be maintained and which will be modified. Finally users can choose the profile segments that need to be modified while the others' appearance and related functional features are preserved. Such feature is useful for the designers who need to consider the limitation of design to fit an existing environment (DFEE) [37], which aims to avoid additional costs caused by design changes.

The proposed generative system is capable of generating large number of samples such that it is not possible to evaluate each of them to find more appropriate solution. Therefore, there is need for narrowing down the generated sample set to the manageable number of solutions. This can be done with a simple option of the system, which retrieves as uniform as possible sample set minimizing the Audze-Eglais potential energy [38]. There is also an interface provided in which additional geometric constraints can be defined by the users to narrow down the solutions. These constraints can be formulated using some built in functions such as volume, surface area, Euclidean distance, vertical and horizontal distances, angle and basic mathematical operators. An example function usage is illustrated in Fig. 1.4, where the samples are filtered, oriented and colored based on the computed values of a function.
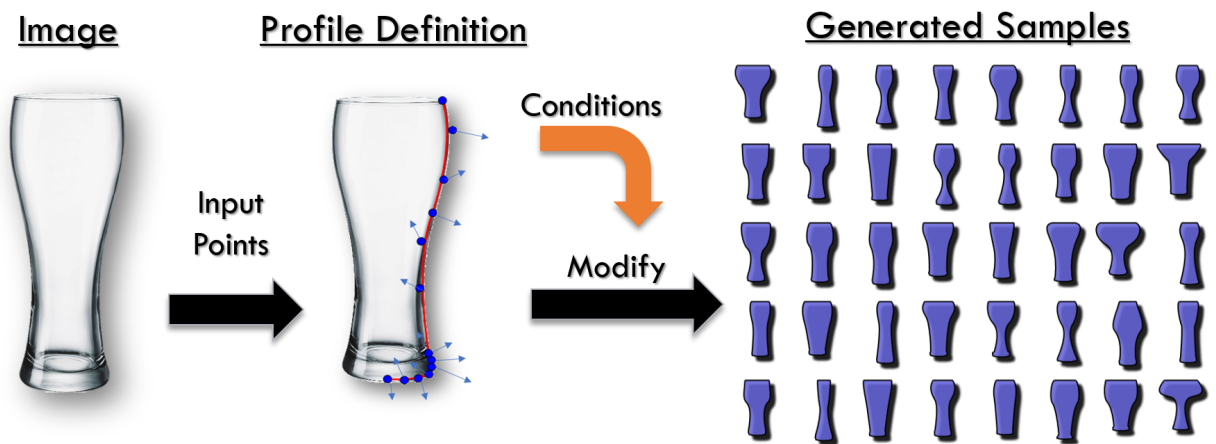
Figure 1.3: Example based generative design method overview. First a profile curve is defined using the input points, then conditions of the profile such as continuity between segments, curve degree and concavity of each segment are extracted. The points are then modified to generate new samples under constraints and maintaining the conditions in generated samples.
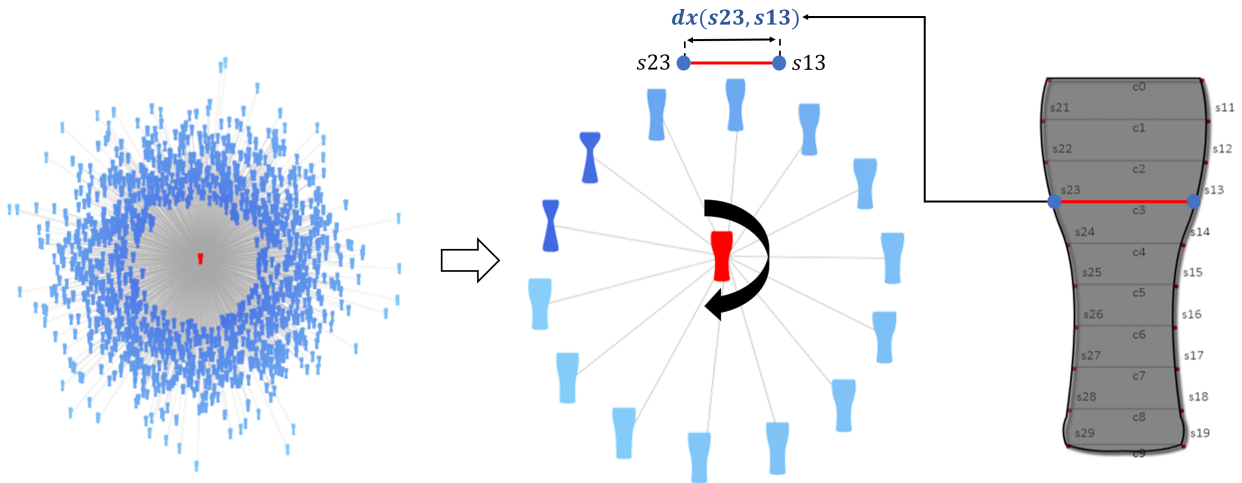
Figure 1.4: The leftmost samples are narrowed down according to $dx(s23, s13)$ where dx is a function to compute horizontal distance between two points that are labeled as $s23$ and $s13$. If the computed distance for a sample is out of a range set by the user, this sample is eliminated. The samples on the right are ordered to be the distance is increasing in clockwise direction starting from the sample with minimum distance that is represented by the darkest blue color to the sample with maximum distance represented by the lightest blue color.

1.3   Research Objectives

As introduced in the previous section, the main motivation is to help users for conceptual design stage to achieve target aesthetic objectives efficiently and effectively through the two major approaches;

- the human-oriented design and

- the generative design.

The human-oriented design method is able to represent aesthetic preferences by mathematical models represented by many design parameters, which can be used for generating infinity number of design samples by changing these parameters. Such capability is considered useful for early stage of the aesthetic design. However, a dataset including irrelevant parameters to the survey participants lowers the reliability of the learned mathematical models. Thus, it is very important to eliminate design parameters, which are not relevant and attractive, for making the sampling system to be usable for designers. For this purpose, the human-oriented design method using the ETAS is proposed that determines the attractive and relevant parameters to the adjectives by examining the subjects' eyes fixation. By discarding the irrelevant and unattractive parameters, the sampling efficiency can be enhanced.

The generative design method is able to generate many design samples even beyond the imagination of designers using computer power. The designers then select solutions out of many that are useful for them. However, the generated samples involve both feasible and infeasible solutions. Thus, the samples must be constrained to be produced only from the feasible regions in the space. However, such requirements are difficult for the stylists who prefer sketching on a paper avoiding computer aided environments to quickly produce their ideas. For the reason that, a generative design approach is also proposed to derive many design samples from a single example that are diverse, regular and similar enough to the exemplar without needing any considerable effort and even designer expertise. The generated samples can also be managed to find a desired solution among them.

1.4   Thesis Outline

This thesis has been organized as follows: Chapter 2 introduces the eye tracking aided survey method to find out attractive and more relevant parameters for the adjectives based on participants' attention and preferences. Chapter 3 proposes the generative sampling method explaining the definition and modification of the original profile curve, the constraining methods and the sampling algorithm used to generate samples satisfying the set of objectives. Chapter 4 introduces the developed software that implements the proposed method in Chapter 3 and also covers the sample management system. Note that, the displayed results in Chapter 3 were obtained using the software proposed in Chapter 4. Chapter 5 summarizes the thesis, discusses the proposed approaches and mentions some future works.

Chapter 2

Eye Tracking for Screening Design Parameters in Adjective-based Design of Yacht Hull

2.1 Introduction

Adjective-based design is a method that translates human perception into design parameters quantitatively in order to achieve better understanding between designers and clients. In this approach, adjectives are used to describe product designs, which are generated via design parameters in terms of geometry. As a requirement of the concept, relations between hull adjectives (e.g., comfortable and aesthetic) and design parameters (e.g., length and width) are learned via a machine-learning algorithm. Nevertheless, the relations cannot be represented by some of the design parameters, although they are in the learning process. This finding shows that the parameters do not affect the adjective choices of the survey participants but add noises to the learning process; therefore, avoiding such parameters beforehand, the reliability of the human-oriented methods' outcomes can be enhanced and samplings can be made efficiently with less number of parameters. However, traditional multiple choice questionnaires are neither reliable nor capable of creating questions to reveal true feelings of people, who do not have background in design and have difficulty to articulate their aesthetic opinions only by words. Eye tracking is one of the methods to study human behaviors based on attention for more objective and accurate data collection regarding subjective feelings of the customers [39]. Therefore, in this study, visual evaluations are made using eye tracking technology for screening the parameters based on their attractiveness and establishing relations between the attractive ones and the adjectives to enhance quality of the relation representations. Eye tracking is used in perceptual research, which proves the existence of correlations between gaze data and human preferences. The main advantage of eye tracking is that reliable human perception data can more likely be collected compared to the user tests, since the evaluation is based on participants' attention rather than applying solely questionnaires that are limited by the question content. In light of the benefits and finding, an eye tracking device is used to collect gaze data, and then, eye tracking tools such as area of interest (AOI), scan path, and heat map are used to evaluate attractiveness of the design parameters. Finally, regression analysis is used to represent relations between gaze data of design parameters and the adjectives.

Adjective-based design

Product performance and qualities are not solely good enough criteria for clients as the market competition has already made them compulsory. For products with high quality and good performance, aesthetic design is highly important for clients to make the final decision [40, 41]. However, this criterion is not a clear target to be reached and is measured through client satisfaction, which is highly related to human feelings; therefore, it is difficult to forecast this criterion before-

hand. Dogan and Gunpinar [27] proposed the adjective-based design method, which quantizes human feelings and represents them as relations between adjectives (e.g., charismatic and modern) and design parameters that are geometrically defined on products (e.g., lengths and widths). Such approach aims to provide better communication between designers and clients [42]. In this method, feelings about designs can be easily expressed using adjectives and their relations with design parameters are used as a guide by designers. Thus, understanding clients and appealing them can be successfully achieved in relatively short times. Dogan and Gunpinar [27] applied the adjective-based method to yacht hulls. They first collected many hull adjectives using a survey method in which survey participants were asked to describe yacht hulls using adjectives, then narrowed down to 10 hull adjectives. Design parameters that can cover common hull shape features were also defined. A second survey was then applied, where a hull design is modified changing the defined design parameters and compared with its initial state, to observe whether the modifications of these parameters affect participants' decisions and eliminated accordingly. After the eliminations, the remaining design parameters were used to generate hull designs via a novel parametric design framework, which is also similar to the method proposed by Khan et al. [28]. Then, another survey was conducted, where the designed hulls were matched with the hull adjectives to create a dataset where inputs are the design parameter values of hulls and the responses are the adjectives selected for these hulls. Finally, a machine-learning algorithm that used neural network was fed with the dataset to represent relations between the adjectives and the design parameters as mathematical models. The mathematical models include the design parameters that have impact on the participant responses; however, some design parameters were absent in some models. In other words, relations of some design parameters with some adjectives could not be established; thus, it was concluded that the design parameters did not affect the adjective choices of the subjects (survey participants). Such noises are caused by unrelated parameters and need to be removed to raise the quality of relation representations. In this chapter, it is assumed that if a shape feature of a product does not attract subjects, the related design parameter with the feature is unattractive and irrelevant to the adjectives as well. An eye tracking device is used to evaluate the degree of attractiveness of design parameters, observing where the subjects' attention is focused.

Eye tracking system

Eye tracking, where eye movements of subjects are recorded as gaze points on given stimuli, is a commonly used method in neuroscience, psychology, computer science, industrial engineering, and marketing [43]. In the eye tracking system, illuminators are used to generate near-infrared

lights and images of their reflections from eyes are captured by cameras. In addition, an external processor is used to process the images to analyze the reflection patterns and generate a 3D model of the eye with its position in space. The 3D eye model is then used to calculate locations of the gaze points on relevant stimuli. Eye movements are illustrated on stimuli via fixations, which are a batch of gaze points accumulated within a predefined span in shape of circles, and saccades are displayed via straight lines that show eye movements from one fixation to another (Fig. 2.1a). In this study, the attractiveness of target areas is analyzed through fixation locations and durations at the locations, as well as scan paths [44], which are combinations of fixations and saccades. Fixations are widely analyzed using the area of interest (AOI) tool and heat maps [45]. Using the AOI tool, targets are surrounded with diverse shapes (Fig. 2.1b) to perform quantitative analysis with various metrics such as fixation duration and visit count. The heat map (Fig. 2.1c) represents fixation-accumulated areas based on a color scale where red indicates more attractive areas than the rest of the image. One method to examine the scan path is defining AOIs (see Fig. 2.1d for yellow rectangular shapes) on the path that needs to be searched and the transitions between the AOIs will indicate how often (frequency) the path is used. A transition matrix is also used to summarize the transitions in matrix form, as illustrated in Fig. 2.1e.

(a)   (b)   (c)

(d)

AOI Group	nowhere	A_1^t	A_2^t	A_3^t	A_4^t
nowhere	120	5	19	9	5
A_1^t	0	0	10	0	0
A_2^t	0	0	22	7	0
A_3^t	0	0	0	4	3
A_4^t	0	0	0	0	0

(e)
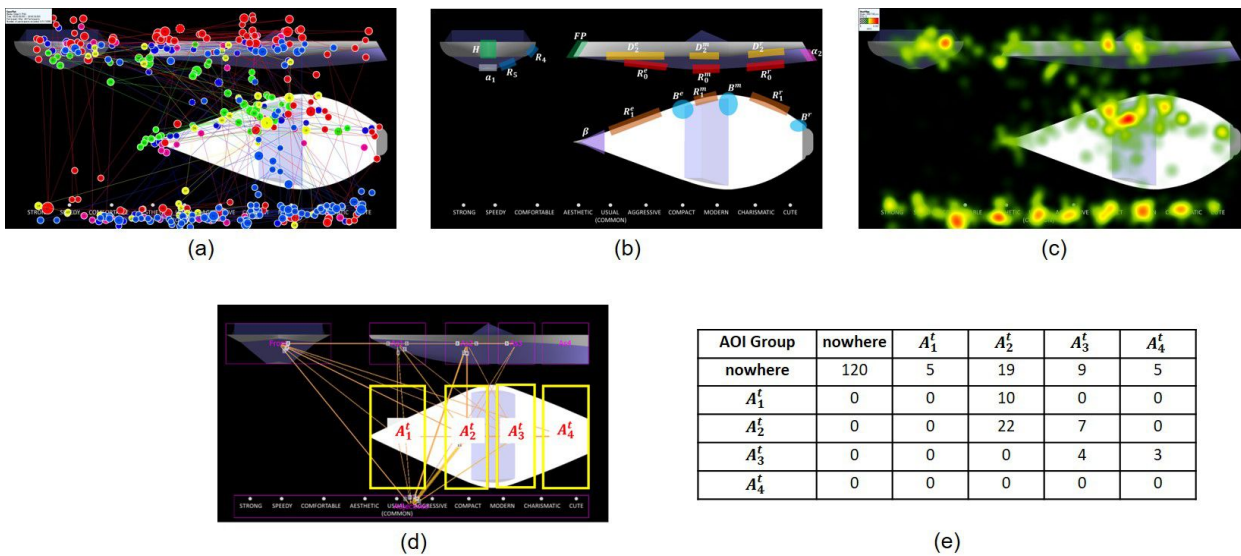
Figure 2.1: (a) Fixations are represented via circles and saccades are straight lines that connect consecutive fixations. (b) AOIs are defined via various shapes on target areas for further statistical analysis. (c) Heat map illustrates gaze point accumulations based on a color scale where red areas depict areas that receive maximum attention. (d) Scan path analysis via AOI transitions. (e) Transition matrix for scan path analysis.

Template Learning Survey (TLS)

Design parameters can be classified as local and global parameters (Fig. 2.2) according to their impact on hull appearance. Local parameters are the ones that have full control on the target shape such as radii of feature curves. On the other hand, global design parameters affect large areas (e.g., lengths and widths) and the recorded gaze data on these areas can be found in any shape related to the search behavior of subjects. Thus, gaze points for global parameters first need to be identified according to the search behavior of subjects in order to analyze them with an appropriate strategy. To do this, a survey is used, called TLS, where all the learned identifier information for the relevant parameter is named as *template*.
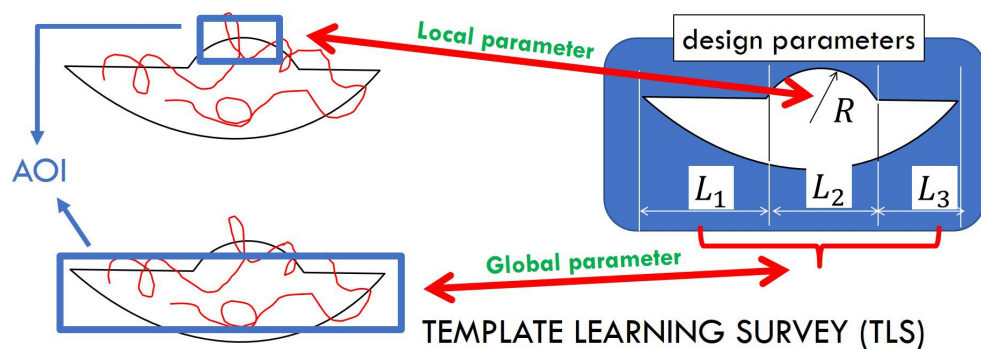
Figure 2.2: Two cases to decide whether AOI will be defined on the relevant parameter or TLS will be applied to learn what the best strategy is.

Proposed approach

According to the flow of the proposed approach depicted in Fig. 2.3, the eye tracking aided survey (ETAS) is first applied, where participants select appropriate adjectives from a given list for the hull images and gaze points of participants are recorded. The local parameters are analyzed by defining AOIs, while the global parameters are first applied TLS to learn their templates to determine a suitable analysis method. If a template of a global parameter shows the gaze points in the shape of accumulation in a particular area, the parameter is also treated as the local parameter since it is searched locally. On the other hand, if the gaze data are spread out instead of being gathered in local areas, scan path analysis is used. Relative time durations (RTDs) are then calculated for local parameters with the outcome of AOI analysis, and transition probabilities (frequency of path usage) are calculated for global parameters, which are analyzed via the scan path. In the end, the two calculated metrics for the design parameters are used to compare their attractiveness.

Finally, relations between gaze data of attractive parameters and the responses (adjective choices) are searched using regression analysis.
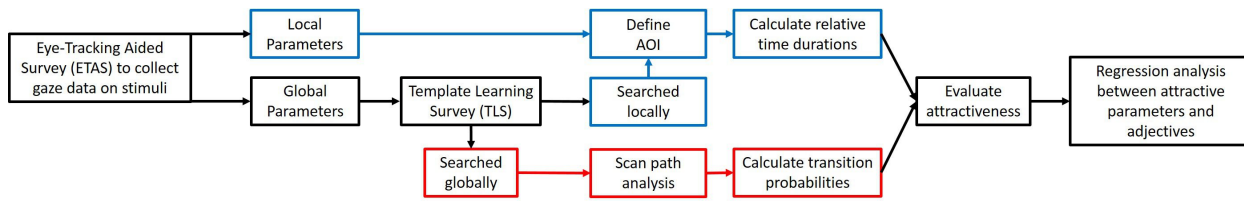
Figure 2.3: Flow of proposed approach.

2.2 Related Works

This study is related to the adjective-based design method, which is similar to other human-oriented design studies such as Kansei engineering [46] and semantic attribute-based concepts [23]. Since these design concepts put the human perception in the center of the design process, this study is also related to the cognitive research conducted to learn human preferences. We are specifically interested in the research where eye tracking systems are used.

Adjective-based design

Literature covers several studies on human preferences to explore, identify, and convert human emotions into physical entities to estimate their possible preferences [46]. For example, Yanagisawa et al. [47] created a model-based design method that used Kansei database to forecast customer preferences and obtain former understanding about human perception of the designs for the designers. Chen and Chang [48] proposed a method to extract appearance attributes and determine mathematical models correlating the attributes with customer responses in order to estimate their possible preferences about product designs. Chaudhuri et al. [23] proposed ATTRIBIT, which assembles 3D models where assembly parts are related to semantic attributes. The relations are explored and the parts are ranked according to their degree of relevant attributes through surveys. In a similar direction, in our previous study, the adjective-based design method [27] is proposed and used in this study to develop a method for screening design parameters.

Eye tracking studies

Gaze data basically show the areas that have and those that have not caught the interest of subjects. There are several studies using eye tracking systems that have found relations between gaze data and emotions and/or preferences. Alshehri and Alghowinem [49] stated that eye movements are related to the emotional states of subjects as they have diverse reactions for pleasant and unpleasant media. Yousefi et al. [50] suggested the use of eye tracking for construction processes, analyzing the relations between gaze data and user satisfaction. Mohammadpour et al. [51] applied user tests recording gaze data, where building designs were evaluated by subjects and long fixation durations for attractive designs were measured. Kim et al. [52] examined correlations between nightscape preference degrees and gaze points, and found that subjects spent more time on the preferred images. Noland et al. [53] used eye tracking in their survey, which allowed qualitative and quantitative investigations of images related to urban planning. The study results showed that *cars* and *parking* were ranked negatively, while new urbanist parts of the images such as *people*

and *pedestrian features* were mostly highly ranked. This study is motivated to use eye tracking technology with these findings to evaluate the attractiveness of the design parameters.

Eye tracking studies for product design

There are a few studies that use the eye tracking framework to particularly understand outstanding design features or how human aesthetic understanding is formed by product appearance. Kukkonen [54] studied product designs with an example of mobile phones where gaze data of subjects were compared through a questionnaire and strong correlations were found between them. In that study, five mobile phones were shown in pairs to the subjects, including designers, and gaze data for product attitudes and preferences were analyzed. Köhler et al. [55] extended the well-known Kansei engineering method using eye tracking, in order to evaluate product aesthetics from the perspective of human perception, and validated the results using descriptive and statistical analysis procedures. Koivunen [56] claimed that the way people look at designs is important and suggested strategies about first impression of the subjects, which they thought can help designers. Du and MacDonald [57] also analyzed the relative importance of visual product attributes and the impact of the attributes' sizes on human preferences by using an eye tracking device. Their study showed the existence of significant relations between the gaze data and attribute importance, and used ordinal logistic regression to predict the importance of both attributes and their size changes. Khalighy et al. [58] formulated aesthetic understanding of subjects through the gaze data depending on *beauty* and *attractiveness* drivers. They asserted that the aesthetic formula succeeds in estimating human preferences via gaze data.

The above studies aimed to learn important geometric features to help designers in understanding customer needs and desires. Our goal is in a similar direction; however, we go further and provide an adjective-based design concept which is a kind of translator that converts adjectives (which is the design aesthetic language of clients) into design parameters (which is the language of designers). Moreover, the importance of design parameters over appearance features is found, which are combination of design parameters. A design framework is also proposed that works with the design parameters, which means that the findings can be directly used by the design framework unless subjective decisions are required by designers. Besides all these benefits, our screening method is conducted more systematically as an orthogonal array is used to sample designs having varied geometric features, where the design parameter values are equally changed through the 54 hull designs. It is believed that to get favorable results from the design evaluations, such systematic approach is needed to observe real perceptions of humans when they see varied

features. To the best of our knowledge, the existing product evaluation studies with eye tracking systems use limited number of existing design samples, which may be good enough to propose their methods, but cannot offer proper evaluation due to lack of systematically prepared enough design variations.

2.3 Experiment Materials and Setup

The experiments were conducted with 54 hull design images and 10 adjectives, which were obtained from Dogan and Gunpinar [27]. In that study, frequently used adjectives were determined via a survey (Fig. 2.5), where participants were shown various yacht hull models and asked to describe them via adjectives. Social listening method was then used to enlarge the adjective dictionary and the retrospective think aloud method [59] was used to validate the determined adjectives via subjects' feedbacks. Finally, the following 10 adjectives were determined: *strong* (A_1), *speedy* (A_2), *comfortable* (A_3), *aesthetic* (A_4), *usual (common)* (A_5), *aggressive* (A_6), *compact* (A_7), *modern* (A_8), *charismatic* (A_9) and *cute* (A_{10}). Before the surveys were conducted, each participant was provided car images related to the adjectives for the illustration. The reason for selecting cars rather than yachts was to not steer the subjects while they were matching adjectives with the hulls, but only show them how an adjective can be related to a product design. The car images were obtained from the Web and are not shared with this thesis due to copyright issues. In addition, dictionaries were used to standardize adjective definitions for the subjects. In the end, each participant was trained with several hull models for warming-up purposes.

Hull models were sampled using the Taguchi experimental method [60], which suggests an L54 orthogonal array for 25 design parameters with three levels and one with two levels. Each level was assigned an appropriate value to determine dimensions for the 54 hulls. The hull models were then generated via a novel parametric design framework proposed by Khan et al. [28], where a hull is divided into three parts: *entrance section*, *middle-body section*, and *run section* (Fig. 2.4). According to the framework, the entrance section surface is obtained via loft operation between forward profile (*FP*) and entrance station profile (SP^e); middle-body section is generated by lofting between SP^e and middle-body station profile (SP^m); and run section is generated by lofting between SP^m and run station profile (SP^r). Note that the lofting processes between profiles were performed following *top*, *bottom*, and *feature (middle)* guide curves to control the surfaces. Furthermore, only half of the model was first lofted and mirroring operation was then performed to obtain the full model. The design parameters with their definitions are given in Table 2.1, and the hull locations are illustrated in Fig. 2.4.

Table 2.1: Design parameters with definitions.

Parameter	Definition
L^e	Entrance section length
L^m	Middle-body section length
L^r	Run section length
B^e	Entrance section width
B^m	Middle-body section width
B^r	Run section width
D_1^e	Entrance section depth
D_1^m	Middle-body section depth
D_1^r	Run section depth
D_2^e	Entrance section upper depth
D_2^m	Middle-body section upper depth
D_2^r	Run section upper depth
a_1	Width of bottom flat panel
α	Deck line angle
α_2	Backward angle
β	Entrance angle
θ	Forward profile angle
H	Height of forward profile
R_1^e	Min. radius of entrance top guide curve
R_1^m	Min. radius of middle-body top guide curve
R_1^r	Min. radius of run top guide curve
R_0^e	Min. radius of entrance bottom guide curve
R_0^m	Min. radius of middle-body bottom guide curve
R_0^r	Min. radius of run bottom guide curve
R_4	Min. radius of upper profile curve
R_5	Min. radius of lower profile curve

Eye tracking aided survey (ETAS)

ETAS questions were prepared using images of 54 hull models, with the front, top, and side views providing the same pixel/meter ratio based on lengths, widths, and depths to simplify the understanding of dimension changes and fair AOI definitions (Section 2.4.1.2). Note that additional
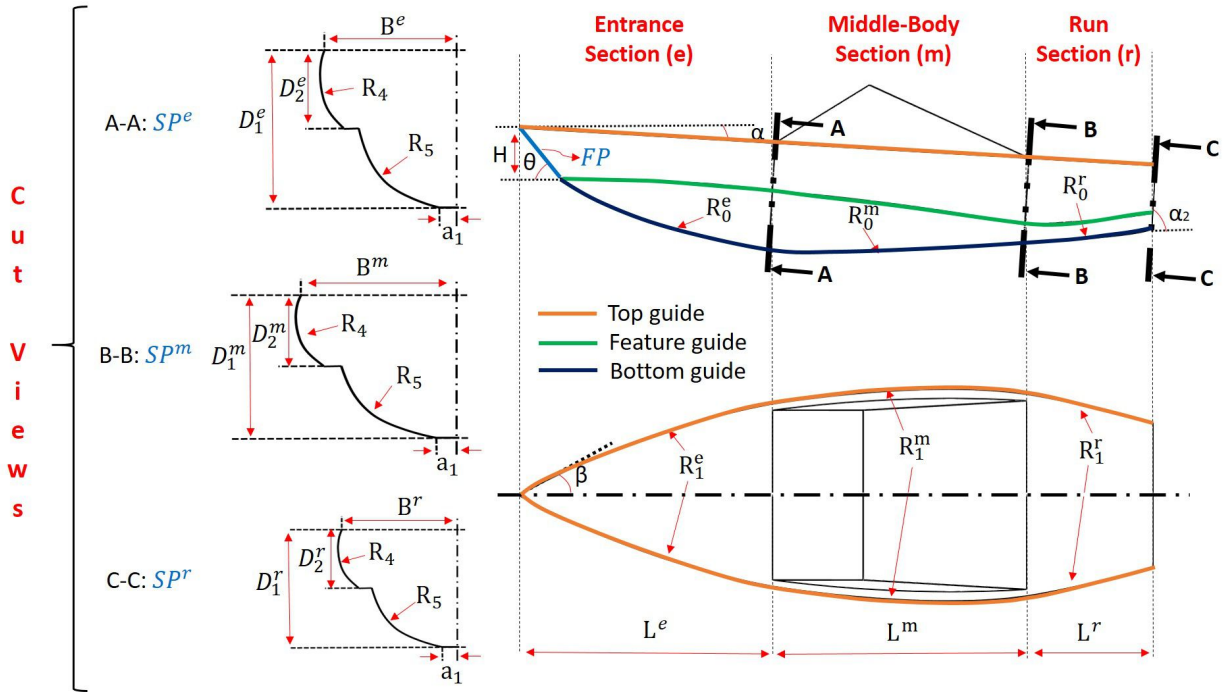
Figure 2.4: Design parameters are demonstrated on side, top, and station profiles, which are illustrated via A-A, B-B, and C-C cut views.

views were not used since they would add nothing to the three views in terms of showing design parameters, but disperse the focus of the subjects to widen areas. Figure 2.6a shows the experimental setup, where the screen was 520 mm wide and 325 mm high (24 inch diagonal) and the image (one of the ETAS questions) had 1920 × 1080 resolution. A screen-based eye tracking device (Tobii Pro X3-120) was used with a sampling rate of 120 Hz. Moreover, participants were free to move their head within 500 mm width and 400 mm height according to the report of the producer. Owing to this setup, the subjects were not disturbed by the device, and hence, could behave more naturally. In addition, the tracker had a reported accuracy of 0.4° and precision of 0.24°. Finally, the distance between the participants and the tracker was set as 650 mm.

The ETAS question interface for a hull design is given in Fig. 2.6b, which shows the design with three views and the location of adjectives. Participants were asked to select at least two appropriate adjectives from the list in order to increase the time spent on the hull, as time limitation was not applied for ETAS. The responses were verbally expressed by the subjects and recorded by an operator via Google Form so that the subjects could keep looking at the screen and not interrupt the gaze recording. This part is important for computing the RTDs since each time a subject looks away from the screen to select an adjective leads to empty gaze data, while the time period of the questionnaire is increasing.
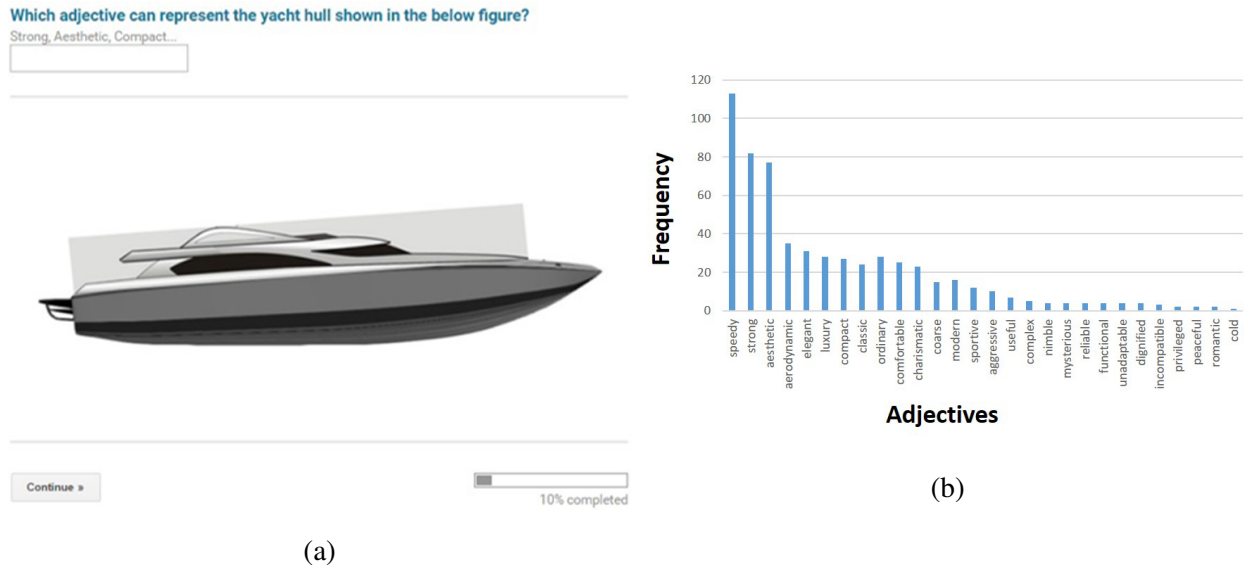
Figure 2.5: A figure taken from Dogan and Gunpinar [27]. (a) A question from adjective learning survey. (b) Hull adjectives that are learned from the survey.

Before each experiment, calibration was made using a calibration tool of the tracker software using nine dots. ETAS was conducted in three sets, where each set consists of 18 hull design images and three calibration images (Fig. 2.6c) between hull images with equal intervals. Note that the calibration images were shown only for two seconds and were used to check if the calibration was missed during the survey. Data of two subjects' tasks were discarded from the analysis due to the calibration problems, which were detected via the calibration images.

Total number of participants for this study were 24, including two females, aged 20 and 42 with mean 24.21 and standard deviation 5.83. The nationalities of the participants were Chinese, Japanese, Korean, and Malaysian. Each participant was given only two tasks out of four (three ETAS sets and one TLS), and on average, 13 subjects participated in each ETAS set and 10 in TLS tasks. A relevant council of The University of Tokyo approved the surveys used in the study.

Figure 2.7 shows some gaze plots and heat maps of ETAS results obtained via Tobi Pro software [39].
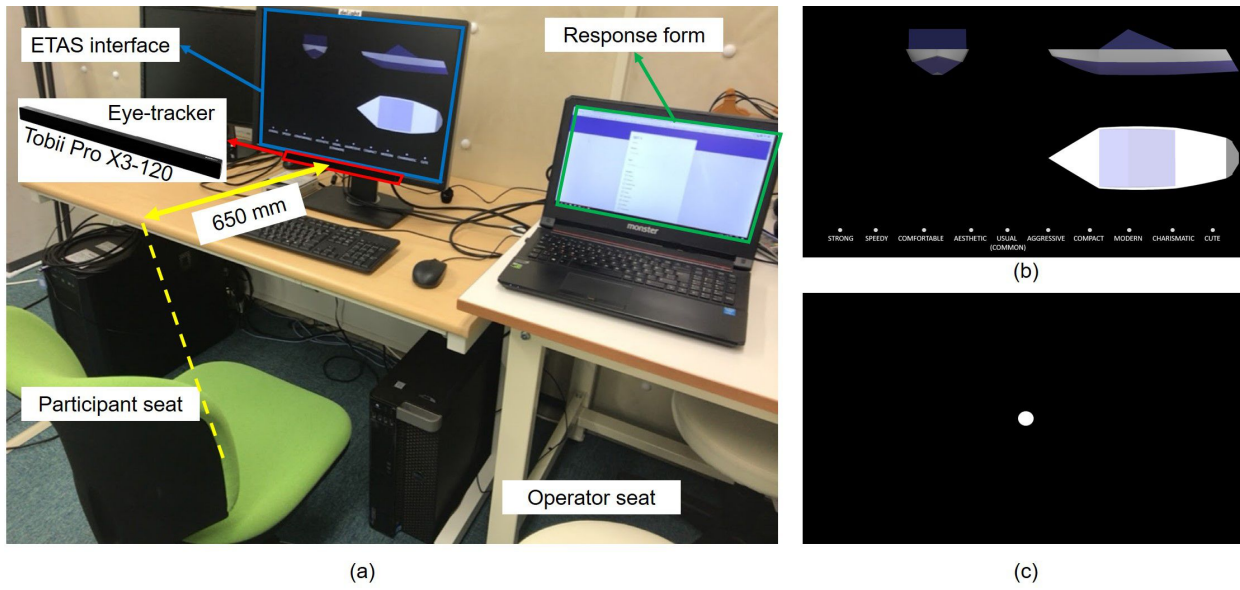
Figure 2.6: (a) Experimental setup. (b) ETAS interface consists of front, side, and top views of a hull design and adjectives placed at bottom of the screen. (c) Calibration image.
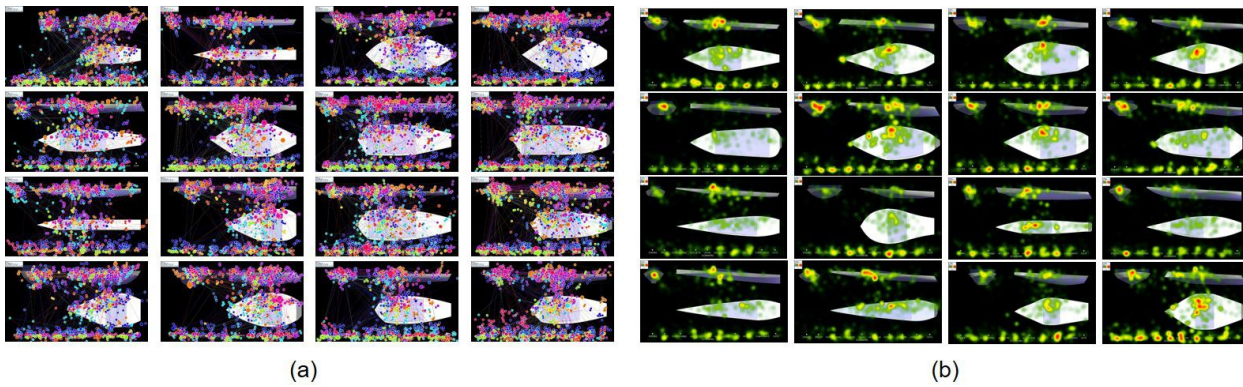
Figure 2.7: (a) Gaze plots of some hulls. (b) Heat maps of some hulls.

2.4 AOI-based Screening Methods for Design Parameters

As mentioned in the first section, the local parameters are evaluated via the AOI tool and global parameters using scan path analysis. The scan path analysis was also conducted by defining AOIs on the path and the transitions between the AOIs refer the usage frequency of the defined paths. To prevent confusion, the AOIs used for scan path are called as *path AOIs*. In this section, first, design parameters will be classified as *local* and *global* based on their impact on the appearance and search areas using TLS. Then, AOI definitions and metrics that will be used will be explained.

2.4.1 Design Parameter Classification

Design parameters that have full control on the target shapes are classified as local parameters since their search area can be limited to particular areas without overlapping with other design parameters. These parameters, which have local impacts on target shape, include minimum radii of feature curves ($R_1^e, R_1^m, R_1^r, R_0^e, R_0^m, R_0^r, R_4, R_5$), bottom width of flat panel (a_1), entrance angle (β), and upper depth parameters (D_2^e, D_2^m, D_2^r). Note that the upper depth parameters are used to control the incline of the feature guide curve between the sections; therefore, the incline is analyzed via AOI to evaluate these parameters. In addition to these, *FP* parameters, which are H and θ, are also classified as local parameters to be evaluated via the AOI tool since the area covered by the profile is relatively small to use the scan path analysis. H can be observed independently from all other parameters over the front view; however, over the side view, overlapping between H and θ is inevitable due to sharing of the same geometric feature. Therefore, an AOI is defined with *FP* label that covers the whole *FP* on the side view; in other words, feature-based screening is performed for *FP*, which is a combination of H and θ, rather than parameter-based.

On the other hand, global design parameters include lengths (L^e, L^m, L^r), widths (B^e, B^m, B^r), and depths (D_1^e, D_1^m, D_1^r), since they impact large areas on the hull shape, and angular parameters (α, α_2), which can be found anywhere through the inclined lines. In brief, we do not know how global parameters are searched by subjects. Therefore, these design parameters first need to be identified based on their search area to determine the best strategy for them. TLS is suggested for the identification and to define templates according to the identities for each global design parameter. Here, the template means the generalized output of TLS for a design parameter that includes information of search area of the parameter, whether local or global, with size and location of the area. Note that all locally searched parameters are analyzed via the AOI tool even if they are classified as global design parameters due to their effects on the hull appearance.

2.4.1.1 Template learning survey (TLS)

TLS tasks are specialized to request participants search only one specific design parameter in order to record gaze data that belong only to this specific parameter. TLS tasks can be categorized into two types. The first task aims to compare a design parameter by sections of one hull model to observe the search behavior of subjects through the hull. Figure 2.8 demonstrates a question example of such task where relevant design parameters are first introduced and the task is explained without time limitation. Whenever participants feel ready, the calibration image is displayed for two seconds and a hull model is then shown for five seconds. Finally, a question (e.g., "Which section is shorter/longer than the others?") is asked related to the task, and after the subject answers, the other hull model is shown. After that, the same task is repeated three more times with other hulls. This task is suitable for lengths, widths, and depths as they are defined for each section separately.

The second task is to compare a design parameter on three different hulls and suitable to be used for all design parameters. Figure 2.9 shows that the task is similarly explained and a calibration image again appears for two seconds, but this time, all hull models are shown consequently and one question (e.g., "Which model has wide/narrow/perpendicular angle?") is asked to compare three hull models for the relevant parameter. The calibration images have extra goal in TLS, which forces participants to start at the same point to increase similarity of initial gaze points in order to get meaningful results for comparison. In addition, the question and answer options that are easy to remember and understand are chosen to enable participants easily focus on the main objective of the task. For example, sections are introduced as left, middle, and right for easy comparison rather than entrance, middle-body, and run, which are difficult to remember. Note that the answers given for the question tasks are not analyzed since their only aim is to give purpose to the subjects and do not add value for gaze data analysis.
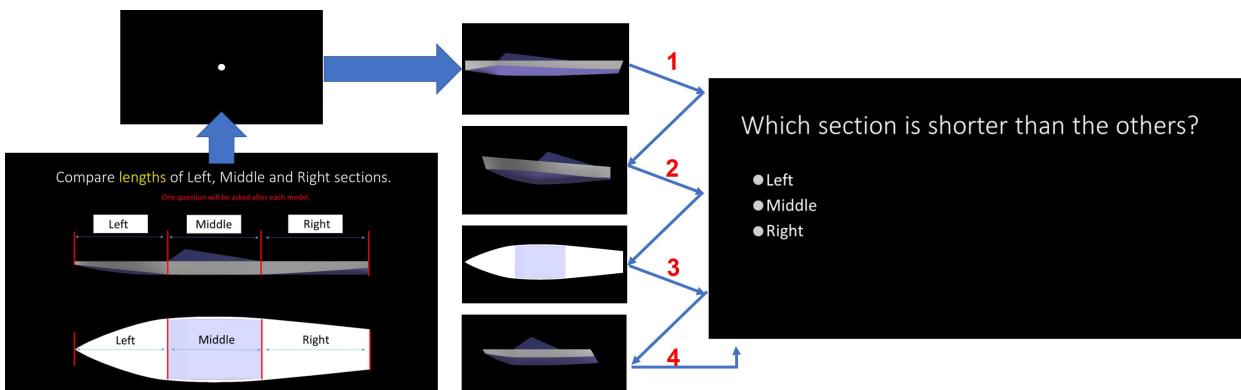
Figure 2.8: TLS task flow of first type, where a question is asked after each hull is displayed to compare the hull sections' relevant design parameter.
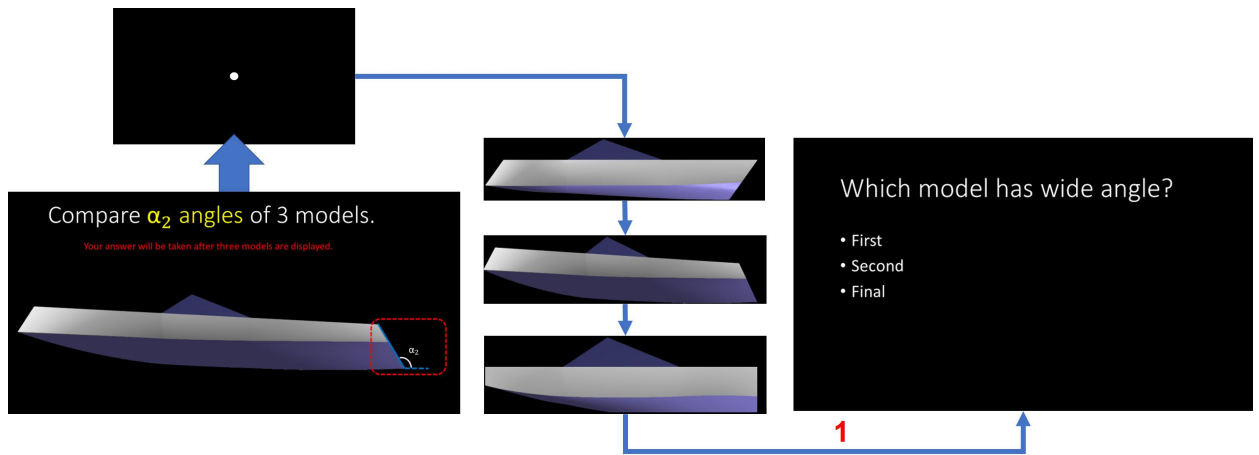
Figure 2.9: TLS task flow of second type, where a question is asked after three hulls are displayed to compare design parameters.

All TLS results are first visualized by heat maps to check whether the parameters are searched locally (fixations are accumulated in particular area) or in a spread-out way, and additional tools are then used to decide if they are suitable for analysis via AOI or scan path. Example TLS outputs for globally searched design parameters are visualized by gaze plot and transition arrows between path AOIs, which are shown in Fig. 2.10a for the first task and in Fig. 2.10b for the second task. On the other hand, example local parameter results are given in Fig. 2.11a for the first task and in Fig. 2.11b for the second task. By evaluating the visual outputs, L^e, L^m, and L^r are classified as global parameters since they are searched horizontally in wide areas. Moreover, B^e, B^m, B^r, and α_2 are classified as local parameters since they are searched on particular areas where AOI definitions are possible without overlapping. Meanwhile, D_1^e, D_1^m, D_1^r, and α parameters cannot be classified due to random gaze plots, which are not suitable for both AOI and scan path analyses. Therefore, they are kept out of the scope of this study.

(a)   (b)
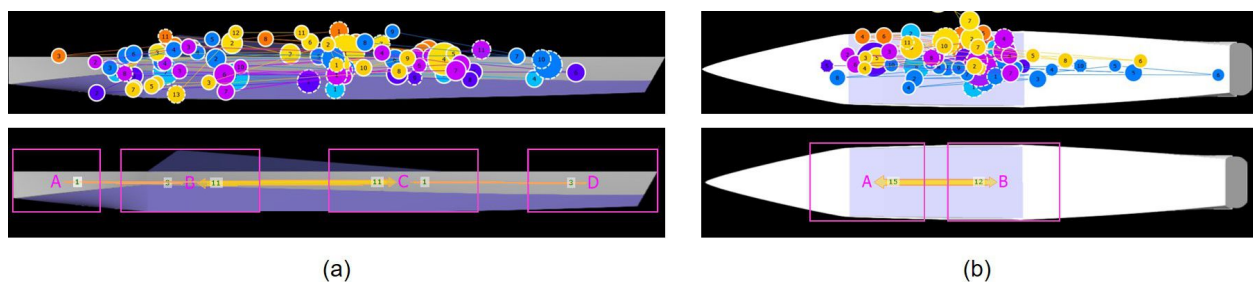
Figure 2.10: (a) An output of first type of TLS task for length parameters (L^e, L^m, and L^r), which requests to compare section lengths. (b) An output of second type of TLS task for length parameters, which requests to compare middle-body lengths (L^m) of different hull models.

(a)   (b)
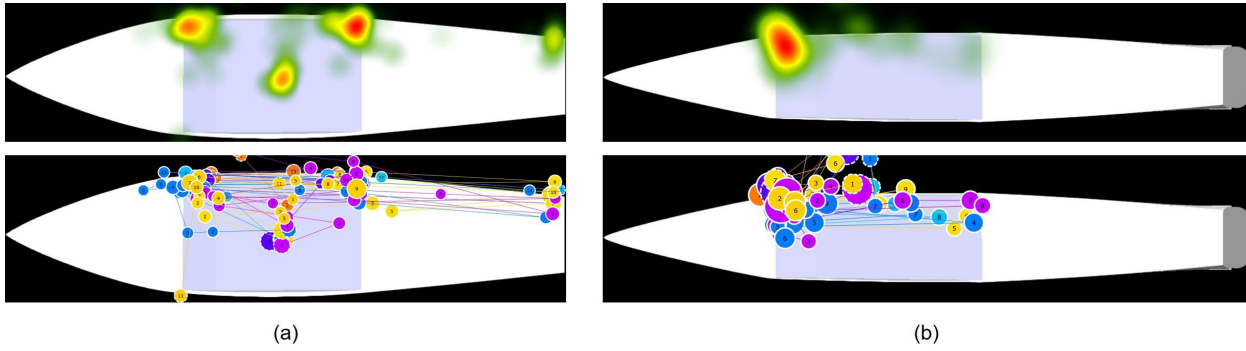
Figure 2.11: (a) An output of first type of TLS task for width parameters (B^e, B^m, and B^r), which requests to compare section widths. (b) An output of second type of TLS task for width parameters, which requests to compare entrance widths (B^e) of different hull models. The outputs are given by the gaze plots, where the eye movements of each subject are represented by different colored circles and straight lines; and the heat maps created based on total time spent by the subjects indicating regions by red in which most of the gaze data are accumulated.

Preliminary search via heat map

The heat map is a well-known method to visualize aggregated gaze points of all subjects at a time on a stimulus using a color scale, as illustrated in Fig. 2.1c. This visualization method gives a general idea about the areas that are attractive to the subjects and those that are completely neglected. As Bojko [61] suggested, instead of using the heat map for extensive analysis, it is recommended to use as a visualization tool for planning the study, mainly to learn where to define AOIs in order to gain time and increase efficiency. Another issue that needs to be considered is the use of relative durations of the total time spent by the subjects in case the time periods of the experiments differ from one subject to another. The final suggestion is to set the total kernel size, which is the diameter of the colored area around the fixation center, with a larger value than the default to spread the colored area to provide higher confidence interval in terms of increasing the search area.

In our study, the heat maps are generated via Tobii Software by applying I-VT filtration [62] with default settings of Tobii Pro software [39] according to relative durations. Furthermore, although the default total kernel size of Tobii Pro software is 100 px, which is determined according to the highest visual span of the human eye, this value is set to 210 px to increase the confidence level of the investigated area. Finally, the parameters that need quantitative examinations by AOI in the colored areas are determined for each image.

As mentioned in Section 3, mirroring operation is used to obtain the final hull models, which

means the hull model is symmetrically generated. Due to this reason, a half of the front and side views has the same design parameters as the other half. However, Fig. 2.12 shows three heat map results, where the searching area of front and side views is indicated by arrow directions. According to this figure and TLS results (Fig. 2.11), only half of the views are investigated by the participants. Therefore, to simplify the study, unnecessary AOI definitions are avoided based on heat map visualizations and define the AOIs for half of the views only.
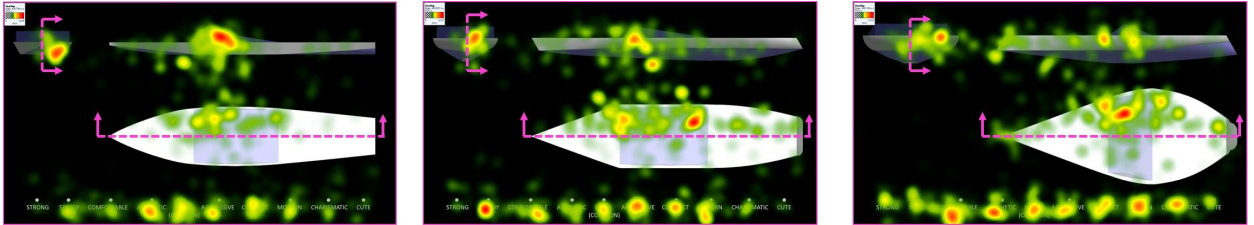
Figure 2.12: Three out of 54 heat map results of ETAS. The investigated areas by the participants are displayed using a color scale, where red depicts the most attractive areas.

2.4.1.2 AOIs for local design parameters

Nineteen design parameters R_1^e, R_1^m, R_1^r, R_0^e, R_0^m, R_0^r, R_4, R_5, D_2^e, D_2^m, D_2^r, α_2, β, θ (FP), H, a_1, B^e, B^m, and B^r are analyzed quantitatively via AOIs, since they are locally searched by the subjects. OGAMA [63] is used to define elliptical AOIs for B^e, B^m, and B^r, since they are observed in an area close to ellipsoidal shape (Fig. 2.11) and tetragonal AOIs for the remaining 16 design parameters. The AOI definition for parametrically generated designs has a critical problem that the dimension of the relevant design parameter differs over the 54 hull models, so the AOIs need to be arranged for each hull model parametrically. Three main issues are considered for AOI definition:

- **Fair comparison:** AOI sizes need to be adjusted by the same proportion for each of the 54 hulls, since comparison is performed between the parameters.

- **Batch AOI definitions:** Nineteen local design parameters for each of the 54 hull models require 1026 AOI definitions, which is impractical to do manually, so automation is needed to define AOIs.

- **Avoid from overlapping:** When AOIs are adjusted for each hull, there may be some circumstances that cause overlapped AOIs. To avoid this problem, the AOIs are defined on the center of the target geometric feature rather than the whole; in other words, the gaze points are sampled from the center of the target feature. This may cause some gaze data loss (decreases sensitivity), but prevents the analysis of incorrect gaze data (increases selectivity).

As the design parameters are compared with batch AOI definitions, it is believed that such an approach is valid when AOI definition is made providing the fairness and necessity to define AOIs automatically without overlapping.

The volume of a 3D product design changes with its length, width, and depth parameters (basic parameters). Therefore, the AOI sizes are varied with equations, making them dependent on the main construction parameters according to the view. In other words, size of an AOI defined for a hull parameter on side view is based on length and depth parameters, while that of a top view parameter depends on width and length parameters. First, template elliptical AOIs are defined as covering the target areas, which are learned from TLS empirically. On the other hand, the templates of the tetragonal AOIs are defined via the oriented bounding box method [64], enclosing the target areas. After that, since the AOIs are managed via four *handle points* (P_0, P_1, P_2, P_3) (see Fig. 2.13), the distances between the handle points of the template AOIs in x and y directions are divided by the relevant basic parameters to compute ratios. Finally, the ratios are used to determine appropriate positions of the handle points for the 54 hulls. In other words, defined templates are reversed based on their hull models' main dimensions and the handle points are relocated according to the new hull dimensions by the amount of the ratios. Note that a fixed reference point P_r^x is selected for each design parameter to compute the ratios and to relocate the handle points of the relevant AOIs.

There are several ways to define AOIs based on the basic parameters, but the one, that is used, is illustrated in Fig. 2.14, where x and y coordinates of P_0, P_1, P_2, P_3 for the elliptical AOI of B^e is parametrically changed in proportion to the empirically found ratios via TLS over width (B^e) and lengths (L^1 and L^2) according to reference point P_r^x. Note that the major axis of the elliptical AOI is computed in two parts based on L^1 and L^2 in proportions of the ratios, and the minor axis is computed based on B^e. Similar and suitable approaches are determined and applied to the other local parameters to parametrically modify and enable them to orient with the various dimensions of the 54 hulls.

2.4.1.3 AOIs for global design parameters

As seen in Fig. 2.10, the sequences of gaze fixations for the global parameters (L^e, L^m, and L^r) are observed in the form of horizontal transitions along the hull on both side and top views. Our aim is to associate transitions made along the sections with the relevant length parameter for each section. This can be done by defining path AOIs to construct a path similar to that observed in TLS and counting the transitions between the path AOIs. Therefore, eight path AOIs are defined:
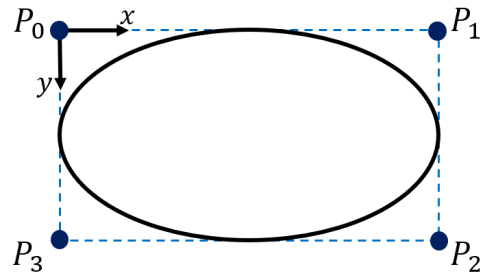
Figure 2.13: AOI shapes are controlled by the handle points (P_0, P_1, P_2, P_3).
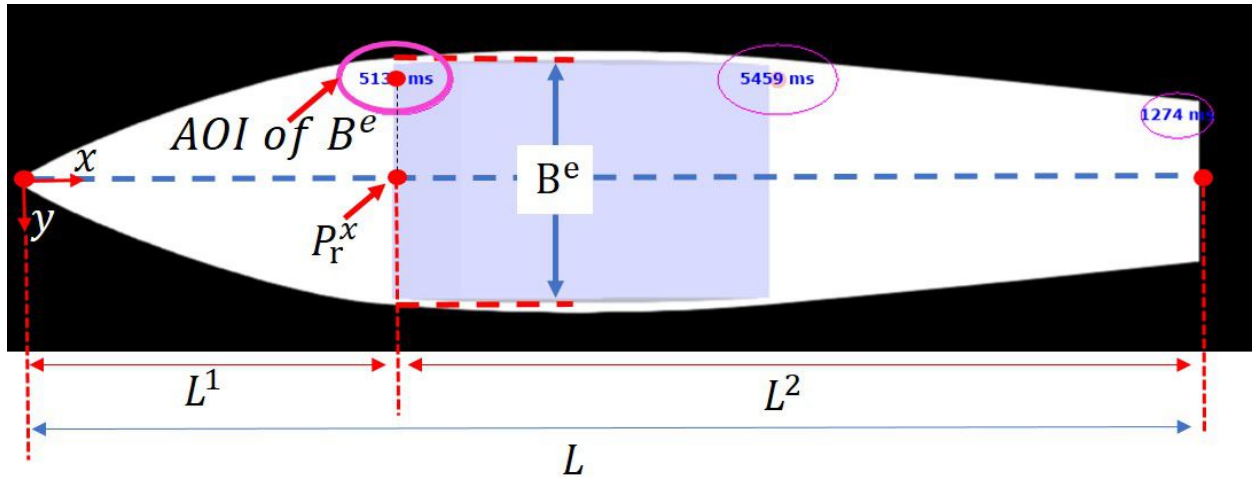
Figure 2.14: AOI location and reference point (P_r^x) demonstration for B^e.

four on the side view, with labels A_1^s, A_2^s, A_3^s, and A_4^s, and four on top view, with labels A_1^t, A_2^t, A_3^t, and A_4^t (Fig. 2.15a). In addition to these eight path AOIs, two extra path AOIs are defined: one for the front view of the hull and one for the whole adjective region in order to be used for transition probability calculation (the reason for this will be explained later). Note that the heights of the path AOIs are equal to the maximum height of the hull on the side view and the maximum width of hull on the top view in order to capture horizontal transitions. Similar to the procedure for local parameters, the handle points of the AOIs in the x direction are defined depending on length parameters and relocated through the 54 hull models using computed ratios. Furthermore, the OGAMA software provides average loci similarities in percentages, which depicts the proportion of the covered scan paths of the subjects by the defined path AOIs. The ratios for path AOIs are computed taking the loci similarities into consideration.

2.4.2 Evaluation Metrics

Two metrics are used in this study: *RTD* for AOI analysis and *transition probability* for scan path analysis.

RTD

Since there are 54 hulls with varied geometries, the AOI sizes are parametrically adjusted for each hull. However, it is not fair to compare AOIs with different sizes [65]. Furthermore, the time periods for ETAS are not fixed, so the periods are different for each subject and the results can be dominated by the one who spends more time than the others. To address these problems, fixation durations are standardized to be relative to the time periods of subjects and the sizes of AOIs for each design parameter.

Equation 2.1 calculates the relative times ($\bar{T}^A$), where T^c is the period of a subject on the relevant hull image and T^A indicates the time spent on a defined AOI for a parameter.

$$\bar{T}^A = \frac{T^A}{T^C} \tag{2.1}$$

Equation 2.2 then normalizes the AOI size of the design parameter, where the sum of relative times of all subjects ($\sum_{subjects} \bar{T}^A$) is divided by AOI proportion of the design parameter to the whole question area (k). These computations are made for each of the 19 local design parameters to obtain the RTD (S^A).

$$S^A = \frac{1}{k} \sum_{subjects} \bar{T}^A \tag{2.2}$$

Transition probability

As in RTDs, the transition counts need to be normalized for comparison of the global parameters of the 54 hulls. To do this, the transition counts are divided by total transitions made in the relevant hull image and the results are interpreted as transition probability [66]. The general formula of transition probability ($p(A_i \mid A_j)$) for a pair of path AOIs (A_i and A_j) is given in Equation 2.3, where the transition count ($C(A_i \parallel A_j)$) is divided by the total count of transitions made on the hull image ($C(A)$). Note that A here refers to a relevant AOI label.

$$p(A_i \mid A_j) = \frac{C(A_i \parallel A_j)}{C(A)} \tag{2.3}$$

Since more than 26 target design parameters can be observed by subjects on given stimuli, many pointless transitions will be made for local parameters, which should be avoided from total transitions. Therefore, the path is constructed via 10 path AOIs covering the major transitions

rather than the minors that are made on the image. $C(A)$ is the number of major transitions, which are the ones among *front view, adjectives region, entrance section, middle-body section,* and *run section* (sections are defined for both top and side views). Minor transitions are assumed as transitions made on black areas of the image and self-transitions ($A_i \parallel A_i$) are the ones made inside of the defined path AOIs, which are usually short saccades and more likely belong to the local parameters. Figure 2.15a shows the defined 10 path AOIs and Fig. 2.15b displays the transition counts between the corresponding AOIs for both side and top views in the matrix form. Figure 2.15c illustrates the transition probability computation (Equation 2.3) over the transition matrix of the top view, where the transition probability between A_1^t and A_2^t ($p(A_1^t \mid A_2^t)$) refers to that of the entrance section length ($p(L^e)$) on the top view, ($p(A_2^t \mid A_3^t)$) is equal to $p(L^m)$ and $p(A_3^t \mid A_4^t)$ is equal to $p(L^r)$. The transition diagram in the Fig. 2.15c is also used to summarize the probabilities between the relevant AOIs, where *nowhere* refers to AOIs other than ($A_1^t, A_2^t, A_3^t, A_4^t$). Similarly, transition probabilities of four path AOIs ($A_1^s, A_2^s, A_3^s, A_4^s$) are used to compute transition probabilities of the section lengths based on the side view. Front view and adjectives are other regions that are involved by the path, as they are important stations for the subjects.
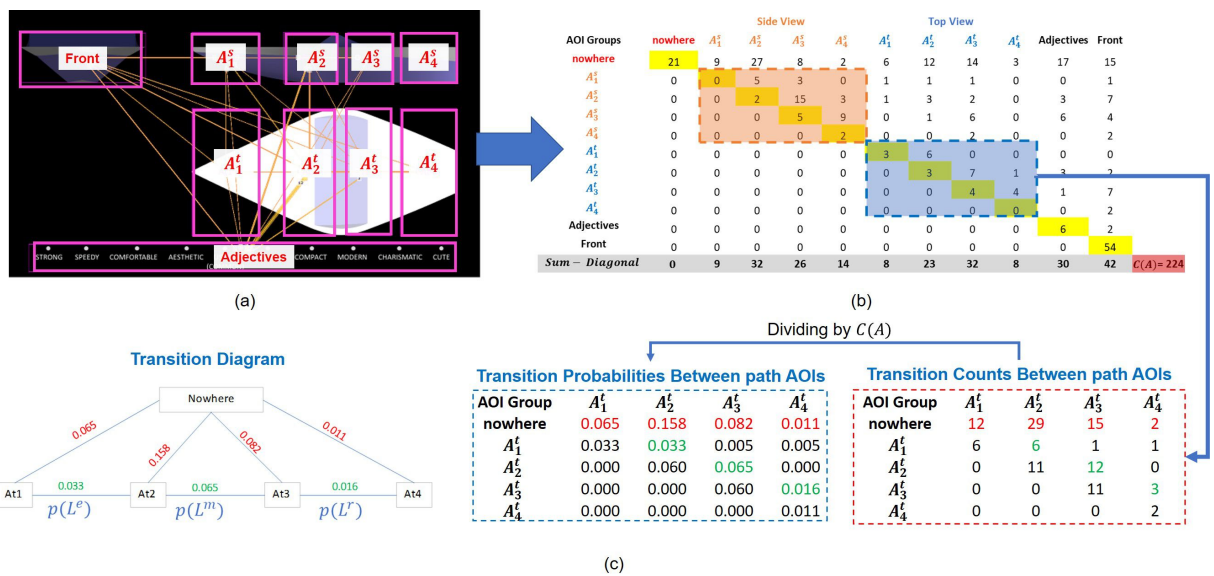
Figure 2.15: (a) Ten path AOIs that cover major transitions. (b) A transition matrix example, which summarizes the transitions in matrix form. (c) Transition probability calculation example over top view path AOIs $\{A_1^t, A_2^t, A_3^t, A_4^t\}$, where the transition matrix members (transition counts) are divided by total transition count $C(A)$. The probabilities between the path AOIs and remaining AOIs (nowhere according to investigated path AOIs) are then represented through a transition diagram.

2.5 Results

2.5.1 Screening-based Evaluation of Design Parameters

2.5.1.1 Evaluation with RTD metric

First, the ETAS questions were roughly examined based on five significant areas: *front view, adjectives, entrance section, middle-body section* and *run section* (the sections are available for both side and top views (Fig. 2.16a)), via their total RTDs computed for the 54 hulls ($\hat{S} = \sum_{i=1}^{54} S^A$). In Fig. 2.16b, $\hat{S}$ values for each area are represented via a pie chart in percentile, which are relative to the sum of all. Note that percentages of sections were calculated according to sum of their computed durations on the side and top views. According to the chart, the regions ordered from the most attractive to the least attractive are as follows: 37% of the total RTD of all 54 hull images for the middle-body section, 20% for the entrance section, 19% for adjectives, 18% for front view, and 6% for the run section. This analysis suggests that the middle-body section is the first section that needs to be modified to appeal clients or achieve any design goals in terms of aesthetics, since people quickly detect the modifications made in this section. Also, the results show that dealing with run section modifications should be considered as last option since the clients will not pay attention to this section in the first place.

Figure 2.16c also shows the comparison of the view-based results with the adjectives. According to the comparison, the side view of the hull design attracts most attention, followed by the top view and then the front view, which means that the side silhouette of the designs need to be studied on priority to appeal clients.
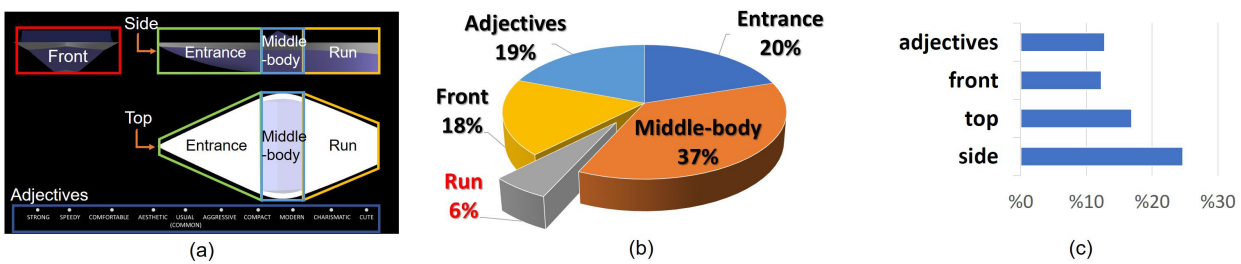
Figure 2.16: (a) Five categorized regions: the front view, adjectives, entrance, middle-body, and run sections. (b) Proportions of relative durations for each categorized region. (c) Comparison of views and adjectives' region based on total RTDs in percentage.

Fine examination is performed with the 19 local design parameters via computed average RTDs ($\bar{S}^A$) over the 54 hulls. The distribution of $\bar{S}^A$ values of the 19 parameters is represented via a

box plot [67] in Fig. 2.17a. The box plot is composed of quartiles, which are used to evaluate the attractiveness of the parameters in four levels. Accordingly, the design parameters whose $\bar{S}^A$ values are above than the third quartile (Q_3) are the most attractive ones (Level 1) among the 19 local parameters. The parameters with $\bar{S}^A$ values between *median* and Q_3 are second-level attractive parameters. The other quartiles below the median value are determined as third and fourth degrees in terms of attractiveness. The local parameters are illustrated in Fig. 2.17a according to their attractiveness levels with different colors, where green demonstrates the most attractive parameters (Level 1), which are listed as follows:

- ***Level 1:*** H, B^e, D_2^m, R_4, and R_1^m.

- ***Level 2:*** $D_2^e, a_1, B^m, R_5, R_0^m$, and *FP*.

- ***Level 3:*** β, R_0^e, R_1^e, and D_2^r.

- ***Level 4:*** R_1^r, B^r, R_0^r, and α_2.

Since the attractiveness of the parameters is measured based on the gaze data, the relations between the gaze data and the hull adjectives must be analyzed. The idea is that if the gaze data have relations with the adjective choices, the attractiveness results obtained will be related to the adjective-based design concept, since it shows that the participants looked at the parameter to select the adjectives. Otherwise, the results will be unrelated to the adjective-based design concept. Therefore, Level 1 and Level 2 parameters are further analyzed via regression analysis to validate the attractiveness results. The parameters lower than the median value are (Level 3 and Level 4 parameters) kept out of the regression analysis. $\bar{S}$ proportions of each parameter relative to the sum of all ($\bar{S}^A / \sum_{i=1}^{19} \bar{S}^A$) are visualized in Fig. 2.17b, where the discarded parameters are surrounded by a red rectangle, indicating the smallness of the area covered by them as compared to the rest.

2.5.1.2 Evaluation with transition probability

Transition probabilities of L^e, L^m, and L^r parameters ($p(L^e), p(L^m)$, and $p(L^r)$) are calculated for each of the 54 hulls via scan path analysis and refer to the usage frequencies (or densities) of the relevant paths. The average probabilities ($\bar{p}(L^e), \bar{p}(L^m)$, and $\bar{p}(L^r)$) for the side and top views with sum of both are given by the bar chart in Fig. 2.18a. The results show that 2.5% of transitions are made for L^m on the side view and 3.8% on the top view, so the total transition percentage for this parameter is 6.3% ($\bar{p}(L^m) = 0.063$). The transition frequencies for L^e on the side and
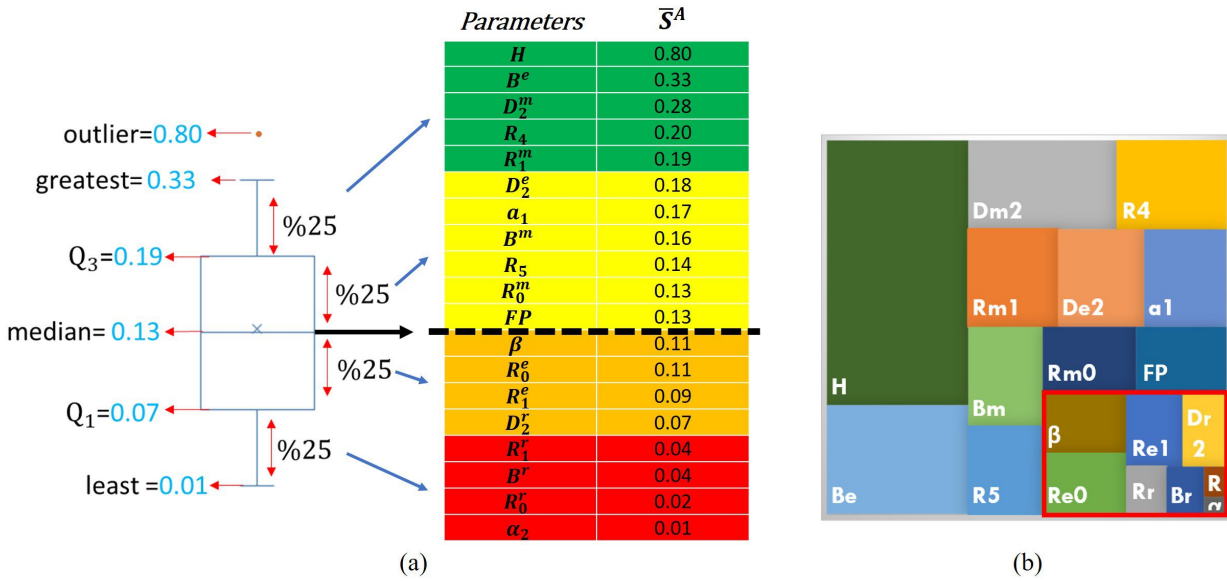
Figure 2.17: (a) Box plot via its elements and $\bar{S}^A$ values of the parameters, which are colored based on attractiveness levels. (b) $\bar{S}$ proportions of each of the 19 design parameters relative to the sum of all.

top views are 1.6% and 1.3%, so the total value is 2.9% ($\bar{p}(L^e) = 0.029$). Finally, L^r transition frequency is calculated as 0.5% on the side view and 1.0% on the top view, and total frequency of the transitions compared to whole transitions made on the question area is 1.5% ($\bar{p}(L^r) = 0.015$). It can be inferred from these results that the attractiveness order of lengths, in other words, priority of the length parameters for the adjective-based design concept is $L^m > L^e > L^r$.

Figure 2.18b also depicts the distributions of the 54 hulls' transition probabilities of L^e, L^m, and L^r (sum of both side and top views for each hull model). In the box plots, each whisker shows the range where 25% of all probabilities are distributed, while the box covers the remaining 50%. Comparing to the range of box plots and median values of L^e, L^m, and L^r (in order $0.03, 0.06$, and 0.01), a big portion of $p(L^r)$ values is distributed under $p(L^e)$ and $p(L^m)$ values. In addition, the run section has already been found unattractive; bringing all the reasons together, L^r is also kept out from the regression analysis.

2.5.2 Relation Analysis via Regression Analysis

In this section, the relations between gaze data and adjective choices are studied. If some relations can be established, they can be used to find unattractive design parameters. For this purpose, regression analysis is applied for estimating the relations between the gaze metrics as independent *input variables* and adjective selections as dependent *response variables*. More specifically, the input
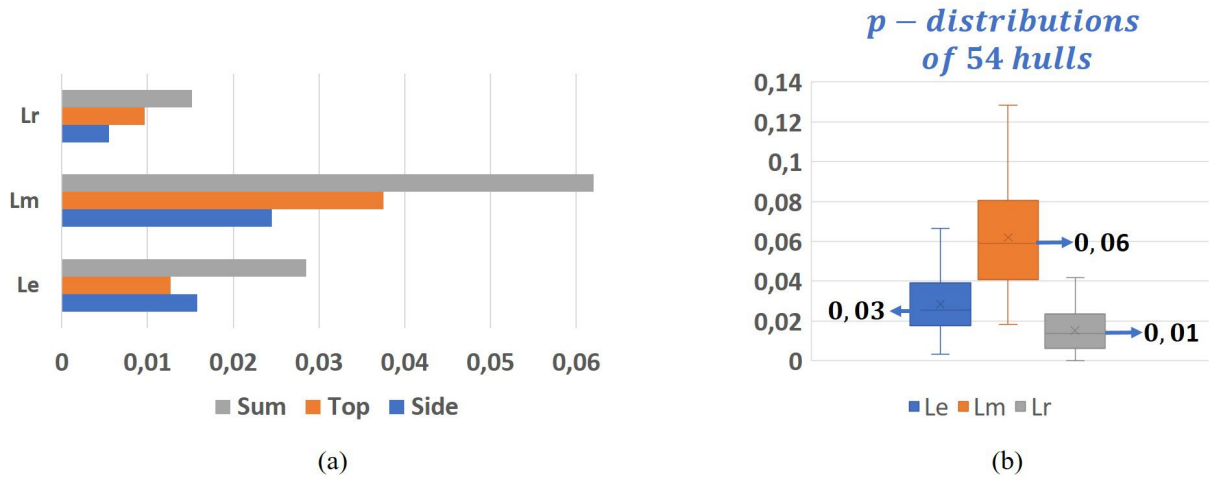
Figure 2.18: (a) Average transition probability of L^e, L^m, and L^r on the side view, top view, and sum of both views. (b) Sum of side and top view transition probability distributions of the 54 hulls for L^e, L^m, and L^r.

variables are the RTD (S^A) and transition probability (p). They are denoted as $X = \{x_i, i = 1...13\}$. The response variables are 10 adjective selections {*strong* (A_1), *speedy* (A_2), *comfortable* (A_3), *aesthetic* (A_4), *usual (common)* (A_5), *aggressive* (A_6), *compact* (A_7), *modern* (A_8), *charismatic* (A_9) and *cute* (A_{10})}. They are denoted as $Y = \{y_i, i = 1...10\}$. As shown in Table 2.2, for each of the 54 hull designs, relevant values for each of x_i and y_i are obtained with the user experiments described in Section 2.4. The regression analysis is conducted on these input and response variables with values from the 54 observations for the hull design $ID = 1...54$. First, a dataset is prepared where input variables are assigned as gaze metrics and the response variables are defined by converting the adjective selections into levels. Next, generalized linear model (GLM) [68] is introduced as the regression analysis method.

A set of input variables, called the regression model, is used for the regression analysis. The set X, including all 13 input variables, cannot be the best choice for the regression model but some subset of X is preferable. Thus, the best-subset selection method [69] is used to determine the final regression model for each adjective. In this method, the residual sum of squares (RSS) of all possible regression models is first calculated to determine the top models, which are then evaluated according to the Akaike Information Criteria (AIC) [70]. The AIC values of the top models are compared according to the Akaike weight ratios [71] and D^2 [72] values. Finally, the performance of the determined models for each adjective is measured via D^2, Mean Absolute Percentage Error (MAPE), and correlation analysis results.

Dataset organization and response variable determination

The gaze data are input for regression analysis and represented by RTD for 11 attractive local parameters and transition probability for two attractive global parameters. The adjective choices are converted into three levels according to the number of selections made by subjects, and then used as response variables for the analysis. Table 2.2 displays dataset organization including input variables, response variables, and observations.

Note that the levels represent the projected values of number of selections and will be analyzed as continuous variables rather than classes. The values of the gaze metrics, RTDs, and transition probabilities increase due to the attention of the subjects. Accordingly, it is hypothesized that the number of selections of an adjective for a hull model is related to the increase in the gaze metric values. In other words, if a design parameter is related to an adjective choice, the value of the relevant metric for the design parameter is increased by the number of participants who select the adjective. However, the amount of increase in the metrics with the number of participants is not expected to be detected clearly, because each additional selection does not guarantee the increase in gaze metrics due to the unstable behavior of subjects during the survey. To clarify the relation between the increase in the gaze metric values and the number of selections, higher jumps between the number of selections are provided projecting them into levels. Therefore, the increase in selections will be easily related to the increase in the metric values and the noises caused by ineffective selections are filtered.

Table 2.2: Dataset for regression analysis.

	Hull ID	$S^{R_1^m}$	S^{B^e}	S^{B^m}	S^{R_4}	S^{R_5}	$S^{R_0^m}$	S^{FP}	S^H	S^{a_1}	$S^{D_2^e}$	$S^{D_2^m}$	$p(L^e)$	$p(L^m)$	A_1	A_2	A_3	A_4	A_5	A_6	A_7	A_8	A_9	A_{10}
					Relative Time Durations								Transition Probabilities		Adjective Levels									
Observations	1	0.12	0.38	0.07	0.39	0.03	0.08	0.11	1.04	0.05	0.05	0.23	0.02	0.04	1	2	1	1	3	1	2	1	1	1
	2	0.18	0.68	0.10	0.10	0.18	0.06	0.11	1.34	0.32	0.09	0.55	0.02	0.05	1	1	2	1	2	1	2	1	1	2
	3	0.35	0.70	0.13	0.50	0.00	0.00	0.18	1.17	0.16	0.17	0.43	0.04	0.05	1	3	1	1	1	2	1	1	2	1
	4	0.10	0.04	0.03	0.40	0.00	0.26	0.30	1.02	0.00	0.50	0.40	0.03	0.04	2	1	2	2	1	1	1	1	1	1
	5	0.10	0.23	0.08	0.56	0.00	0.03	0.17	1.05	0.46	0.41	0.12	0.02	0.05	2	1	2	1	1	1	1	2	1	1
	6	0.12	0.43	0.06	0.24	0.05	0.16	0.36	1.97	0.20	0.25	0.48	0.02	0.06	2	2	2	2	1	1	1	1	1	1
	7	0.13	0.07	0.17	0.11	0.27	0.19	0.09	1.15	0.25	0.11	0.10	0.02	0.03	1	2	1	1	1	1	1	2	1	1
	8	0.09	0.20	0.04	1.14	0.03	0.11	0.00	0.82	0.19	0.99	0.04	0.03	0.06	2	1	2	1	1	1	1	1	1	1
	9	0.09	0.10	0.14	0.00	0.03	0.14	0.00	1.31	0.30	0.00	0.16	0.01	0.03	3	1	2	2	1	2	1	1	1	1
	.	.	.	.	.	.	.	.	.	.	.	.	.	.	.	.	.	.	.	.	.	.	.	.
	52	0.02	0.08	0.15	0.00	0.11	0.44	0.15	0.22	0.18	0.16	0.28	0.02	0.10	1	3	1	2	1	3	1	2	1	1
	53	0.06	0.10	0.14	0.18	0.00	0.33	0.00	0.23	0.46	0.06	0.33	0.03	0.06	1	3	1	1	1	3	2	3	1	1
	54	0.07	0.40	0.15	0.18	0.38	0.39	0.45	0.99	0.05	0.01	0.39	0.02	0.08	1	3	1	2	1	2	2	2	2	1

As it is mentioned before, each participant was given only two tasks out of four and some data were discarded due to calibration problems. Thus, the number of participants, namely the

maximum possible number of selections, are different for each ETAS set, so the assignment of levels for the adjective choices must be done accordingly. Therefore, instead of using the number of selections directly, selection indexes are calculated dividing them by the number of subjects participating in the relevant set. The 540 index values (54 hulls and 10 adjectives) are plotted against the hull ID using the histogram type graph to examine their distributions (Fig. 2.19). The histogram is first was divided into two parts by a median value of 0.46, and it is seen that the upper portion is randomly distributed. The stable part is then divided into two equal intervals. As a consequence, the levels are assigned using the following conditions:

- Level 1: $index < 0.23$

- Level 2: $0.23 \leq index < 0.46$

- Level 3: $index \geq 0.46$
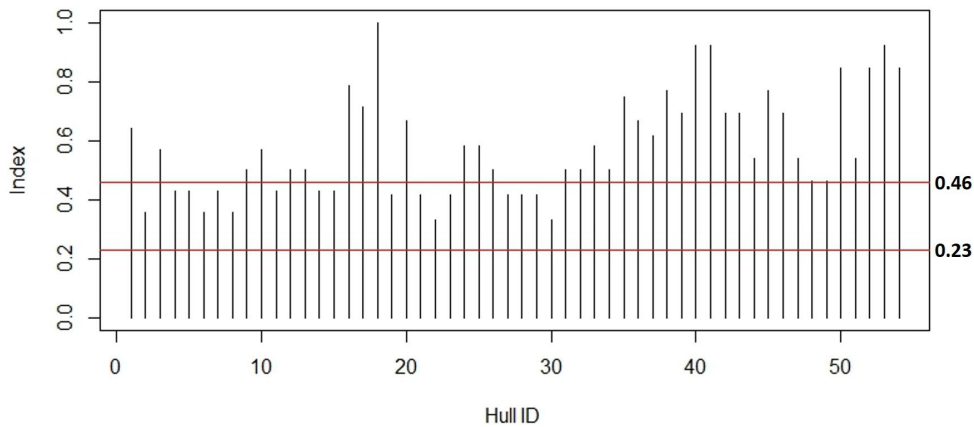
Figure 2.19: Histogram of selection index values versus hull ID and red threshold lines for levels.

Generalized linear model (GLM)

In this study, GLM [68] is used for the regression analysis. In addition, as the response variables (adjective levels) are non-negative continuous variables and limited between 1 and 3, which makes the distribution skewed since the bounds cannot be exceeded, the Gamma family [73] is found suitable for the data distribution after comparing and testing with the other families (e.g., Gaussian, Poisson, and Quasi). The general formula of GLM is as follows:

$$g(E(y_i)) = \beta_0 + \beta_1 x_1 + ... + \beta_k x_k \tag{2.4}$$

where $E(y_i)$ is estimation of the response value (adjective choices) corresponding to $A_1, A_2, ..., A_{10}$; $x_1....x_k$ are independent input variables (gaze metrics) corresponding to $S^{R_1^m}$, S^{B^e}, S^{B^m}, S^{R_4}, S^{R_5}, $S^{R_0^m}$, S^{FP}, S^H, S^{a_1}, $S^{D_2^e}$, $S^{D_2^m}$, $p(L^e)$, and $p(L^m)$; β_0 is intercept, and $\beta_1....\beta_k$ are the coefficients for the estimation. *Inverse* link function ($g(\mu) = \mu^{-1}$) [73] is also used to relate the mean (μ) of the Gamma distribution and the linear estimation model.

Best-subset selection

In general, a regression deviation consists of two parts:

$$regression\,deviation = explained\,variance + residuals \qquad (2.5)$$

where variances are explained by the input variables (gaze metrics) and the residuals are remaining random variances that cannot be explained by the existing variables of the regression model. It is clear that our target is to increase the explained variances as much as possible, to decrease the residuals. To do this, the input variables, which are unrelated to the relevant response variable, need to be discarded from the regression model. This can be achieved via the subset selection method [69]. One way to select the best subsets is calculating the RSS via Equation 2.6 for each of the possible regression models, namely each $\hat{X}$ of the power set of X, 2^X. After that, the first m best subsets, which have the least RSS values, are found using an exhaustive search algorithm proposed by Morgan and Tatar [74]. RSS is computed for each $\hat{X}$ of 2^X as follows:

$$RSS = \sum_{i=0}^{n}(y_i - \hat{y}_i)^2 \qquad (2.6)$$

where n is the number of observations (54, the number of hull designs), y_i is the observed response value, and $\hat{y}_i$ represents the estimated value via the subset $\hat{X}$. $\{\hat{X}_1, \hat{X}_2, ..., \hat{X}_m\}$ can be found having the smallest RSS values. Then, $\{\hat{X}_1, \hat{X}_2, ..., \hat{X}_m\}$ are further analyzed according to one of the quality measures, i.e., AIC [70] value:

$$AIC = -2 \times ln(L) + 2k \qquad (2.7)$$

for each $\hat{X}\epsilon\{\hat{X}_1, \hat{X}_2, ..., \hat{X}_m\}$. L is the value of maximized likelihood function $L(\psi; x)$, which is calculated by setting its derivative (with respect to unknown parameter ψ) to zero and solving the derived equation for ψ; k is the cardinality of $\hat{X}$. Since the AIC value is a measure of information loss, the model with the smallest AIC is the best. On the other hand, in case the AIC values are close to each other, another model close to the best model (having AIC value close to smallest)

can be selected if it explains more portion of variance of the data. D^2 (Equation 2.8a) [72] is a measure of the explained variance for a GLM model, which is also equivalent to the well-known measure R^2. The value of D^2 increases with the number of variables involved in the regression model and causes unfair comparison between the models having different numbers of variables. Therefore, the regression models are compared via *adjusted D^2* (Equation 2.8b) [72] to eliminate this problem.

$$D^2 = 1 - \frac{Residual\ Deviance}{Null\ Deviance} \tag{2.8a}$$

$$adjusted\ D^2 = 1 - \frac{(n-1)}{(n-k)} \times [1 - D^2] \tag{2.8b}$$

where *Residual Deviance* refers to the residuals of the model including all model variables ($\beta_0 + \beta_1 x_1 + ... + \beta_k x_k$) and *Null Deviance* is the residual of the intercept-only model (β_0). Additionally, the AIC values of the models are compared via the following equation [71]:

$$w_{ij} = \frac{L_i}{L_j} \times (k_j - k_i) \tag{2.9}$$

where w_{ij} is the ratio of Akaike weights [75], which indicates how much i^{th} model $\hat{X}_i$ is better in terms of minimization of the information loss over j^{th} model $\hat{X}_j$.

To sum up, the subset selection starts with finding several best-subsets, which have the least RSS values. AIC is then used to find the best among them, which has the smallest AIC value. The best subsets having AIC values close to the best model are then checked to see if their D^2 values are higher than those of the best model without dramatically raising w_{ij}, which is computed between the best model (which has minimum AIC value) and the inquired model. In the end, if the increase in D^2 value is not sufficient to afford the increase in w_{ij}, the search is concluded.

Performance results of determined regression models

To conduct the GLM analysis supporting the subset selection method based on RSS and AIC values, the best-subset GLM (*bestglm*) package is used proposed by McLeod and Xu [76] through R-Studio software [77]. Table 2.3 shows the summary of the results for the determined model for each adjective in matrix form, where the first column represents the adjective labels. The second column indicates MAPE, which is computed via Equation 2.10 to obtain the error between the estimated ($\hat{y}_i$) and observed (y_i) response values scaling from 0 to 1, where 0 refers to 100% prediction accuracy.

$$MAPE = \frac{1}{n} \sum_{i=0}^{n} \left| \frac{y_i - \hat{y}_i}{y_i} \right| \tag{2.10}$$

Next, four columns represent correlation analysis results, which are measured with 95% confidence level, between the relevant adjective response of the data and fitted values of the models, where *cor* represents correlation value, CI^L and CI^U are lower and upper bounds of the confidence interval, and p-value is significance level of the correlation. Furthermore, GLM assumes that all input variables are independent. This assumption is checked via a multicollinearity test where the generalized variance inflation factor (GVIF) [78] values are used for the judgment. The last row shows that the computed GVIF values for each variable are less than 3, which indicates low correlation between the input variables, namely their independency [79].

The results show that the ratio of explained variances (D^2), which can be interpreted in percentile multiplying them by 100, ranges between 16% and 45%. Since the human perception is a complicated issue, the collected data for social research are usually very noisy and the D^2 values even under 50% are acceptable in the context of the research [80]. Also note that, the regression analysis in this study is conducted to show the existence of correlation between gaze data and preferences, but not for the prediction purposes. Moreover, the computed MAPE values range between 0.16 and 0.39, which shows relatively good results to claim the existence of the relations considering the noisy data. Correlation values, where " -1" indicates perfect negative correlation and "0" depicts no correlation while "1" represents perfect positive correlation between the models and the responses, are found between 0.37 and 0.67, which refer to positive correlations between the gaze data and the preferences. The correlations for the A_4, A_5, and A_{10} models are weak compared to the others, but still show the existence of positive relations. The $p-$values also indicate that all correlations are significant since all of them are lower than the 0.05 value (according to 95% confidence level).

The overall performance results of the determined regression models validate the existence of relations between human preferences (adjective choices) and subject attention (gaze data). The parameters of the found regression models (determined $\hat{X}$ subsets for each adjective) are also represented in Table 2.3 with black color, which are highly related to the relevant adjectives in terms of attention. For example, the regression model variables of A_1 are $R_1^m, R_4, FP, H, D_2^e, D_2^m$ and L^m. A designer can use these significant parameters in the first stage to get the hull model according to the desired adjective by modifying an existing hull model as they are attractive and have impact on the adjective choices.

Note that the unattractive parameters determined in Sections 2.5.1.1 and 2.5.1.2 were also

Table 2.3: Regression analysis results and the related parameters with the relevant adjectives represented by black cells.

Adjective	D^2	MAPE	cor	CI^L	CI^U	$p-value$	R_1^m	R_4	R_5	R_0^m	FP	H	a_1	D_2^e	D_2^m	B^e	B^m	L^e	L^m
A_1	0.38	0.31	0.62	0.43	0.76	5.02E-07	■	■			■	■		■	■				■
A_2	0.25	0.39	0.51	0.28	0.69	7.54E-05	■	■						■		■			
A_3	0.45	0.31	0.67	0.49	0.80	2.60E-08	■	■						■		■	■		
A_4	0.16	0.23	0.37	0.11	0.58	0.00606			■				■		■		■		
A_5	0.20	0.31	0.38	0.13	0.59	0.00408	■			■			■			■			■
A_6	0.35	0.31	0.60	0.39	0.75	1.73E-06		■	■					■			■	■	
A_7	0.38	0.20	0.57	0.36	0.73	5.46E-06		■		■			■		■				
A_8	0.30	0.32	0.54	0.31	0.70	2.83E-05			■		■		■				■		
A_9	0.41	0.16	0.62	0.43	0.76	4.93E-07		■	■			■			■		■		■
A_{10}	0.22	0.28	0.42	0.17	0.62	0.001735		■								■		■	
						GVIF	1.96	1.74	1.75	2.03	1.27	1.43	2.07	1.43	1.62	2.02	2.37	1.75	1.57

analyzed via plots against residuals of the regression models (Fig. 2.20) in order to check if the parameter can explain some portion of the residual part of the model. However, the residual plots show that the parameters have still totally random distributions, which means they are not explanatory, or the randomness is broken locally but the performance measures are not raised to be involved in the regression models. For example, the plot for R_0^e and β is relatively symmetric according to the line $y = 0$, so it is not possible to estimate the residuals via them. On the other hand, in the plot of R_1^e, some residuals can be estimated by the increase in this parameter. However, after adding the parameter to the relevant model, the *adjusted D^2* value decreases and MAPE value increases. Based on this, it can be said that the previous determination of the unattractive parameters is valid since they failed to explain the variances.
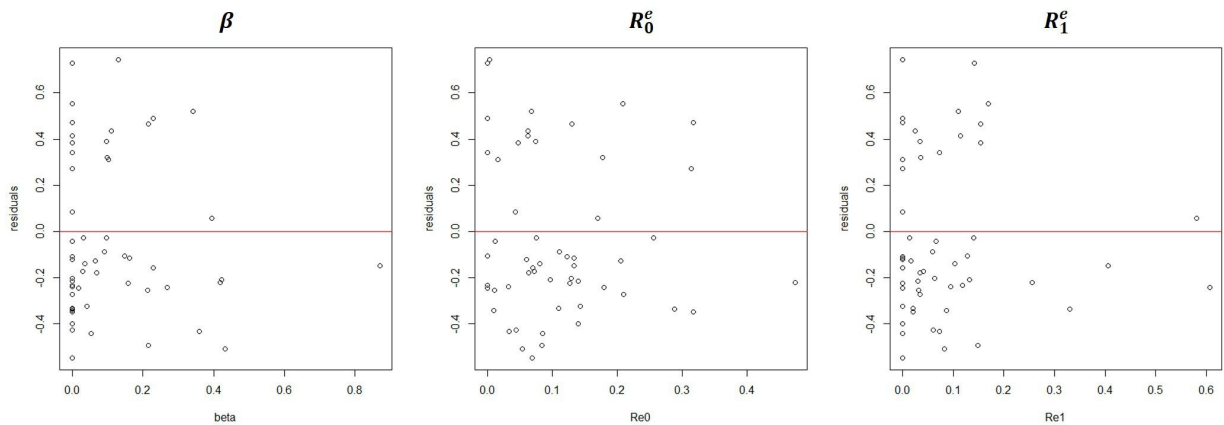
Figure 2.20: Residual plots of some of the unattractive parameters for regression model of strong adjective (A_1).

Further analysis

Pearson's product moment correlation [81] is also used between time spent on each adjective (each adjective was surrounded by an AOI separately) and the adjective levels (Fig. 2.19). Such analysis can provide following information:

- **How comfortable the subjects are with the adjectives:** If the subjects spend more time on an adjective even it is not selected, negative correlation is expected, which means that the adjective is difficult to match with the hulls or somehow confusing, which makes the subjects think more about it. So, in that case, it can be concluded that it needs to be replaced with a better adjective in the future surveys.

- **Consistency of gaze data and selection:** Reliability of the responses can be confirmed in cases where positive correlations are observed. However, negative correlations do not indicate bad reliability.

Table 2.4: Correlation results for adjectives based on durations

	Correlation Value	$p < .05$	t
strong	0.37	0.0059	2.8694
speedy	0.23	0.0905	1.7248
comfortable	0.42	0.0014	3.3837
aesthetic	0.32	0.0202	2.3966
usual	0.41	0.0023	3.2022
aggressive	0.44	0.0010	3.4863
compact	0.43	0.0013	3.4115
modern	0.25	0.0708	1.8447
charismatic	0.47	0.0003	3.8656
cute	0.08	0.5898	0.5425

Table 2.4 shows the correlation results for the adjectives. According to the results, the correlations for *speedy, modern,* and *cute* are found insignificant as the *p*-values are higher than 0.05, which means the gaze data for them are random relative to the selections. Therefore, nothing can be claimed about them. On the other hand, remaining adjectives have weak positive correlations (0.32-0.47). Considering the noisy data that make the correlations weak, it still validates that the adjectives are perceived by the subjects and they find the adjectives suitable to match with the hulls.

Several correlation analyses are also conducted based on the time to first fixation (TTFF) metric, which indicate the time spent before the subjects' first attention for a target AOI. The analyses are made for the adjective selections to inquire their relations with each adjective's AOIs and with local design parameters. However, significant correlations are not found, which means that subjects do not have specific parameter targets related to the adjectives to search in the first place, but they examine the designs until finding meaningful reasons for their choices. On the other hand, the relation between TTFF and RTD metrics of local design parameters is also checked and find interestingly significant correlations for R_4 ($cor = 0.40; p \leq 0.05; t = 3.1890$), R_0^m ($cor = 0.33; p \leq 0.05; t = 2.5578$), FP ($cor = 0.52; p \leq 0.05; t = 4.3646$) and a_1 ($cor = 0.28; p \leq 0.05; t = 2.0723$) (see Table 2.5). The existence of the correlation between RTD and TTFF for the parameters is also represented by graphs in Fig. 2.21 with relation equations and R^2 values (represents how much variance is covered by the equation). Although it cannot be claimed that they are more significant than the other parameters based on these results, it is apparent that they require special attention in the design process.

Table 2.5: Correlation values between TTFF and RTD metrics of local design parameters

	Correlation Value	p < .05	t
R_1^m	-0.19	0.1678	-1.3989
R_4	0.40	0.0024	3.1890
R_5	0.00	0.9864	0.0171
R_0^m	0.33	0.0135	2.5578
FP	0.52	0.0001	4.3646
H	-0.19	0.1757	-1.3729
a_1	0.28	0.0432	2.0723
D_2^e	-0.10	0.4850	-0.7034
D_2^m	0.17	0.2315	1.2106
B^e	-0.15	0.2756	-1.1020
B^m	-0.01	0.9149	-0.1074
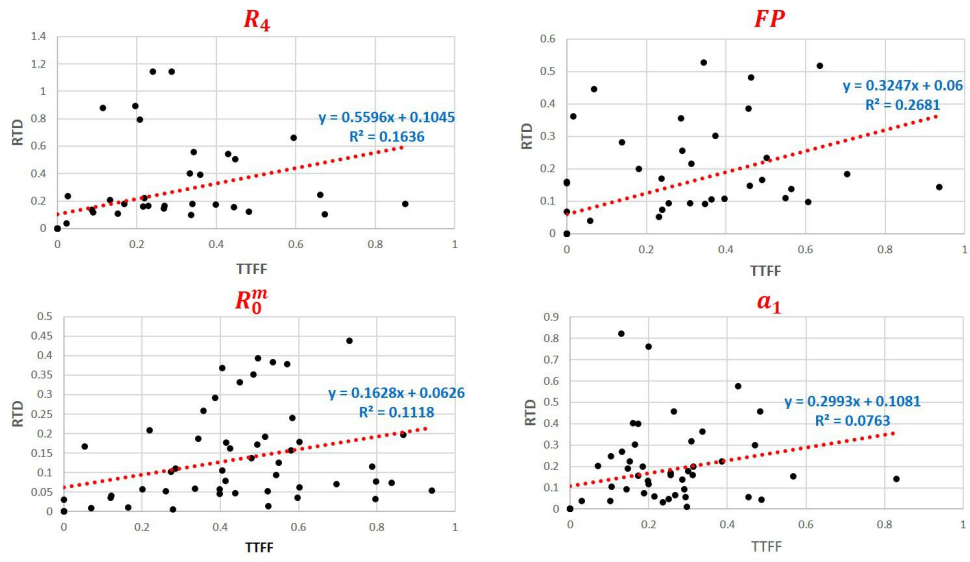
Figure 2.21: TTFF versus RTD of R_4, R_0^m, FP and $a1$.

2.6 Conclusion and Discussion

In this study, the adjective-based design concept is used, where hulls are parameterized and the adjectives are related to the designs at the parametric level. This provides relatively more detailed examination compared to the studies conducted with appearance features of designs, which are obtained by a combination of varied values of relevant design parameters. As the design elements are correlated to the targets at the parametric level, such approach provides flexibility and more control on sampling designs that meet the targets, specifically after the outcomes of this perception study are integrated into the design concept. However, working with the design parameters requires more attention as different dimension values and various combinations of the design parameters can be interpreted differently by subjects. Therefore, the Taguchi experimental method is also used to sample models, where each design parameter value is shown to be able to cover various features equivalently in the same number of times.

TLS is first proposed, which is used to classify the global design parameters based on search behavior of the subjects. One output of TLS is a *template*, which conveys the required information about AOI definitions based on search areas of the relevant design parameters. An ETAS method was then utilized to collect gaze data, which were evaluated via RTD and transition probability metrics. The evaluations were conducted in three parts: rough examination (section based and view based), fine examination (design parameters), and finally, regression analysis. Rough examinations indicated the most attractive section as middle-body section and view as side view. Such results can be used by designers to decrease labor times working only on the attractive areas. Fine examinations were first used to determine attractive parameters in four levels for local parameters and priorities for the global parameters interpreting a box plot. The determined attractive parameters for fine examination results were then used in the regression analysis to validate that attractive parameters are really useful for the adjective-based design concept.

GLM with the best-subset selection method was used to find regression models for each adjective depending on some performance measures (D^2 to measure explained variance ratio and MAPE for accuracy check) and best-subset $\hat{X}$ determination criteria (RSS and AIC). In addition, correlation analyses were conducted to confirm and measure levels of relations. The results proved the existence of correlation between gaze data and adjective choices, even though the performance measures were relatively low compared to the predictive models. However, our aim was not to get predictive models but to show the relations. Social science is complicated to study, since the human understanding is difficult to estimate and this problem is getting even more complex with the unclear and varied targets. 54 yacht hulls are studied, which are generated by 26 design

parameters, and developed 26 targets from our viewpoint; however, there are even more targets for the subjects as a hull design has many more design details that can be detected. Moreover, they are asked to match 10 adjectives with 54 hulls having all the design details, which makes the problem even harder, since the decision-making mechanism is also developed and changed by seeing various hull models and unstable decisions (noises) are observed besides the useful data. Moreover, they are not designers, who change their decision criteria for no tangible reasons. This has also been proved by Kukkonen [54], where gaze data correlations with the goals were very low for the subjects who were not designers, and very high for designers. After all of this, despite the weakness of the performance measures compared to the predictive models, significant results are found that validate the attractiveness of the design parameters determined by the gaze metrics. Specifically, the related design parameters with an adjective, which are the variables of a relevant subset, should have priorities to get desired adjective-based design among all attractive design parameters. Designers can generate many solutions only using these parameters, preferably combining with a generative design software, without making redundant modifications by the irrelevant parameters, which may cause problems for engineering design, cost and time. In other words, this study lets designers to narrow down the space of solutions getting rid of infeasible sub regions in terms of aesthetic. After that, the product-related requirements can be considered for filtering out the undesired design options. In this study, a yacht hull was used, in which the hydrodynamic and hydrostatic performances are crucial. As such performance properties in addition to aesthetic properties are important, the aesthetics are handled first to be then combined with a performance-based system, which is considered as future work.

Chapter 3

A Generative Sampling System for Profile Designs with Shape Constraints and User Evaluation

3.1 Introduction

A sampling approach is proposed for deriving profiles of an existing product design using profile similarities and primitive shapes, such as circles, triangles, and ellipses, as constraints. A common approach for a designer is to generate or collect sketches to create a design space. The design space can be explored to retrieve the samples directly based on requirements or crossing over them to obtain new design variations. In this stage, the proposed method can be used to derive a large number of samples from a design image to work with. First, the user clicks on the image to define each design feature as cubic Bézier curve segment. The primitive shapes are then constructed for each segment and used as constraints, such that adjacent triangles are not allowed to be flipped onto each other to prevent loop and cusp at the segments, sides of internal points respect to the circle diameter is used to prevent inflections, and control points are not allowed to cross the ellipse boundary to limit their excessive modifications. Moreover, the design similarities are computed using the triangles based on their anisotropy ratios, which are measures of the deformation between corresponding triangles and which are used to ensure that they are highly related samples in the example design. Modified Hausdorff distances are also computed between the control points of the samples. There is diversity provided that these distances are large enough. A customized sampling algorithm that fulfills our constraints is executed several times synchronously via parallel programming to create a design space. Finally, the user-specified number of distinct samples is retrieved from the design space by minimizing the Audze-Eglais potential energy. We provide an additional tool with which the users can adjust the weights for each control point to guide the sampling process and record the chosen samples. The main goal of this study is to generate samples, which are diverse but still convey the key features of the supplied shape. Using the settings related to similarity, a designer can derive samples sticking to their initial idea to explore its better version or more creative results that they could not imagine on their own. The proposed system offers simplicity automating every step that must be done by the user. Thus even inexperienced users without needing any programming skill can vary shapes defined using a set of points in a matter of seconds, and experienced users can even focus on specific shape features weighting them without dealing any constraint or rule definition requirements. Besides, the proposed system allows partial modifications, in which users can select a specific region to modify while the rest of the shape maintains the original appearance and functionality of the exemplary design.

3.1.1 Generative Design Methods

Although the definition of generative design can vary depending on the context, it can be generalized as generating new design samples using computer power. Various *generative design methods* [82, 83, 84, 85, 86] are evolved to support design process with different design requirements such as those from manufacturing, conceptual design, architecture, engineering and construction that raised throughout the years.

This study focuses on the design aesthetics at the conceptual stage, which has become an essential part of product design. To realize a target design, the designers must first generate or collect various design samples mostly as 2D sketches and images, which are used to develop their ideas. However, such ideas are not easily shaped and each of them may require serious amount of time. In addition, the solutions generated by designers are often limited due to the inadequacy of their imagination, preconceptions and personal preferences.

Generative systems are useful solutions to be able to generate many unbiased design samples efficiently. Various generative design methods for aesthetic design have been proposed so far. Notwithstanding, we found these methods are not usually preferred by designers, who find sketching on paper easier than meeting the requirements of generative methods. In order to help designers, their requirements must be well understood. In the next subsection we discuss such requirements which we take into consideration in our approach proposed in this chapter.

3.1.2 Requirements for Generative Aesthetic Design Methods

In this subsection, we discuss requirements considered in this study for generative design methods.

In generative design methods, an object to be designed is usually represented by a set of design elements, and variant samples are generated by changing these design elements. A region that covers the set of all such samples is called the design space of the object, and it also includes creative samples beyond the designers' imagination.

The space is first limited to the samples by defining the lower and upper bounds of each dimension [30]. Then, a sampling process is applied to obtain feasible samples from the bounded space. This is achieved by searching the samples that satisfy the physical constraints and using a predefined objective criterion integrated into the search algorithm. Ultimately, the designers choose one sample as the solution and use it directly as the concept or as an idea to shape their concepts.

However, owing to the difficulty in creating such a constrained and bounded design space, designers cannot make full use of generative design methods to achieve aesthetic results. Thus, generative methods often use a very limited number of design parameters to search for new ex-

ternal appearance. The searches use basic features such as length, height and width [87, 31], which require additional work and designer expertise to define. It is required to minimize user involvement automatizing the parameterization, constraining and bounding operations as much as possible to allow for more parameter definitions.

Besides, currently available methods are mostly problem specific, so users need to define new rules by themselves, or even need to manipulate source codes of sampling algorithms to make them appropriate for their different problems [88]. This is not convenient for those who want to use generative system to create quick ideas for conceptual design stage. Thus it is also required that the generative system should be able to handle various type of designs with the built in problem solutions.

In addition, designers often have to deal with the limitation of "design to fit an existing environment" (*DFEE*) [37] in which the product must fit to the existing facility to avoid extra equipment and assembly costs, in case of upgrading a given design. If new designs are obtained over the existing models to get new outer appearance, larger modifications are refrained due to the limitation of existing production lines. Therefore, the system should also allow the modifications to be within specific portions of the product keeping the rest as possible as original, but with remarkable aesthetic impacts to achieve both generating new appearances and maintaining suitability to the existing environment. However, most of the current studies are aimed to explore only novel shapes ignoring this requirement.

3.1.3 Objectives

In this study, the main goal is to develop a tool to generate various distinct samples from a single exemplar to extend the design options in an easy way while remaining faithful to the exemplar. In our tool, the design of a target product is represented by its profile curve, which is defined using composite Bézier curves with control points. Each of the control points is a design parameter and can be used to generate new samples. Figure 3.1 shows car design samples generated by manipulating the control points of a profile curve.

For a given original profile D_{org} we can generate various sample profiles D by changing the control points of D_{org}. All of these samples form a *design space* centered at D_{org}. Our aim is to obtain a set of such samples $\Omega = \{D_j\}$ in the design space. However, simply changing the control points does not always produce good samples. For instance, a sample profile may look very different from D_{org}, or two samples may be very similar. Further, we also wish to avoid curves with inflections, cusps or loops. Our objective is to generate a sample set Ω such that:

- It consists of distinct samples covering a sufficient range of the design space (*diversity*).

- The samples are not far from D_{org} (*similarity*).

- It does not include inappropriate samples (*regularity*).

Our method is designed to be general enough to deal with various product profiles by using a composite Bézier curve to define them. Besides, the constraints which are needed to generate desired samples are represented also by using the control points of the curve. Therefore, the constraints are not dependent on any specific profiles. They are geometrical constraints on circles, triangles and ellipses defined by the control points.
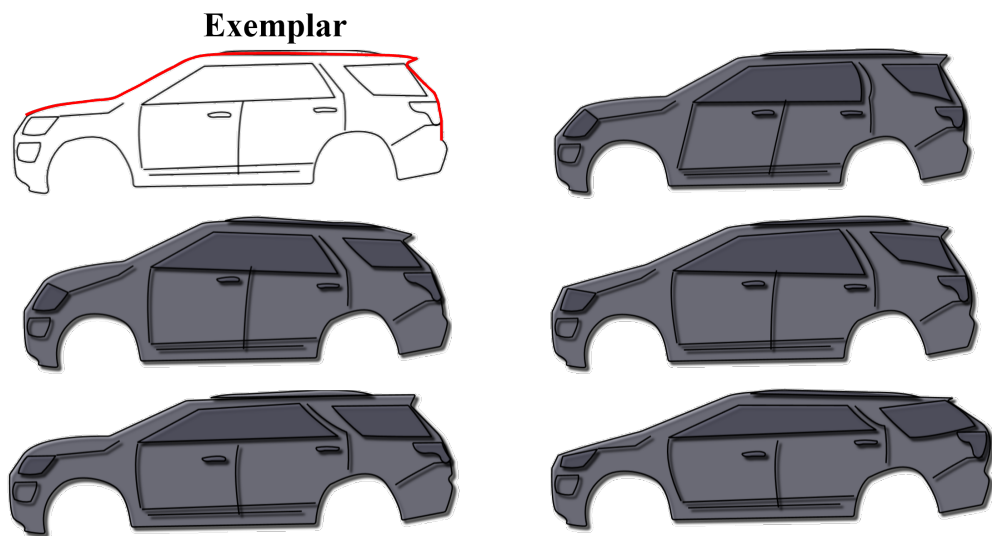
Figure 3.1: Generated samples from an exemplar. The modified part is indicated by red.

3.1.4 Overview of the Proposed Concept

Figure 3.2 draws a general method flow, which is explained step by step as follows:

- **Model definition**

  Initially, a profile curve is defined with user-provided points as composite Bézier curve (Section 3.3.1) (Fig. 3.2a).

- **Condition Extraction and Constraint Construction**

  In the stage depicted by Fig. 3.2b, the profile curve is first analyzed to determine the continuity conditions between the curve segments of the composite curve. These are used as

rules when generating new profiles. Moreover, the segments of the composite curve are categorized based on the degree of Bézier curve (Section 3.3.2) and the concavity properties, which are also maintained in all samples generated for each segment.

The constraints are geometrically constructed as circles, triangles and ellipses using the control points of the profile curve (Section 3.4.1). Finally, user-provided similarity thresholds are used to define a region in the design space, in which the target samples are possibly existing.

- **Sample Generation**

  Figure 3.2c indicates the final stage where samples are produced modifying the exemplar profile (Section 3.3.3). The extracted conditions are used here to preserve basic shape features maintaining the relevant curve degree and continuity conditions between segments in the generated samples. Afterward, two types of constraints are checked by the sampling algorithm to accept or reject a generated sample: regularity (Section 3.4.1.2) and similarity (Section 3.4.1.3). These constraints are converted into energy functions and the sampling algorithm (Section 3.4.2) iterates the modification process to reduce total energy (Section 3.4.1.4) and find the samples without failures within the defined region in the space. To increase efficiency while a larger design space is created, the algorithm is synchronously executed using parallel programming. After that, users are able to retrieve samples as many as they need from the pool. This can be done manually by the user simply picking desired ones or using a provided button to retrieve diverse samples from the pool based on the Audze-Eglais potential energy [38].

To handle these steps, we also developed a tool in which everything is automatically handled, but users only provide points and adjust the sampling settings such as similarity thresholds based on their needs. Thus, our tool is flexible and can easily be used by inexperienced users. Starting with a sketch of the product profile, it generates new designs. The system has the following features:

- The constraints can be visualized.

- Specific parts of a design can be chosen for modification, and the rest of the design is kept as close as possible to the original.

- Control points can be dragged to allow the user to implement the final touches.
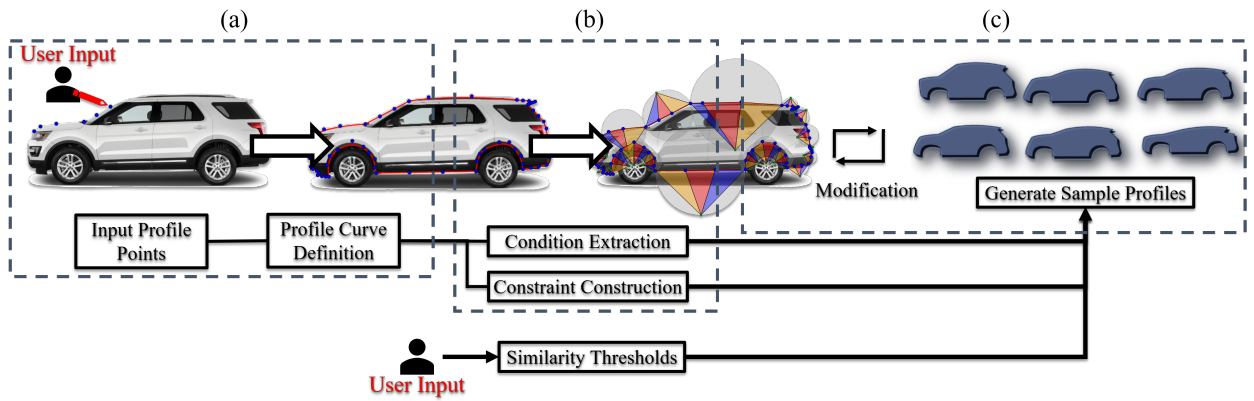
Figure 3.2: (a) The profile curve is defined as composite Bézier curve with user-provided points over the input shape. (b) Constraints are constructed using the curve's control points and conditions that are continuities at the joints of the segments, curve degrees, and concavity properties are extracted. (c) Samples are produced by modifying the profile curve and the sampling algorithm finds the ones within the bounds specified by user-provided similarity thresholds satisfying the conditions and constraints.

The system has an easy-to-use interface. A user can guide the sampling process by adjusting the modification weights for each control point. Moreover, the user can select or reject samples and modify samples before accepting them.

The control points of the selected samples are finally exported to a computer aided design (CAD) tool for further embodiment of the design.

This chapter is organized as follows. Related works are described and compared with the proposed method in Section 3.2. Section 3.3 shows how a product profile is represented and introduces our method for generating new profile samples. The sampling algorithm and constraints are explained in Section 3.4. The proposed tool is introduced in Section 4.1, and Section 3.5 shows the results of this study.

3.2 Related Works

In this section, generative design methods from different fields are first introduced, and their disadvantages for the conceptual design stage comparing to our approach are then explained.

3.2.1 Generative Design

3.2.1.1 Parametric modeling

As a basic definition, generative design means using computer power to generate many design alternatives, which can be hard to imagine or create manually. In parametric modeling generative studies, a single parameterized CAD model is treated as input in general, and new samples are generated changing the defined parameter within bounds and under constraints. Gunpinar and Gunpinar [30] proposed a generative sampling approach that works with defined constraints. Khan and Gunpinar [87] suggested a teaching-learning-based optimization method for product sampling. First, unconstrained space is used to learn user preferences, and the constrained space is then created using the preferences as constraints. Krish [31] proposed a generative CAD tool that explores creative designs by randomly sampling from a bounded design space. His tool can communicate with external CAD systems to create 3D models. An approximate filter is used to create distinctive designs and to narrow down the number of presented solutions. This tool also relies on the external CAD tool systems to filter out infeasible designs. Khan and Awan [32] introduced a space-filling generative design method to create novel samples from a given CAD model.

3.2.1.2 Generative design for manufacturing

Performance driven studies also use generative design concept for manufacturing. Autodesk [89] proposed a generative design tool whose input parameters are the manufacturing methods, cost, size, weight, and material to explore design variations that are presented to the user, who can select a solution based on criteria such as low cost, light-weight, and high durability. Other tools with similar inputs can also generate and optimize designs for additive manufacturing [90, 91]. Kazi et al. [92] proposed a tool called *DreamSketch* in which users are able to sketch their models and the system generates optimal 3D models modifying the design variables. Users can also check model properties such as volume, weight, and stress while they are navigating the results. However, since the generated 3D models are topologically optimized, generating a single solution takes a long time specifically to reach high-quality results even with fewer design variables. Dhokia et al. [93] proposed a method for additive manufacturing that was inspired by termite behavior to generate

structurally optimized and production-ready designs. Shea et al. [94] also incorporated graph-based geometrical modeling in a design system based on structural optimization called *eifForm*. It produces designs using performance criteria so that the models generated are ready for designers to use.

3.2.1.3 Shape grammar

A special design language called a shape grammar was introduced by Stiny [85]. It aids designers when they are generating unique designs. Pugliese and Cagan [95] introduced a 2D shape grammar for generating motorcycles and demonstrated it by encoding a brand-new model. Orsborn et al. [96] used a shape grammar to generate new vehicle designs by crossing different models based on defined rules and parametric ranges. Hsiao et al. [97] merged a semantic approach with a shape grammar. Agarwall and Cagan [98] proposed a shape grammar for coffee makers. Agarwall et al. [99] presented a way to involve designers in the early stages, by selecting rules based on the production costs of coffee makers.

3.2.1.4 Evolutionary computation

Evolutionary computation has been proposed to solve complicated computational problems, such as for subjective human decisions in product design. The method is usually an iterative process that runs until terminated by the user or predetermined criteria are met. Xu et al. [100] developed a crossover operator to generate new 3D models synthesizing parts of a set of designs and used preference scores of users to evaluate fitness of the evolved models. Lee et al. [101] proposed a shape-grammar-based methodology in which generative methods are used together with evolutionary computation to produce creative design solutions. O'Neill et al. [102] suggested using a grammar with evolutionary computation, and they demonstrated their method by designing a shelter. Kielarova et al. [103] proposed an interactive generative system in which a shape grammar is combined with an evolutionary algorithm. They demonstrated the methodology by designing jewelry. Guoyan et al. [104] combined a constraint-based design methodology with an interactive genetic algorithm to explore optimal solutions. Yannou et al. [105] proposed a sketching tool to create car designs using genetic algorithms. In their study, users interactively evaluate an existing set of car shapes. This genetic approach considers the user preferences for the models, and the output designs are often surprising. They used similarity tests to show that the output designs are innovative. Cluzel et al. [106] developed a similar approach. Kelly et al. [107] used an interactive genetic methodology with an initial design population to aid designers in being creative.

3.2.1.5 Data-driven methods

This section covers some generative methods whose common point is their need for data, which can be collection of user preferences, set of designs, or both together. Unlike the evolutionary computation, the researches under this title usually do not require collecting user preferences interactively to evolve a fitness function, but the data is often collected with offline procedures.

Chen and Fuge [108] proposed a data-driven sampling method, in which given data set of initial designs with implicit constraints are used to exploit the decision boundary exploring feasible regions in an unbounded space efficiently. Kalogerakis et al. [33] suggested a probabilistic shape synthesis method in which the components of various shapes are combined to generate new models. In the study of Xie et al. [109], users are asked to provide 2D strokes of parts that will be retrieved from existing data set and combined to suggest new models. Averkiou et al. [110] proposed a method where collection of design models are parameterized to synthesize new designs. Alhashim et al.[111] introduced a generative algorithm that uses a topology-varying 3D shape blending method to produce new samples.

There are numerous semantic based methods where designs are represented with adjectives to make them more understandable even by non-experts. Furthermore, since the adjectives are usually learned using crowd sources, such approaches are considered being human-oriented and makes easier the expression of target designs for users. Chaudhuri et al. [23] studied on an assembly-based model where attribute strength of each assembly part for different categories (e.g. head, tail and leg of a creature) is determined using crowd-sourcing. The parts are then assembled in real time based on user preferences about the adjectives with their strength using an easy to use interface. Yumer et al. [112] proposed also a semantic based design exploration, but in this study a given shape is deformed to produce a new one rather than combining existing assembly parts. They also used crowd-sourcing to learn and relate adjectives with design geometries. The relations are used to create a continues color-coded 2D map, where the colors refer to attribute strength. Users are provided an interface to obtain samples that meet available attributes with desired strength. Dang et al. [113] also collected preference scores to learn probability density functions for shape grammars and used them to generate new models that reflect the preferences as much as possible.

Neural networks are utilized in various generative concepts such as indoor scene synthesizing [114], generation of styling images varying human pose, texture and shape for fashion [115, 116], and interactive procedural model sketching for urban modeling [117]. Li et al. [118] offered an encoder for 3D shapes using neural networks, and generated new designs synthesizing the encoded

shape structures. Zhu et al. [119] also made use of an auto-encoder network to creatively compose shapes. Sinha et al. [120] used deep neural networks to reconstruct 3D shape surface from a single image and generate samples utilizing interpolation between two surfaces. Nash and Williams [121] suggested a variational auto-encoder method, in which 3D shape samples are synthesized from part-segmented input models. Tan et al. [34] also took advantage of variational encoders to generate new deformable models from 3D homogeneous mesh models. Huang et al. [122] suggested a probabilistic generative model that is learned via deep neural network. Liu et al. [123] utilized generative adversarial network (GAN) to produce 3D voxel based realistic models and they supported their system with a simple interface, which allows interactive editing a voxel grid. Smith and Meger [124] also used GAN with variational auto-encoders to reconstruct 3D shapes from 2D images and interpolation to produce models between different objects.

3.2.2 Advantages of the Proposed Method over the Existing Methods

This section briefly summarizes disadvantages of the generative studies to be used for the conceptual design comparing with our proposal. All generative methods explained so far have great contributions and are milestones for the generative design field. However, each of them is developed to solve different problems than ours or have drawbacks that detract designers from using them. This study aimed to remove barriers between designers and generative design concept so that anyone without needing any experience about CAD systems or statistical knowledge can produce conceptual designs using computer power. Moreover, designer expertise related to constraint definitions, and collecting or creating samples to be an initial data set are also not needed to use our tool. On the other hand, our claim is not the ability of generating samples that the others cannot create. We believe that all can generate various useful samples that inspire users under optimal conditions according to their requirements. However, the question is how much effort and devotion can be expected from the users, specifically those who are responsible to create conceptual designs before the model prototyping and gaining functionality to the final 3D models.

Our system requires only an image of an example product and some mouse clicks. The product profile is first defined with composite Bézier curves, whose segments are then constrained automatically and the control points are the design parameters. A user does not need considerable design skills to get started, even for complex shapes. The input exemplar can be prepared in the design system, and the design space can be controlled with clear settings, such as similarity, which can be understood by anyone. Moreover, modifications can be weighted to ensure that the designs created include or exclude desired shape features. The tool can populate a drawn 2D sketch, but

it is also easily able to convert a revolvable or closed 2D sketch into 3D owing to communication with the Rhino/Grasshopper [125]. The provided tool is also able to visualize constraints and variations, user evaluation and repetitively execute the sampling algorithm to reach a large number of samples in seconds.

The parametric modeling studies (Section 3.2.1.1) are the most relevant to our study among others in terms of objectives and sampling methods. However, they need a parameterized model, which is not always available and hard to create for non-experts. The parameters and their interactions also need to be bounded and constrained, which require expertise and higher labor than our approach. Such initialization is a heavy burden for the users and hard to expect from them in the early stages of the modeling, during which conceptual ideas are developed. Also, these requirements impair their usability for complex shapes since the number of parameters that need to be defined, bounded and constrained also increases. In our method, design parameters are selected automatically from the provided points, constraint definitions are not expected from the users and bounding as simple as defining only two similarity thresholds.

The generative design for manufacturing methods (Section 3.2.1.2) often use heavy optimization processes that take a long time without given explicit control for aesthetics but with the basic functionality such as durability and weight. Despite the possibility of finding an aesthetically plausible design among many generated samples, it is getting harder if the input shape is complex as an even longer time required to create a sample set that includes both functional and aesthetic designs. The design aesthetic is still mostly obtained with pencil and paper to realize their ideas as quickly as possible without deeply concerning about the functions. Thus, our method is more applicable to the conceptual design stage, in which many design ideas are quickly generated to inspire designers. Nevertheless, in the conceptual design stage, the functionality can be considered with the best possible estimations made by experienced designers observing existing shapes' functionality. Therefore, we believe that it would be helpful for the experts if some functionality can be queried from the strokes of a sketch to narrow down the design space. We keep it as a future work where users will be able to define and use functional constraints to make their decisions.

The usage of shape grammars (Section 3.2.1.3) for product design requires a considerable amount of expertise and time for creating a sample set and defining grammars with their rules, if they are not already available. Although the aesthetics can be controlled during the design stage, they are still somewhat limited in terms of variations since the grammars are usually extracted from man-made shapes.

Evolutionary computational methods (Section 3.2.1.4) are useful to generate samples in the direction of user preferences; however, these methods suffer from human fatigue problems despite

several attempts to reduce it [126, 127, 128]. Furthermore, to produce targeted design suggestions, the parent population should include sufficient design variations, which may not always be easily provided. Such necessity about the creation of the population makes this method less practical comparing with our method, which needs only a single input. However, since aesthetic is a subjective phenomenon, considering user evaluations during the sampling is sometimes important to meet the targets. Hence, we provide an additional interface in our tool in order to integrate user preferences with the sampling procedures (see Figure 4.6). This interface creates a population with the desired number of samples allowing users to adjust the modifications by weighting the control points, evaluate the generated samples to accept or reject, and collect scores to further analyze with an statistical software. However, the current version of the tool cannot evolve a fitness function like the evolutionary methods; thus, the weights must be assigned manually or found statistically based on the evaluations using an external tool.

Data-driven methods (Section 3.2.1.5) are widely preferred due to satisfactory results and usually come up with easy to use interfaces for non-experts to achieve their targets. However, their main drawback is that a new problem needs a new data set, which is not always available or easy to create due to specific input requirements such as being part-based [23, 118, 121] or deformable mesh models [34]. In addition, due to dependency on the diversity of the input models, the output variations are directly affected such that the generated samples may not meet the targets. The attribute-based researches [23, 112] are also very limited because they depend on the small number of subjective attributes that are learned via crowd-sourcing. If the available data, such as attributes and input models, is not enough to solve a user's problem, the preparation of new suitable data requires some knowledge about data collection and interpretation. Such requirements to set up a problem detract those who already refuse using CAD environments to speed up their work.

As an overview, the introduced methods usually require an initial design set with suitable models and variations, grammar definition, or crowd-sourcing. Although all of them can define a design space, such requirements could not be expected from the users in practice. On the other hand, the parametric modeling requires only a single model like our method; nonetheless, the design space definition is difficult due to all the bounding and constraining definitions. We eliminate these disadvantages proposing a method, in which a single 2D image is enough and the design space definition is remarkably simpler as we handle the constraining and bounding operations using automatically defined fan polygons and similarity measures. Thanks to such easiness of the method, the input can be replaced or modified quickly in case the outcomes do not satisfy the users. Overall, our method is quick in generating product designs for the conceptual design stage comparing to the all other works starting from the input preparation to the obtaining results.

3.3 Profile Curve Definition

In this research, a product design is represented by a profile curve, as shown in Fig. 3.3a. The profile curve is defined by a composite curve D composed of n cubic Bézier curve segments $s^i, i = 0, \ldots, n - 1$. We assume that each segment of the composite Bézier curve is without inflection points. Each segment i consists of four control points represented by $\Gamma^i = \left\{ P_0^i, Q_0^i, Q_1^i, P_1^i \right\}$, where P_0^i and P_1^i are the two end points and Q_0^i and Q_1^i are internal control points. The segments satisfy C^0 continuity, that is, $P_1^i = P_0^{i+1}$ for $i = 0, \ldots, n - 2$. Therefore, n is determined as "$(N - 1)/3$" if N is the number of input points and there should be at least four points for each shape feature to define a segment on it. A design system is developed to make this step easier (Section 4.1.1). Note that when the composite curve is closed, $P_1^{n-1} = P_0^0$ must also be satisfied.

We use the following notation throughout this chapter:

- AB is a segment with two ends A and B. In general, $P_0 P_1 \ldots P_{N-1}$ is a polygon with N points P_0 to P_{N-1}.

- $\overrightarrow{AB}$ is a vector from A to B. $\|\overrightarrow{AB}\|$ is the norm of $\overrightarrow{AB}$.

- $\overline{AB}$ is an infinite line passing through A and B.

3.3.1 Original Profile

The original profile curve D_{org} is generated using our own curve editing system (Figure 4.2), or it can be imported from a CAD system.

D_{org} is used as a reference. Various profile curves are generated by modifying its control points. There are nominally $4n$ control points $\left(P_0^i, Q_0^i, Q_1^i, P_1^i \right)$, $i = 0, \ldots, n - 1$, but the end points of adjacent segments s^i and s^{i+1} are equivalent, that is, P_1^i is equivalent to P_0^{i+1}. A new profile curve is obtained by manipulating the $3n$ control points $\left(Q_0^i, Q_1^i, P_1^i \right)$ of segments $s^i, i = 0, \ldots, n - 1$ as shown in Fig. 3.3b.

3.3.2 Reducing the Number of Control Points

We constrain some of the internal control points to be dependent on others. In other words, these dependent internal control points can be computed from other control points. In this way, we can reduce the number of control points, which reduces the degrees of freedom of the design space.
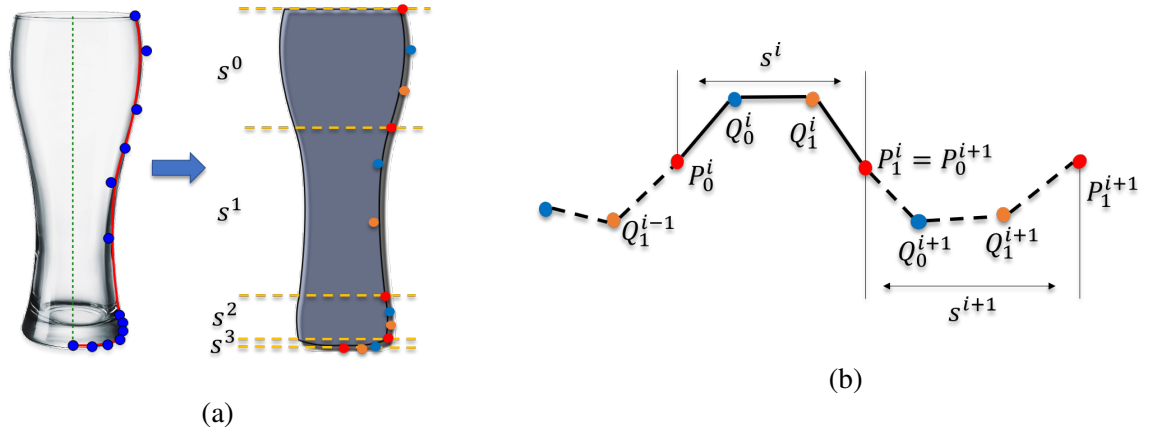
Figure 3.3: (a) Profile curve of a glass example (b) s^i and its control points.

In the following sub sections, the Bézier curve segments are classified into three types based on the tangency condition with the adjacent segment. For each of the types, the dependency of some of the internal control points is defined. These are the conditions of the proposed approach, where the generated samples are derived from an exemplar and should carry the shape features of it to preserve initial ideas in some level that might be related to aesthetics and functionality. Therefore, if a segment is defined as linear, or either a corner or continuity is existing between adjacent segments, such conditions are extracted from the defined profile curve in the beginning and maintained throughout the sampling process while a new sample is generated.

3.3.2.1 Linear segments

If the four control points, P_0^i, Q_0^i, Q_1^i and P_1^i, are collinear (Fig. 3.4a), the segment s^i is a linear segment. The internal control points Q_0^i and Q_1^i are computed using the following equations from the two end control points P_0^i and P_1^i.

$$Q_0^i = (2 \times P_0^i + P_1^i)/3 \tag{3.1a}$$

$$Q_1^i = (P_0^i + 2 \times P_1^i)/3 \tag{3.1b}$$

A linear segment has one independent control point P_1^i. The two internal control points Q_0^i and Q_1^i, are dependent on it. Note that P_0^i is a control point of the previous segment s^{i-1}.

3.3.2.2 Cubic segment

We check the tangent continuity between adjacent segments s^i and s^{i+1}. If $\overrightarrow{Q_1^i P_1^i} \parallel \overrightarrow{P_0^{i+1} Q_0^{i+1}}$, they are tangent continuous at their junction and the end point P_1^i is said to be a *tangent*; otherwise, it

is a *corner*.

If the end control point P_1^i is a tangent, as shown in Fig. 3.4b, the segment s^i is cubic. This tangency must be retained by each modified sample. For a cubic segment, the internal control point Q_1^i satisfies the C^1 condition:

$$Q_1^i = P_1^i + \overrightarrow{Q_0^{i+1} P_1^i} \tag{3.2a}$$

Thus, a cubic segment has two independent control points, Q_0^i and P_1^i.

G^1 and C^1 continuities are often used for styling [28, 129] and considered enough in this thesis for the aesthetic design represented by simple forms. The higher continuities require higher degree curves to work with, thus the problem is getting more complicated. Furthermore, since G^1 has an extra freedom at one direction of the relevant point, C^1 is selected over G^1 to further simplify the problem. Such simplifications are made for users, to let them guide the sampling processes by weight modifications that will be explained later. Complicated requirements in profile definition would make difficult to follow sampling procedures for them.

3.3.2.3 Quadratic segment

If the end control point P_1^i is a corner as shown in Fig. 3.4c, s^i is quadratic. For such a segment, since we do not have to consider the tangency with the adjacent segments, we do not need both internal control points, and we can merge them to form a new internal control point Q_2^i, which is computed from P_0^i, Q_0^i, Q_1^i and P_1^i.

Q_2^i is an independent control point of s^i. Thus, s^i has two independent control points, Q_2^i and P_1^i. The internal control points Q_0^i and Q_1^i are computed using

$$Q_0^i = \left(2 \times Q_2^i + P_0^i\right)/3 \tag{3.3a}$$
$$Q_1^i = \left(2 \times Q_2^i + P_1^i\right)/3 \tag{3.3b}$$

3.3.3 Generating a New Profile

New profile samples are generated by modifying D_{org}. When the original profile D_{org} is modified to be a sample profile D_{new}, each segment $\hat{s}^i$ of D_{org} is modified to become s^i of D_{new}. We write the control points of $\hat{s}^i$ as $\hat{\Gamma}^i = \left\{\hat{P}_0^i, \hat{Q}_0^i, \hat{Q}_1^i, \hat{P}_1^i\right\}$.
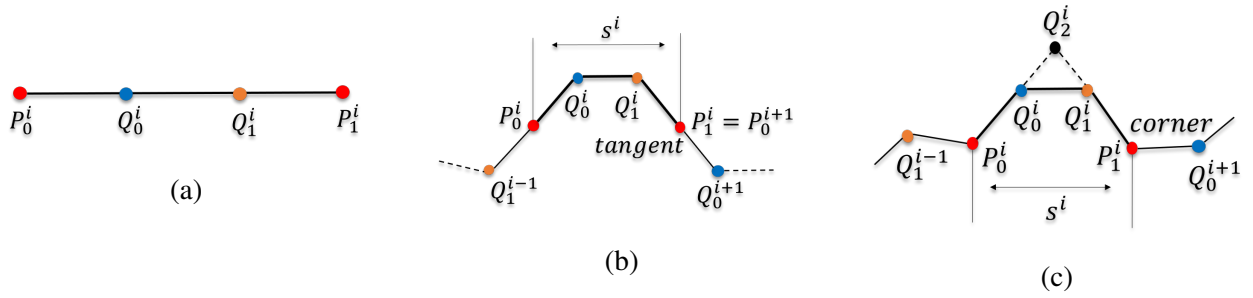
Figure 3.4: (a) Linear segment where internal points are always on the line. (b) s^i is a cubic segment if tangent at P_1^i. (c) s^i is a quadratic segment if P_1^i is a corner.

The modification is achieved via a two-pass algorithm. In the first pass, D_{org} is modified by adding a displacement $\Delta(w)$ to all of the independent control points. The dependent control points are then computed in the second pass to generate a new profile D_{new}. $\Delta(w)$ is defined as follows:

$$\Delta(w) = diag(w_x, w_y)\vec{r} \tag{3.4}$$

where $\vec{r}$ is a random vector with length $d_{min} \leq \left\|\vec{r}\right\| < d_{max}$. Note that the randomness is provided for each point separately. That is, the length and direction of $\vec{r}$ are different for each independent point. Therefore, all independent control points in $\hat{\Gamma}^i$ are modified as

$$\Gamma_j^i = \hat{\Gamma}_j^i + \Delta(w) \times \frac{l}{l_{max}} \tag{3.5}$$

where l is the length of s^i computed as Euclidean distance between P_0^i and P_1^i, and l_{max} is the maximum length among all segments. See also Fig. 3.5 for illustration of the segment modification.

The weights $w = (w_x, w_y)$ are assigned for each independent control point separately by the user:

- to fix some control points by assigning $w_x = w_y = 0$, and

- to adjust the modification amount.

By default, the weights w_x and w_y are set to 1. The usage of weights are explained in Chapter 4 under Section 4.1.2.2 in detail, but for this chapter default value is used for all weights.

Note that, if the profile curve is closed, since $P_1^{n-1} = P_0^0$ needs to be satisfied, P_1^{n-1} is a dependent control point and is not modified.

Users are also allowed to partially modify the curve by selecting a range $[s^{first}, s^{last}]$, where s^{first} is the first segment and s^{last} is the last segment of a sequence that will be modified. Note that, s^{first} does not necessarily refer to segment s^0 unless the user sets the *first* as 0 (*first* = 0); and s^{last} is not same with s^{n-1}, unless user sets it as *last* = $n - 1$. The segments out of the range are preserved to maintain the original appearance of the product profile at these unmodified parts.
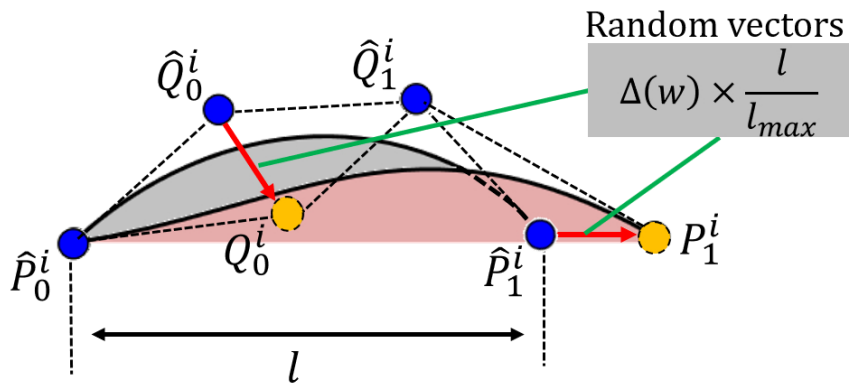
Figure 3.5: Modification of a segment using Equation 3.5 where $\hat{\Gamma}^i = \left\{\hat{P}_0^i, \hat{Q}_0^i, \hat{Q}_1^i, \hat{P}_1^i\right\}$, $\Gamma^i = \left\{P_0^i, Q_0^i, Q_1^i, P_1^i\right\}$ and $\Delta(w)$ is random for both $\hat{Q}_0^i$ and $\hat{P}_1^i$.

3.4   Sampling Methods

3.4.1   Constraints and Similarity

As mentioned in Section 3.1.3, to generate a sample set with diversity, similarity, and regularity, heuristic constraints on various features of the sample profiles are used. The design space includes both feasible and infeasible regions [108] where a feasible region covers the samples that satisfy the objectives. Similarity and violations of each segment constraint are converted to constraint energy computed as a difference between two states of a sample that are the state at that moment and the closest state that does not have the relevant failure. For example, if a sample is not dissimilar enough that does not satisfy the diversity objective, similarity energy is computed by subtracting the sample's current similarity value from a threshold that is minimum required dissimilarity value between the samples (see Equation 3.7). The sum of all energies is assumed as a distance of the sample to the closest feasible region in the design space. Thus, the total energy is then used to determine if a new sample D_{new} can be accepted as a member of the set of samples Ω.

We tested various kinds of features, and proposed those introduced in this section.

To capture the characteristic of a Bézier curve segment, we introduce a *fan polygon* defined by the four control points of Γ^i and one extra point. Γ^i is used to evaluate the distance between two segments.

In the following, several functions are defined to compute constraint energies with the fan polygon and the control points.

We use the ramp function $\mathcal{R}(x) \equiv \max(x, 0)$ to define constraint energies.

3.4.1.1   Fan polygon and fan triangles

We first construct a circle for the segment s^i (Fig. 3.9a). The diameter $P_0^i P_1^i$ is between the two end control points of s^i. The top point of s^i, P_T^i, is defined as the midpoint of the semi circle on the opposite side to Q_0^i and Q_1^i (see Fig. 3.9b). If Q_0^i and Q_1^i are on the diameter, either side of the diameter line for P_T^i has equal distance to these internal points. Therefore, any side can be selected since it does not make any difference for the segment, and it is selected to be a point outside of the profile for clear visualization. A *fan polygon* is an octagon $P_T^i P_0^i Q_0^i Q_1^i P_1^i$. It is also a composition of three *fan triangles* $FT^i = \left(T_1^i, T_2^i, T_3^i \right)$ where $T_1^i = P_T^i P_0^i Q_0^i$, $T_2^i = P_T^i Q_0^i Q_1^i$ and $T_3^i = P_T^i Q_1^i P_1^i$. Figure 3.11 depicts some profiles overlaid with circles and fan triangles.

3.4.1.2 Segment constraint energies

This section explains how to constrain segments to get rid of the cusp, loop, and inflection from the generated profiles using fan polygons. In addition, an ellipse with user-specified size is used to limit the movement area of the internal points so that user has control on the modifications before the samples are generated. Finally, one more constraint is defined for symmetric shapes to prevent overlapping of symmetric parts onto each other.

Note that, the constraints are defined to prevent possible failures considering various product profiles. That is to say, some introduced constraints may not be required for some profiles. For example, inflection must be prevented for a yacht hull profile (see Fig. 3.7); on the other hand, the inflection may not need to be discarded for bottle or glass profiles. Similarly, the ellipse boundary constraint is defined to let users control modifications of internal points for the case they need to be further bounded. In this chapter we define and use all constraints together in the sampling algorithm as default to show how they work; however, border constraint energy and inverting energy defined below could be disabled through software proposed in Chapter 4.

Flipping Constraint Energy This energy is used to penalize the flipping of control points to prevent a curve segment from being twisted (see Fig. 3.6). We compute the (signed) apex angles α_1^i, α_2^i and α_3^i at P_T^i for fan triangles T_1^i, T_2^i and T_3^i for each s^i. They are measured in the clockwise direction (Fig. 3.9c).

A negative angle indicates that a control point has flipped. Therefore, if an apex angle is negative, we take its absolute value as its energy. By summing the absolute values of the negative angles for all of the curve segments of D, the flipping constraint energy (E_{flip}) of D is obtained as

$$E_{flip} = \sum_{i=0}^{n-1} \left(C_{flip}(\alpha_1^i) + C_{flip}(\alpha_2^i) + C_{flip}(\alpha_3^i) \right)$$

where $C_{flip}(\alpha) = \mathcal{R}(-\alpha)$.

Inverting Constraint Energy To constrain each segment $\hat{s}^i$ of D_{org} from inverting its convex direction (Fig. 3.7), we use a penalty on the internal control points to ensure that they are on the same side (right or left) of the diameter $\hat{P}_0^i \hat{P}_1^i$ (Fig. 3.9b). For instance, if $\hat{Q}_0^i$ is on the right-hand side of the diameter $\hat{\delta} \equiv \overline{\hat{P}_0^i \hat{P}_1^i}$ in $\hat{s}^i$ and moves to Q_0^i in s^i on the left-hand side of the diameter $\delta \equiv \overline{P_0^i P_1^i}$, then it violates the constraint. We use the cross product $\chi_\delta(P)$ of $\overrightarrow{P_0^i P_1^i}$ and $\overrightarrow{P_0^i P}$ to judge the side of P with respect to the line δ where $\chi_\delta(P) < 0$ refers one side while $\chi_\delta(P) > 0$ refers to another side, and $\chi_\delta(P) = 0$ when P is on the line. Then, the
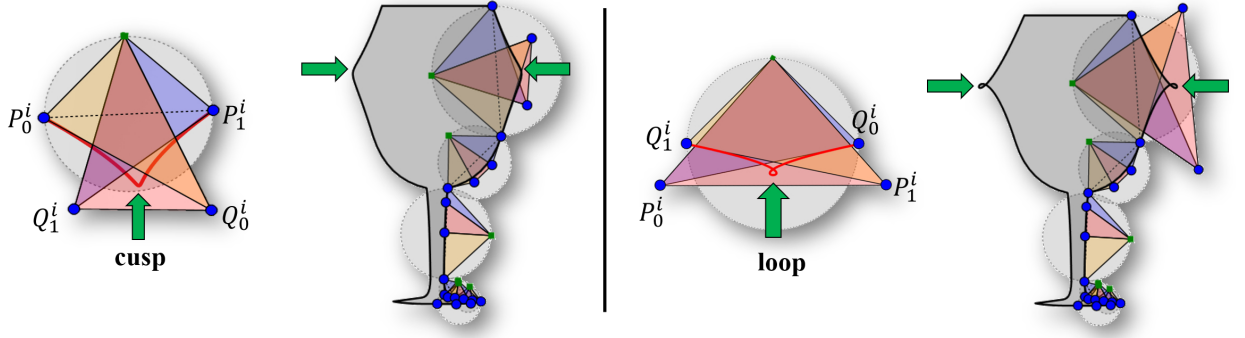
Figure 3.6: Flipping of triangles causes cusp (on the left) and loop (on the right).

condition that $\hat{Q}_0^i$ and Q_0^i are on the same side can be written as $sgn(\chi_{\hat{\delta}}(\hat{Q}_0^i)) = sgn(\chi_\delta(Q_0^i))$, where sgn is the signum function. Therefore, the inverting constraint energy (E_{invert}) is

$$E_{invert} = \sum_{i=0}^{n-1} \left(C_{invert}(Q_0^i) + C_{invert}(Q_1^i) \right)$$

where $C_{invert}(P) = \mathcal{R}(-\sigma\,|\chi_\delta(P)|)$ for an arbitrary point P with $\sigma = sgn\left(\chi_{\hat{\delta}}(\hat{P})\chi_\delta(P)\right)$.
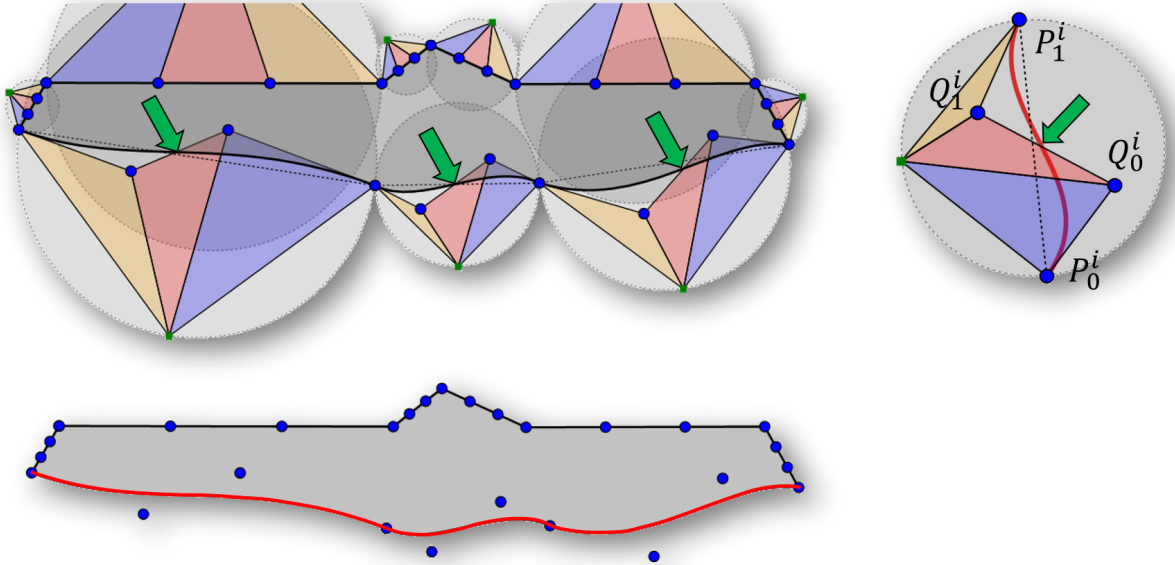
Figure 3.7: Unwanted undulations occur if the inverting constraint is violated.

Border Constraint Energy To avoid large modifications to the control points, we define for each segment s^i a half elliptic region from P_0^i to P_1^i opposite to P_T^i (Fig. 3.9d) in which the internal control points Q_0^i and Q_1^i must exist. This region has the same center as the segment's circle defined above. Its minor axis is the circle's radius R, and its major axis is ψR, where ψ can

be set by the user. We set the default value of ψ to be the golden ratio (1.618), since it mostly gives aesthetically pleasant proportions. The energy for violating this constraint E_{border} is:

$$E_{border} = \sum_{i=0}^{n-1} \left(C_{border}(Q_0^i, f^i) + C_{border}(Q_1^i, f^i) \right)$$

where C_{border} is defined with the equation of the relevant ellipse $f(P) - 1 = 0$ for an arbitrary point P. That is $C_{border}(P, f) = \mathcal{R}(f(P) - 1)$.

Symmetry-Axis Constraint Energy If the profile curve is mirror symmetric with respect to a center line, only one half of the shape is drawn, modified, and then mirrored to get the whole. The profile (the control polygon) should not intersect the center line (Fig. 3.8). The energy for the control points crossing the center line γ is

$$E_{sym} = \sum_{i=0}^{n-1} \left(C_{sym}(P_0^i) + C_{sym}(Q_0^i) + C_{sym}(Q_1^i) + C_{sym}(P_1^i) \right)$$

where $C_{sym}(P) = \mathcal{R}\left(-\sigma \left| \chi_\gamma(P) \right|\right)$ with $\sigma = sgn\left(\chi_{\hat{\gamma}}(\hat{P})\chi_\gamma(P)\right)$ for an arbitrary point P. If the profile is not symmetric, the constraint is not checked, and $E_{sym} = 0$.
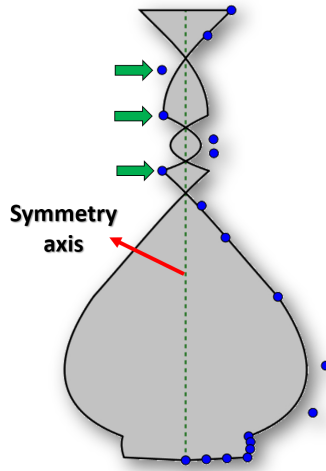
Figure 3.8: Symmetric shape failure due to intersection of some control points with the symmetry axis.

3.4.1.3   Shape similarity energy

Shape similarities are constrained using anisotropy and distances between the control points of the profiles. Anisotropy is used to ensure that the generated samples are not too dissimilar than the

Figure 3.9: (a) Construction of a fan polygon for s^i with a circle and three fan triangles. (b) The top point (P_T^i) side is the midpoint of the arc on the side opposite to Q_0^i and Q_1^i. (c) Fan triangle vectors and the angles between them. (d) Internal points Q_0^i and Q_1^i must remain in the blue region.

exemplar, while the control points' distance is used to check if the generated profile is different from all other samples in the set to ensure the diversity.

In the following subsections, the mathematical backgrounds of the similarity metrics are first explained and implemented on some profiles, their effectiveness is then discussed.

Anisotropy Ratio Energy The shape similarity of segments $\hat{s}^i$ of D_{org} and s^i of D_{new} is evaluated by the distortion of fan triangles T_1^i, T_2^i and T_3^i using the Bookstein shape coordinate method [35]. We first compute a *landmark L* for each of the fan triangles T_1^i, T_2^i and T_3^i. Denote a fan triangle as ABC, where C corresponds to the top point P_T^i and A and B correspond to the control points. A is mapped to $A'(0,0)$ in the xy coordinate system, and B is mapped to $B'(1,0)$, which gives a unit baseline on the x-axis. By applying an affine transformation which maps A to A' and B to B', C is mapped to a landmark L whose coordinates are given by

$$L = \frac{1}{\|\overrightarrow{AB}\|} = \begin{pmatrix} \overrightarrow{AB} \cdot \overrightarrow{AC} \\ \overrightarrow{AC} \cdot \overrightarrow{AB}^\perp \end{pmatrix},$$

where $\cdot$ denotes the inner product and $\overrightarrow{AB}^\perp$ is the vector obtained by rotating $\overrightarrow{AB}$ by $90°$ counterclockwise.

The landmarks are used to evaluate the distortion of the fan triangles using log-anisotropy [35, 130]. As shown in Fig. 3.12, landmark $\hat{L}$ is computed for a fan triangle $\hat{T}$ of $\hat{s}^i$ and a landmark L for a fan triangle T of s^i corresponding to $\hat{T}$. The affine transformation mapping a triangle $A\hat{L}B$ to a triangle ALB is easily obtained. The log-anisotropy ρ of $(A\hat{L}B, ALB)$ is

Figure 3.10: Irregular samples generated without applying the segment constraints.

defined as the logarithm of the ratio of the semi-major (β_1) and semi-minor (β_2) axes of an ellipse that is obtained as a result of the applied affine transformation to an imaginary unit circle that is assumed in $\hat{T}$. $\rho = \log(\beta_1/\beta_2))$ is called the log-anisotropy.

The similarity of segments $\hat{s}^i$ and s^i is defined using the log-anisotropies ρ_1^i, ρ_2^i and ρ_3^i, which are defined for $(\hat{T}_1^i, T_1^i)$, $(\hat{T}_2^i, T_2^i)$ and $(\hat{T}_3^i, T_3^i)$ respectively. Therefore, the total shape similarity based on anisotropy is

$$\rho^{total} = \sum_{i=0}^{n-1} \left(\rho_1^i + \rho_2^i + \rho_3^i \right)$$

We constrain the total ρ^{total} over the whole D to be smaller than a threshold θ_{sim}. Thus, the energy for the shape similarity constraint E_{sim} for D_{new} is defined by

$$E_{sim} = \mathcal{R} \left(\rho^{total} - \theta_{sim} \right)$$

Similarity of shape using anisotropy ratio (ρ^{total})

Figure 3.13 compares some simple shapes with the same number of segments to show the detection ability of the shape similarity ρ^{total}. This measure simply compares corresponding segments by removing all transition and rotation differences between the shapes. When such
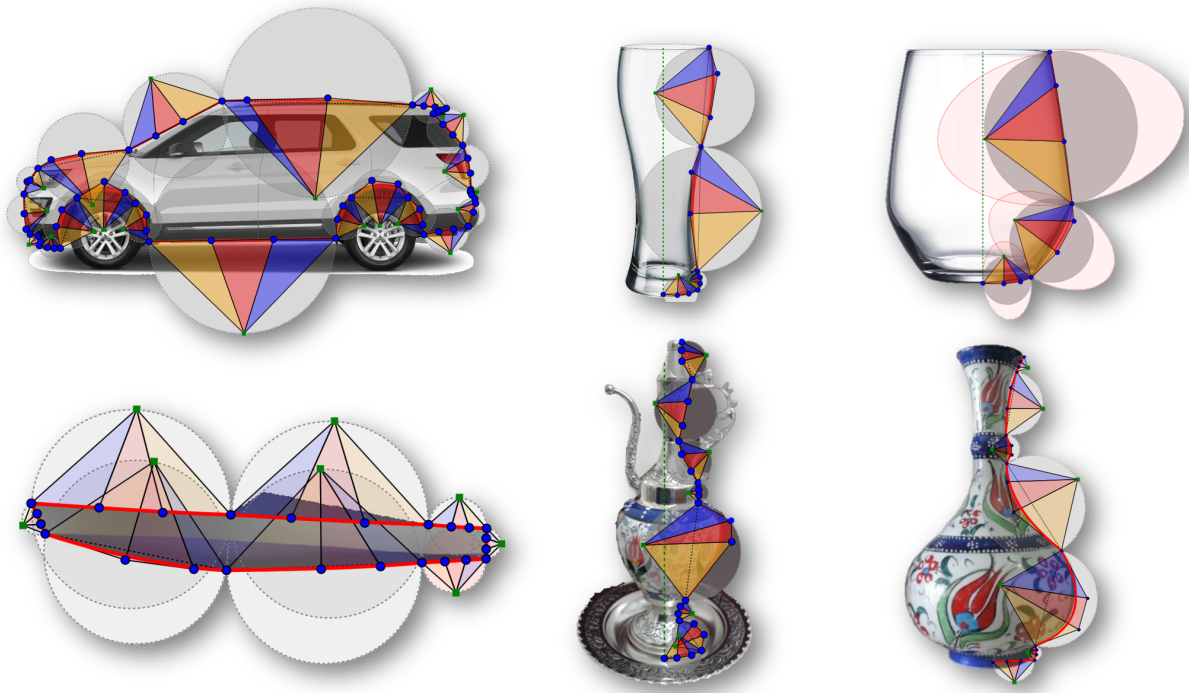
Figure 3.11: Various shapes are visualized via circles and triangles.
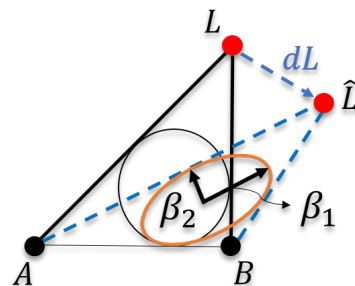
Figure 3.12: Strain deformation between triangles represented via single point.

transformations are applied to linear segments, they will look similar; therefore, line-line correspondences decrease ρ^{total}. On the other hand, a curve-line correspondence increases ρ^{total}, since they are still different after a translation and scaling. For example, compare the rectangular shape with 5, which consists of four straight lines, with the other shapes in Fig. 3.13. ρ^{total} decreases from left to right as the corresponding segments become straight lines.

Modified Hausdorff Distance Modified Hausdorff distance [36] between two point sets is computed as:

$$mhd(A, B) = max\left(d(A, B), d(B, A)\right)$$
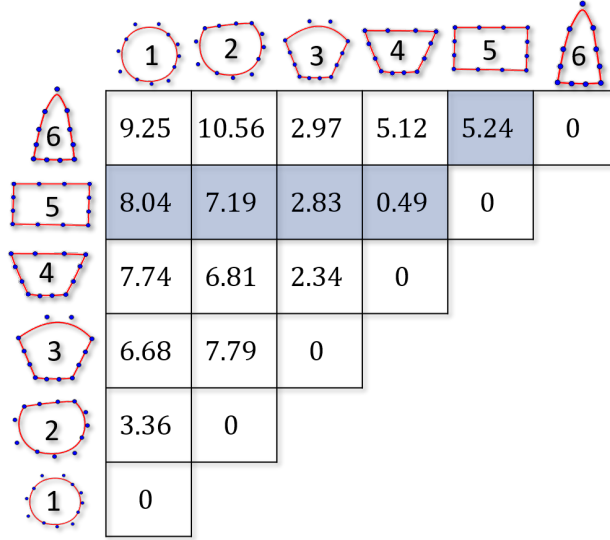
Figure 3.13: Pairwise similarity test for object detection using the ρ^{total}.

where $d(A, B)$ is:

$$d(A, B) = \frac{1}{N_A} \sum_{a \in A} min_{b \in B} \|a - b\|$$

where N_A is the number of points in A and $\|a - b\|$ is Euclidean distance between a and b.

We compute $mhd\left(\Gamma^i, \Gamma'^i\right)$ for the two segments s^i and s'^i. The modified Hausdorff distance between two profiles D and D' represented by $MHD(D, D')$, which is the sum of the mhds of all of the segments $s^i \in D$ and $s'^i \in D'$.

$$MHD(D, D') = \sum_{i=0}^{n-1} mhd\left(\Gamma^i, \Gamma'^i\right) \tag{3.6}$$

Using $MHD(D, D')$, the energy E_{MHD} for D_{new} is

$$E_{MHD} = C_{MHD}(D_{new}, D_{org}) + \sum_{j=1}^{K} C_{MHD}(D_{new}, D_j) \tag{3.7}$$

where $C_{MHD}(D_1, D_2) = \mathcal{R}\left(\theta_{MHD} - MHD(D_1, D_2)\right)$ for any two profiles D_1 and D_2. This is used to define a constraint such that the distance from D_{org} and each of the K samples in $\Omega = \{D_j\}$ must be higher than a threshold θ_{MHD}, as described in the next section. This ensures that D_{new} is different enough for diversity.

Since our proposed algorithm starts sampling from an exemplar profile D_{org}, the samples generated tend to be close to the exemplar. The MHD is used to ensure that variations

exceed the threshold θ_{MHD}. The impact of different θ_{MHD} values is illustrated on the glass, car and ewer profiles shown in Fig. 3.14. The generated profiles overlap at a fixed point indicated in red. In this figure, it can be seen from the scattered profiles that a higher θ_{MHD} increases the diversity.

Effectiveness of similarity constraints

Both *MHD* and ρ^{total} relate to the similarity of the profiles. Six different samples of the glass profile are compared in Fig. 3.15. The larger values indicate more dissimilar designs, which are estimated by both similarity metrics accurately respect to each other. Note that the values are not used to compare the similarity between the samples, since the metrics are computed only against the exemplar.

As it is already discussed, the higher θ_{MHD} lead more modifications on the original profile (Fig. 3.14). Fig. 3.16 shows the impact of θ_{sim} on two sample sets, which are generated under same conditions. According to this figure, using same θ_{MHD} value, which pushes the algorithm to modify the profiles more, lower anisotropy value successfully prevents dissimilar shapes than desired. Therefore, Fig. 3.14 and Fig. 3.16 show that *MHD* and ρ^{total} together are able to define a sampling region in the design space where the generated samples' similarity is controlled by user input thresholds. In other words, the similarity constraints let users explore similar or very dissimilar design alternatives based on their needs.
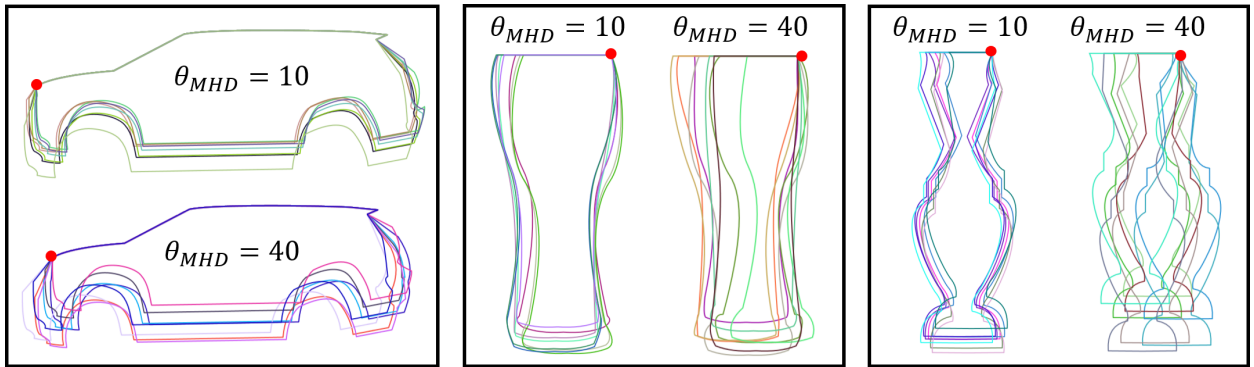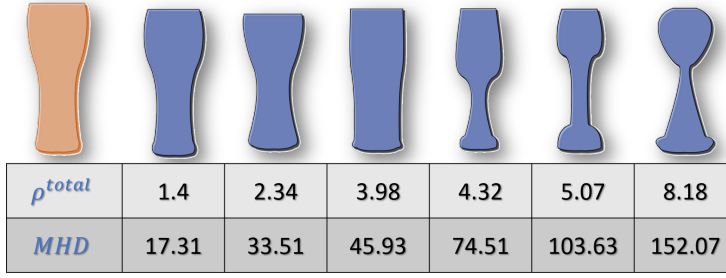
Figure 3.14: Impact of the θ_{MHD} on sample variations is illustrated with car, glass and ewer profile.

3.4.1.4 Total energy

All the defined energy functions are independent of each other; therefore, they have equal importance and must be taken care of individually. However, their sum *total energy* is used in sampling algorithm to monitor their convergence easily. In summary, the total constraining energy that needs to be minimized before adding D_{new} to Ω is

ρ^{total}	1.4	2.34	3.98	4.32	5.07	8.18
MHD	17.31	33.51	45.93	74.51	103.63	152.07

Figure 3.15: Similarity comparison with ρ^{total} and $MHD(D, D_{org})$, where larger values refer to more dissimilar profiles than the D_{org}.
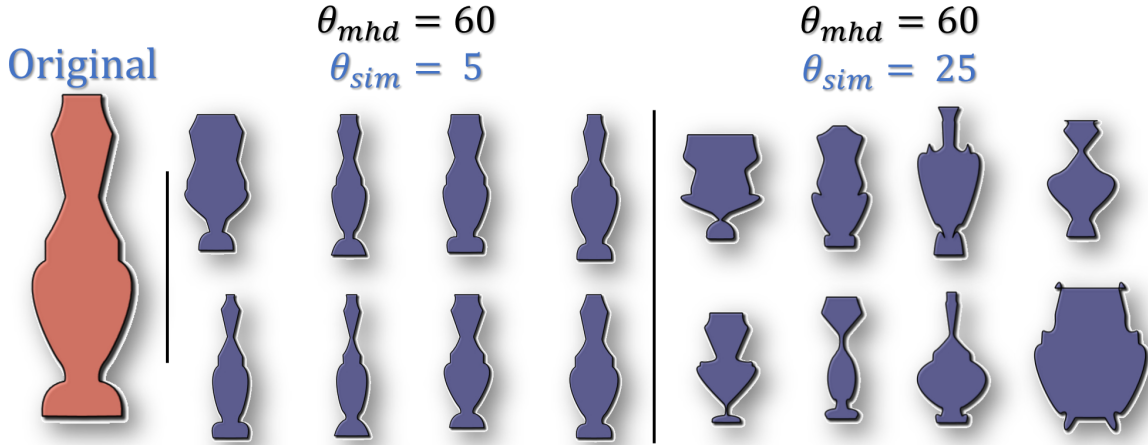
Figure 3.16: Impact of θ_{sim} on two sample sets generated using same θ_{MHD} value.

$$E_{total} = E_{MHD} + E_{sim} + E_{flip} + E_{invert} + E_{border} + E_{sym} \qquad (3.8)$$

3.4.2 Sampling Algorithm

Our sampling algorithm is based on iterated local search [131] and customized to work with the proposed constraining methods, such that D_{new} must satisfy $E_{total} = 0$.

It is composed of two parts: (1) a perturbation is used to generate large modifications of the original shape (D_{org}) to get a D_{new}, and (2) the local search shifts D_{new} within its neighborhood via relatively smaller modifications until it satisfies the stopping criterion $E_{total} = 0$. Both the perturbation and local search use the same modification procedure to generate and move D_{new} (Section 3.3.3). The only difference between the perturbation and the local search is the definition of d_{min} and d_{max} for $\overrightarrow{r}$, which are set to allow larger modifications by the perturbation than the local search, that is, $[d_{min}^{local}, d_{max}^{local}] \subset [d_{min}^{perturbation}, d_{max}^{perturbation}]$. The algorithm uses the following

procedure:

1. Let $\Omega = \varnothing$.

2. Repeat steps $3 - 7$ until M samples have been added to Ω or the maximum allowed time is consumed (time constraint).

3. Repeat step 4 until $E_{total} < \theta_{energy}$, where θ_{energy} is a threshold set to increase the probability of meeting the stopping criteria $E_{total} = 0$ in the local search.

4. Generate D_{new} by modifying the independent control points of D_{org} for the segments in $[s^{first}, s^{last}]$ using Equation 3.5 with $[d_{min}^{perturbation}, d_{max}^{perturbation}]$.

5. Repeat step 6 until $E_{total} = 0$. If it is not finished after η iterations, finish the local search and go to step 2.

6. Move each independent point within segments $[s^{first}, s^{last}]$ of D_{new} using Equation 3.5, with $[d_{min}^{local}, d_{max}^{local}]$.

7. If $E_{total} = 0$, add D_{new} to the sample list Ω.

Figure 3.17 illustrates the computation of E_{MHD} during the sampling procedure as it is formulated in Equation 3.7. According to this figure, if D_{new} is the $(K + 1)$th generated design $((K + 1) \leq M)$, its MHD is compared the D_{org} and with each $D_1, D_2, \ldots, D_K$ that are added to Ω after K iterations. In other words, the algorithm ensures that the current D_{new} is far enough from D_{org} and all samples that have been generated until then. In this way, the computation time is decreased significantly since D_{new} can readily be added to the list and it does not need to be moved again to maintain the distance between samples. This procedure is called chain sampling.

However, the performance of this sampling method in terms of time and quality is very much reduced if poor solutions are generated. These result in a broken chain as they affect the following samples in the chain. Therefore, instead of generating all samples in a single chain, ϕ small chains are synchronously started via parallel programming, where each chain produces sub-sample-lists Ω_n $(n = 1, \ldots, \phi)$ such that $\Omega_n \in \Omega$. Moreover, to stop the chain when a poor sample slows down the sampling, there is a user-defined time constraint. Thus, $\Omega_n \in \Omega$ may have different sizes. Finally, N distinct samples are retrieved from Ω ($\Omega = \bigcup_{n=1}^{\phi} \Omega_n$) by minimizing the Audze-Eglais energy (Equation 3.9) [38]:

$$E^{AE}(L_k) = \sum_{p=1}^{N-1} \sum_{q=p+1}^{N} \frac{1}{\sum_{i=0}^{n-1} \sum_{j=1}^{4} \|\bar{\Gamma}_{p,j}^i - \bar{\Gamma}_{q,j}^i\|^2} \tag{3.9}$$

where $\bar{\Gamma}^i = \left\{ \bar{P}_0^i, \bar{Q}_0^i, \bar{Q}_1^i, \bar{P}_1^i \right\}$ is the set of scaled control points of s^i, and p and q are the sample indexes in the list of N randomly selected samples L_k ($L_k \subseteq \Omega$). If $E^{AE}(L_k) > E^{AE}(L_{k+1})$, then L_{k+1} is better than L_k, where L_{k+1} is obtained by randomly changing one sample in L_k. This procedure is repeated with various combinations until E^{AE} does not get any better. This satisfies the space-filling condition and ensures that the samples are distinct. For more detail and the application to product sampling, refer to [30, 87, 38].
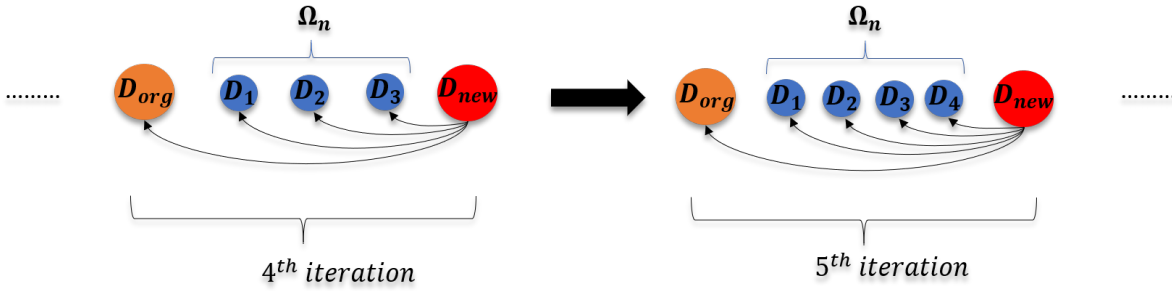
Figure 3.17: Illustration of the fourth and fifth iterations. The *MHD* (Equation 3.7) of the current sample (D_{new}) is compared with those of the original sample (D_{org}), and the samples generated so far ($D_{1,...,K}$). Ω_k grows with the number of iterations.

3.5 Results

3.5.1 Computation Time

The computation times needed to generate samples very much depend on the number of samples in a single chain and the number of parallel threads. Each thread executes a single-chain sampling procedure. An essential requirement for smooth sampling is finding a balance among the size of the search area (determined by $d_{min}^{perturbation}$ and $d_{max}^{perturbation}$), the number of independent control points within $[s^{first}, s^{last}]$, θ_{sim} as an upper bound, and θ_{MHD} as a lower bound. For example, more creativity requires higher θ_{MHD} values, which need more independent control points and higher θ_{sim} values. Note that complex shapes with more degrees of freedom, a wider perturbation range, and larger θ_{MHD}, such as a car profile, will take longer than a simple profile, such as a glass. However, the computation time can be restricted using the time constraint, as explained in Section 3.4.2.

Once all of the settings are defined optimally after several trials, single chain can often produce up to 16 samples in milliseconds. Even when pushing limits of the sampling settings the computation time is usually less than $15s$.

3.5.2 Sampling

In the algorithm described in Section 3.4.2, ϕ sub-sample-lists Ω_n ($n = 1, \ldots, \phi$) are synchronously generated to create the sample list Ω. A random subset $L_k \subseteq \Omega$ with N samples is then searched to minimize the potential energy E^{AE}. Ω is not changed to allow that procedure to be used many times until the user is satisfied with the presented samples. Moreover, parallel computation can be used to start that procedure from different random subsets L_k and the subset with lowest E^{AE} is shown to the user. Although this is not the goal of this study, such approach can be used to catch sufficient space filling property of the sample set when it matters for the user.

3.5.2.1 Variation of samples

The sampling algorithm is used to generate diverse and regular samples from an exemplar profile while the similarity with D_{org} is preserved to some degree. Figure 3.18 shows 8 samples D_j ($j = 1, \ldots, 8$) for each ewer, glass and car profiles that are generated by this algorithm. This figure also depicts *MHD* values of D_j, where the $MHD(D, D_{org})$ indicates the amount of modification of D_{org}, and $MHD(D, D_{closest})$ indicates the distance of each sample from the closest other sample in the set. $MHD(D, D_{closest})$ values are determined by a pairwise *MHD* computation. All samples D_j exceed the defined threshold θ_{MHD}, which means that the desired amount of variation is achieved

and all designs are sufficiently far from each other and D_{org}. A greater variation between the generated samples can be obtained with a higher θ_{MHD}, as illustrated in Fig. 3.14.

Furthermore, it can be observed from the Fig. 3.18 that all produced samples are regular because they satisfy the constraints, and owing to this regularity, 3D models can be successfully generated. Also note that, generally, the sets obtained in the first execution are not the final collection of samples. When the sampling settings are tuned to be optimal for a relevant sample, failed designs are rarely observed. A known constraining problem is also discussed in Section 3.5.3.

Figure 3.20 shows a ceramic vase profile defined using the tool. It was exported to the Grasshopper environment (Fig. 4.11) to get the 3D models. The texture from the original vase was simply extracted and applied to the 3D models to give a similar appearance. Once the 3D model is complete, the user can analyze the cost, appropriate manufacturing method, weight and so on. A first-year undergraduate student with no CAD experience obtained a set of vase samples in less than 5 minutes, running all of these processes by following simple instructions.

Figures 4.23 to 4.25 in Chapter 4 display more examples of using the proposed system.

3.5.2.2 Analysis of sample diversity

To represent a profile D in the design space, a feature vector composed of $3m$ landmarks L (Section 3.4.1.3) is used, where m is the number of modified segments and 3 is the number of fan triangles for each segment. This feature is a visual aid, and the details are out of the scope of this thesis, but one can find the details of the usage of landmarks to represent shapes in other studies [35, 130, 132]. The feature vectors can be plotted using a dimensional reduction method such as the non-linear technique t-SNE [133], which can visualize the samples in a 2D plot. The samples are placed according to probabilistic based similarities while preserving the spatial information in the underlying data.

Figure 3.19 shows three sets of car profile samples represented by feature vectors with their t-SNE plots. These plots are created using Accord.NET Framework [134]. Each set consists of 20 final samples $D_{1,\dots,20}$ retrieved from three different design spaces (three sample lists, Ω). The sample list of the set at top Ω^{top} is created with $\theta_{MHD} = 10$, and for Ω^{middle}, $\theta_{MHD} = 40$, and the rest of the settings are the same. Ω^{top} and Ω^{middle} originally had 400 samples, that are the collection of Ω_n ($n = 1, \dots, \phi$) where each of Ω_n includes 8 samples ϕ is set as 50. The Ω^{bottom} is created with the LHS samples used in the tuning interface (Section 4.1.2.1). Since θ_{MHD} is not applied when creating LHS samples, instead, to obtain Ω^{bottom}, we set d (Section 4.1.2.1) to the $d_{max}^{perturbation}$ value used to create Ω^{top} and Ω^{middle}, which is 15. The Ω^{bottom} was created with 5000 samples, which was

reduced to 357 after the constraints (Section 3.4.1.2) were applied. The generation times of Ω^{top}, Ω^{middle} and Ω^{bottom} were 9.7s, 15s and 47ms in order. The 20 final samples $D_{1,\dots,20}$ were retrieved by minimizing the potential energy E^{AE}, which was 0.406, 0.212, and 0.515 in the same order. A lower E^{AE} indicates that the space-filling ratio is higher and the set has more diversity, which can be also observed in the plots. Of the three sets, the middle has the lowest E^{AE} value, thus the sample diversity is better than the other sets. Furthermore, these are typical results from a first execution. This shows that, using our algorithm with a high θ_{MHD}, more uniform sets are obtained than with a lower θ_{MHD} or constrained *LHS* samples.

Moreover, we defined ranges for $MHD(D, D_{closest})$. The samples in a plot are then colored based on these levels, to make it easier for the user to interpret the minimum distances of the samples D_j.

Side Views   **3D Perspectives**
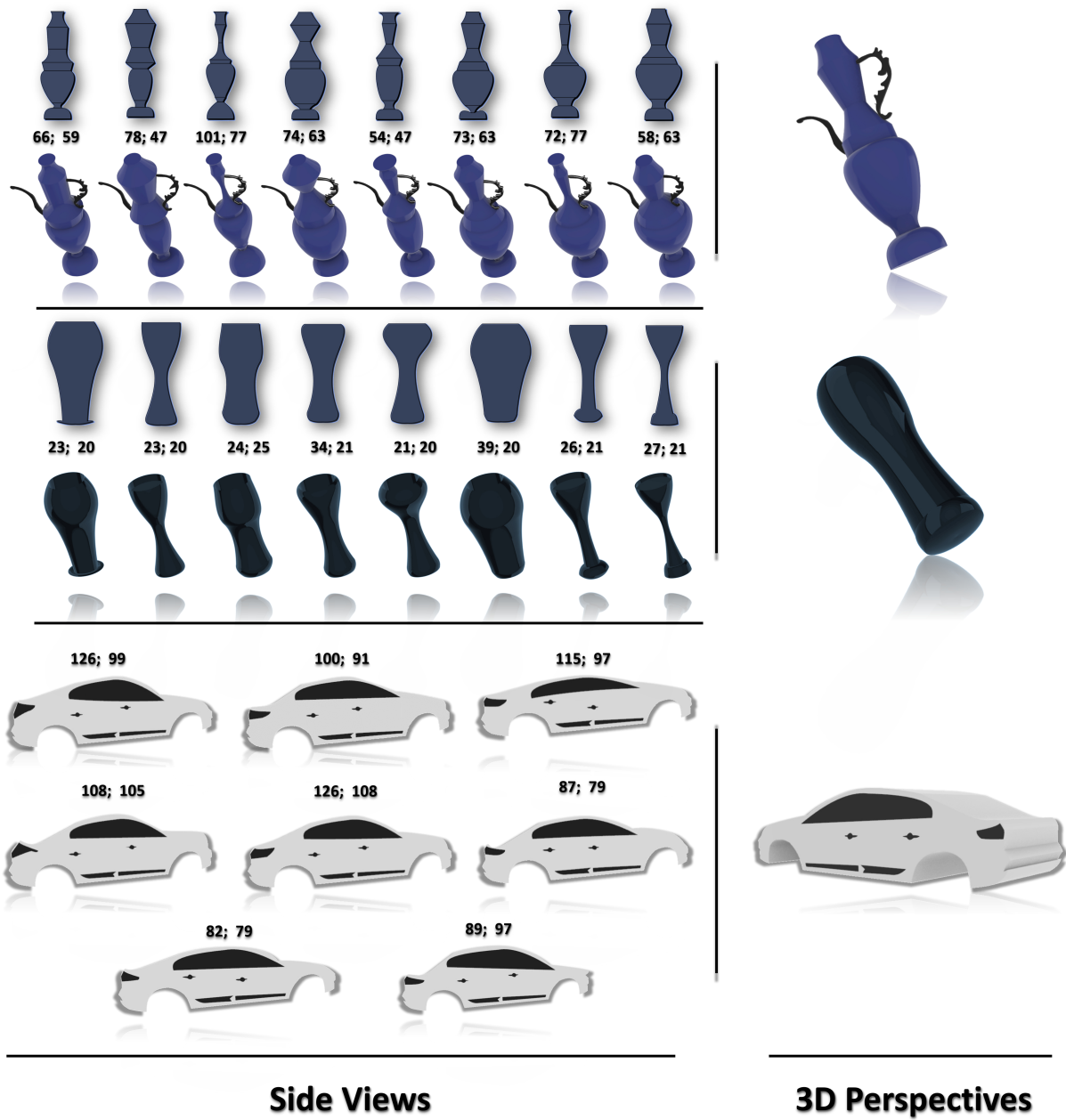
Figure 3.18: Ewer, glass and car profiles are sampled and converted into 3D. $MHD(D, D_{org})$ and $MHD(D, D_{closest})$ are separated by semi-colons.

$$E^{AE} = 0.406 \quad \theta_{MHD}=10 \quad t=9.7\,s$$

$$E^{AE} = 0.212 \quad \theta_{MHD}=40 \quad t=15\,s$$

$$E^{AE} = 0.515 \quad d=15 \quad t=47\,ms$$

Figure 3.19: Three sets of car profile samples are displayed with Audze-Eglais potential energy E^{AE}, *MHD* threshold θ_{MHD} and, t, the time spent in creating sample lists Ω^{top}, Ω^{middle} and Ω^{bottom}. The *t-SNE* plots are also displayed next to each set.

Figure 3.20: 3D samples derived from a ceramic vase with applied texture.

3.5.3 Limitations

In this section some limitations of the proposed approach will be discussed.

3.5.3.1 Similarity evaluation with anisotropy ratio and MHD

ρ^{total} is a coarse similarity measure since it is computed after an affine transformation has been applied to the shapes, which removes all scaling and transition differences between the samples. Therefore, it is not useful to measure the variation between samples D_j from the same product family since the ρ^{total} values are often very close, which makes it hard to control the variation using them. However, it is good in object detection for distinguishing between unrelated designs efficiently. Therefore, we use it to prevent excessive dissimilarities. For a successful application of this measure in object detection, see Felzenszwalb [135].

On the other hand, the *MHD* is sensitive to all modifications made to the independent control points without requiring any transformations. Thus, we use it to ensure that the control points have been modified enough to give distinct design samples. However, its sensitivity can produce large values, that can make comparing the similarity between samples intractable. Therefore, setting the upper bound with *MHD* to prevent the excessive dissimilarity is more difficult than ρ^{total}.

To sum up, to overcome the deficiencies of each other, ρ^{total} is used as insurance to prevent generating abnormal samples while the creativity is pushed by *MHD*.

3.5.3.2 Constraint problems

We observed that, if a segment is too small, the impact of modifications on this segment can be extreme. One example is given in Fig. 3.21. The red point on the left unmodified car is moved up after the modification, which produces overlapping segments. This type of problem can actually easily be handled by checking all possible intersections in the shape; however, this drastically increases the computational time. Instead, the user can handle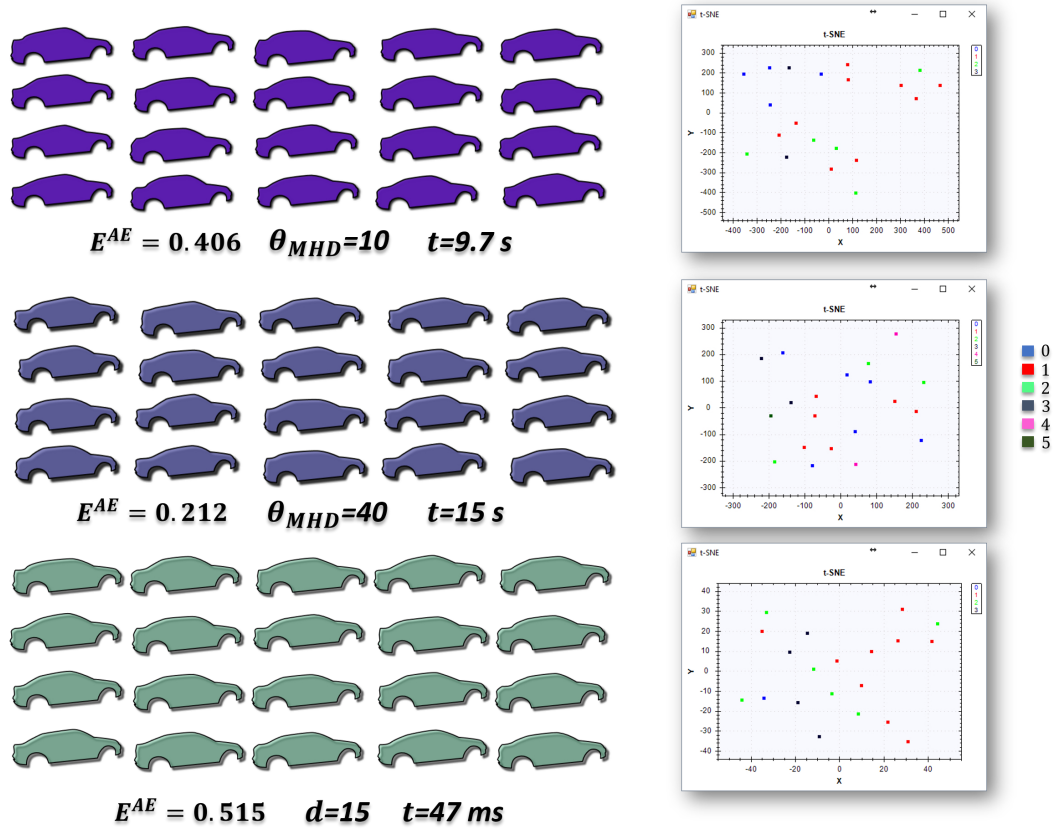 this problem in a few different ways. The first solution is just to reject the failed sample or to correct the point by dragging it manually. As a second option, the weight w (Section 3.3.3) of the relevant control point (the red point in Fig. 3.21) can be reduced or set to zero to prevent this failure. The final option is to put the problematic segment outside the modification range $\left[s^{first}, s^{last} \right]$.
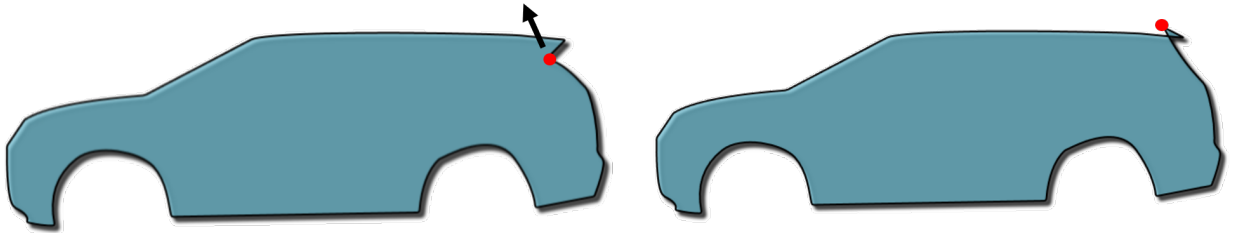
Figure 3.21: Example of a constraint failure.

3.6   Conclusion

Our approach minimizes the effort needed to generate designs, since it requires nothing but control points of cubic Bézier curves. The fan polygons constructed are used in constraints with two main benefits. First, they can be constructed for any cubic Bézier curve; thus, they are applicable to any shape profile created by these cubics. Second, they can be visualized through the interface for the samples generated; therefore, the user can clearly see the defined constraints, which makes the sampling system more manageable. Furthermore, similarity measures ρ^{total} and *MHD* are also defined to bound the design space, rather than the conventional method of bounding each parameter for a shape. The search area can easily be extended by changing parameters such as $d_{max}^{perturbation}$. The samples generated from a 2D profile defined as a composite Bézier curve can be then converted to 3D in an external CAD environment.

The earlier mentioned limitations of the proposed method have been scheduled to be fixed in future studies. Moreover, the applicability of the constraining approach can be extended to handle various unexpected circumstances, such as the problem illustrated in Fig. 3.21.

The proposed method can create a large set of samples using the proposed *Generative Design Software* (Chapter 4), and a subset with desired number of samples are retrieved from the set by minimizing the potential energy or selected by the user one by one. In addition to that, *Sample Management Interface* (Section 4.1.3) can be used to narrow down the generated samples based on user-defined geometric constraints.

Chapter 4

Generative Design Software

4.1 Generative Design Software

The software has been developed using the C# programming language. It has several features to make sampling easy, even for inexperienced users. A typical user flow of the proposed system is given in Fig. 4.1. According to this flow:

- Profile points are provided by mouse clicks on a selected image or importing from an external source using *Design System Interface*.

- Settings are tuned by observing their impacts on the test samples through *Tuning Interface*.

- Samples are generated

    - interactively evaluating them one by one and weighting modifications to guide sampling via *User Evaluation Interface*,

    - or all at a time using *Sampling Interface*.

- The generated samples are exported for 3D visualization,

    - but the samples can also be narrowed down through *Sample Management Interface* defining a geometric constraint before exporting for 3D visualization.

Note that, the system records the initial points and its relevant settings for each design. Therefore, once the points are defined in the system, th samples can be generated directly opening the "Sampling Interface" without needing any other step. The following sections explain these main interfaces in detail.
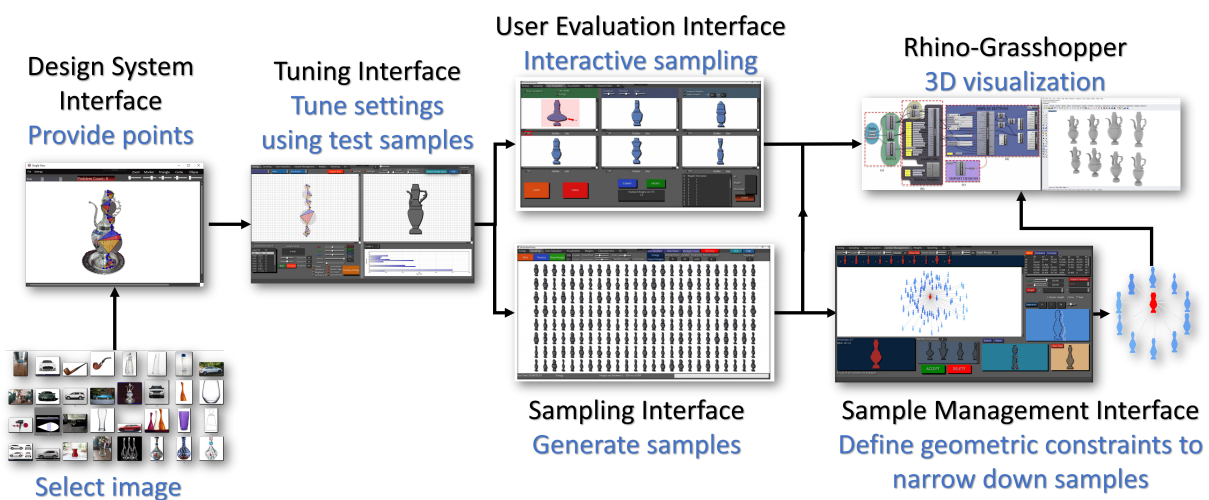

Figure 4.1: A typical user flow of the proposed generative system.

4.1.1 Design System Interface

Figure 4.2 displays the interface that is used to get the control points of a composite Bézier curve of a profile D_{org}. The user can also import control points from a CAD system. The user can import an image of a product and define a curve by clicking control points with a mouse, as shown in this figure. The interface allows dragging and delete operations on points. The fan polygon, which consists of fan triangles FT^i, and the circles are constructed for each segment simultaneously as the points are supplied. This system also checks for constraint violations and displays them by turning the relevant part red, with a warning text block indicating how many constraining rules have been violated.

Furthermore, each of characteristic lines, which are shape details other than the outer profile of the design, can also be provided as composite Bézier curve (Fig. 4.2). These lines are not modified to generate new samples but transformed to be fitted for new generated outer profiles to enhance sketches visually. The transformations are made for each characteristic line maintaining relative positions of them to the closest control points of the outer profile curve.

In addition, Fig. 4.3 shows an additional interface that supports multiple profile definition at the same time for up to 3 different views. This interface is designed for surfaces generated via sweep and network surface methods of Rhino software. The sweep method that we used to generate surface requires two profile curves and at least one cross-section, while the network surface requires at least three profile curves and at least one cross-section. Thus, the top left canvas is reserved for a view with two rails and bottom left one is reserved for another view with two rails so that user can define up to 4 profile curves using them. On the other hand, the top right canvas is reserved for cross-sections. The cross-sections are automatically placed between the profile curve segments' corresponding start and end points in order, so the maximum number of cross-section slots depend on the profile curve with minimum number of segments. Note that, the cross-section is used to control interior shape of the design; thus, a new cross-section is only needed at a point that shape starts to change. If the interior shape is constant, a single cross-section definition will be enough. Finally, the interface have mirroring operations such that it is enough to draw one of the profile curves (e.g. bottom left in Fig. 4.3) if they are symmetrical or half of a profile curve (e.g. top right in Fig. 4.3) if it is symmetrical.

4.1.2 User-Guided Sampling Interfaces

The main sampling process is done automatically by the algorithm described in Section 3.4.2. However, to generate samples that fully reflect the user's intention, we provide a user-guided
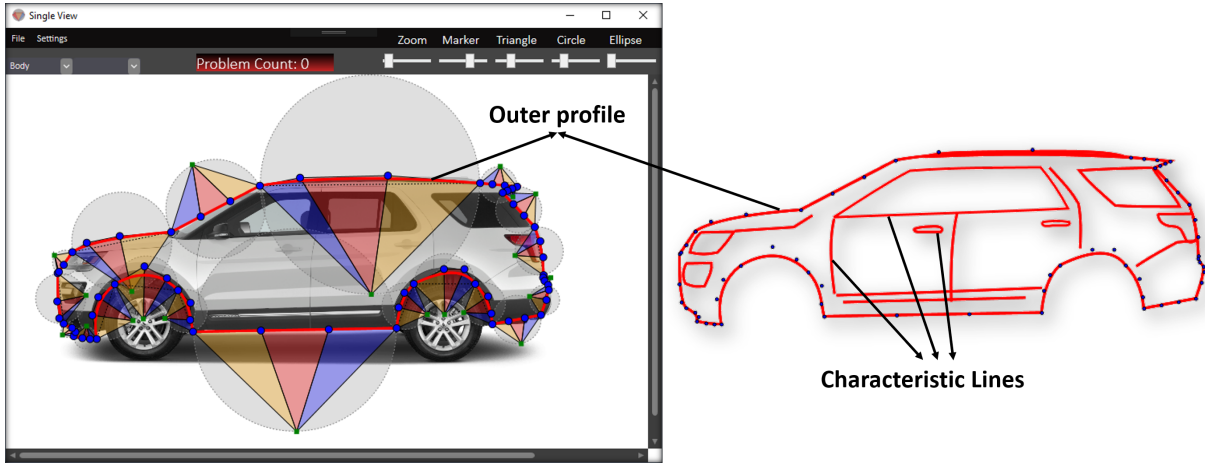
Figure 4.2: The interface for adding points to the outer profile and characteristic lines.

sampling interface. The sampling module consists of three interfaces:

1. Tuning interface

2. User evaluation sampling interface

3. Generative design interface.

4.1.2.1 Tuning interface

In our sampling algorithm, there are some thresholds and parameters. An interactive tuning interface is provided to make setting them easy (Fig. 4.4). First many samples are tentatively generated using a simple method, the space-filling algorithm of Latin hypercube sampling (LHS) [136]. This algorithm manipulates the independent control points of D_{org} by Equation 3.5 to get D_{new}, where $\overrightarrow{r} = d \times lhs$ (Equation 3.4). lhs is also manipulated by the LHS. d is a constant value that can be changed with a slider on the tuning interface to give immediate results. On the basis of these tentative samples, the user can set the sampling parameters, such as the thresholds θ_{MHD}, θ_{sim}, d_{min}^{local}, d_{max}^{local}, $d_{min}^{perturbation}$, and $d_{max}^{perturbation}$. For example, ρ^{total} and $MHD(D, D_{org})$ can be observed for various d values, which helps in choosing the parameters. To generate samples with good variations quickly, optimal parameters values must be selected based on the test samples. For example, if a design is extremely dissimilar, θ_{sim} should be chosen to exclude it. In the same way, if a sample profile D is too similar to D_{org}, then θ_{MHD} must be set higher than $MHD(D, D_{org})$. In addition, d affects how many modifications lie within the extreme values of the d_{min}^{local}, d_{max}^{local}, $d_{min}^{perturbation}$, and $d_{max}^{perturbation}$ and how many designs are eliminated because of constraint violations. Note that, the sampling is hard if few designs survive after they are filtered out because of constraints.
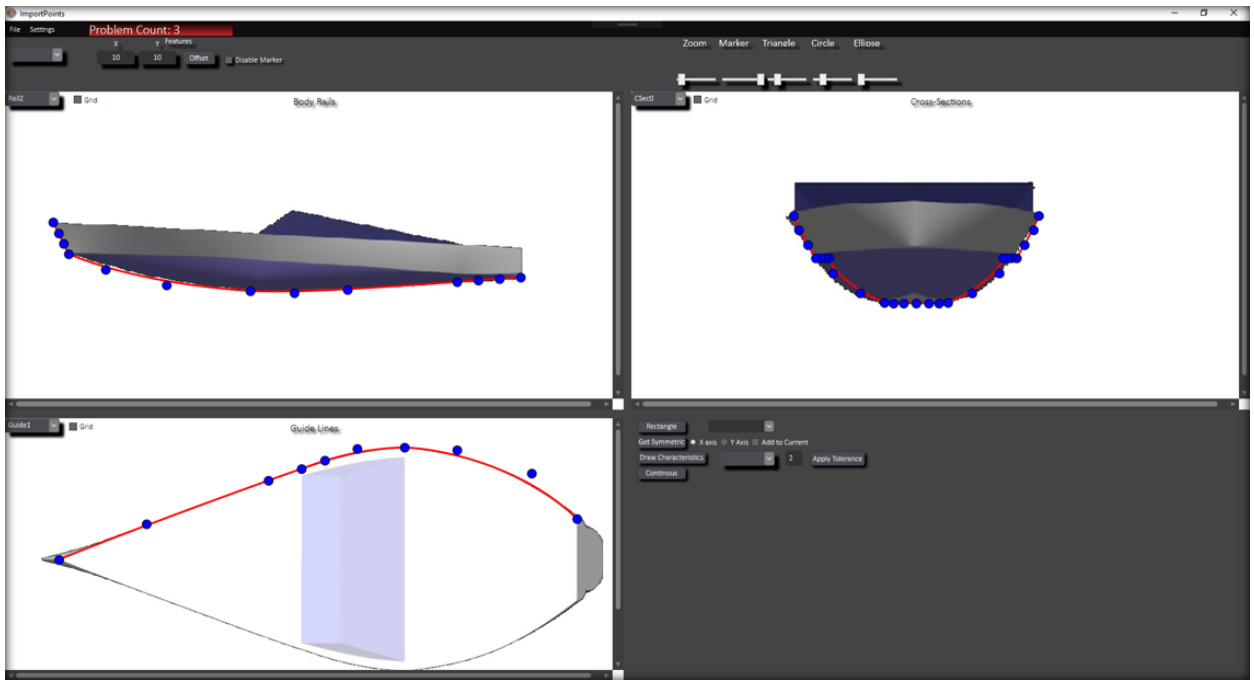
Figure 4.3: The interface for adding points to the multiple profiles of different views.

Moreover, the primitive shapes and biarcs are also visualized to give an insight into the designs generated with different parameter settings.

Note that, the *LHS* is default for generating the test samples; however, there is also a button to import a design table (see Fig. 4.26) that consists of coefficients to manipulate the independent points to be used instead of the *LHS*. Thanks to this option, users can also create a sample set to be suitable for controlled studies like human-oriented designs explained in Chapter 1.

Tuning interface has four areas, namely **A**, **B**, **C**, and **D** in Fig. 4.4:

- **A:** The test samples are visualized with circles, circle diameters, fan triangles, and ellipses. The points of Γ^i and P_T^i are also marked. Each of these items can be disabled or enabled to give a suitable visual combination. This area is mainly used to observe the constraints and the simplified structure of the relevant design.

- **B:** The outer profile curve D and characteristic lines (if they are defined), of a design are drawn in this area. Biarcs $BA(s^i)$ are also displayed. Corners can be filleted.

- **C:** This area shows ρ^{total} and $MHD(D, D_{org})$. The *MHD* values of each segment are also displayed to show how much each segment has been modified. The constant d value can be changed with a slider. User-defined weights can be applied by enabling the check box; otherwise, all weights are set to 1 by default. There is also an option in the sampling settings to disable the randomness in the direction of $\overrightarrow{r}$ to control the direction of modification. This

is done by adding a sign to the weights. Constraints can be applied. The design can be mirrored if symmetry is enabled and an open shape can be closed. Moreover, the colors, opacity and the shadow effect can be set.

- **D:** A biarc is a curve segment comprising two arcs joined smoothly, as shown in Fig. 4.5. We generate an approximating biarc $BA(s^i)$ for the curve segment s^i, as proposed by Šír et al. [137]. $BA(s^i)$ is defined by two arcs: $P_0^i J^i$ with radius and center angle (R_1^i, θ_1^i) and $J^i P_1^i$ with (R_2^i, θ_2^i). J^i is a point on the curve of s^i that ensures the G^1 continuity between the arcs. The radii of biarcs $R_1^i, R_2^i, \ldots, R_2^{n-1}$ are scaled to $0-1$ and plotted to display the distribution of the curvature of D.
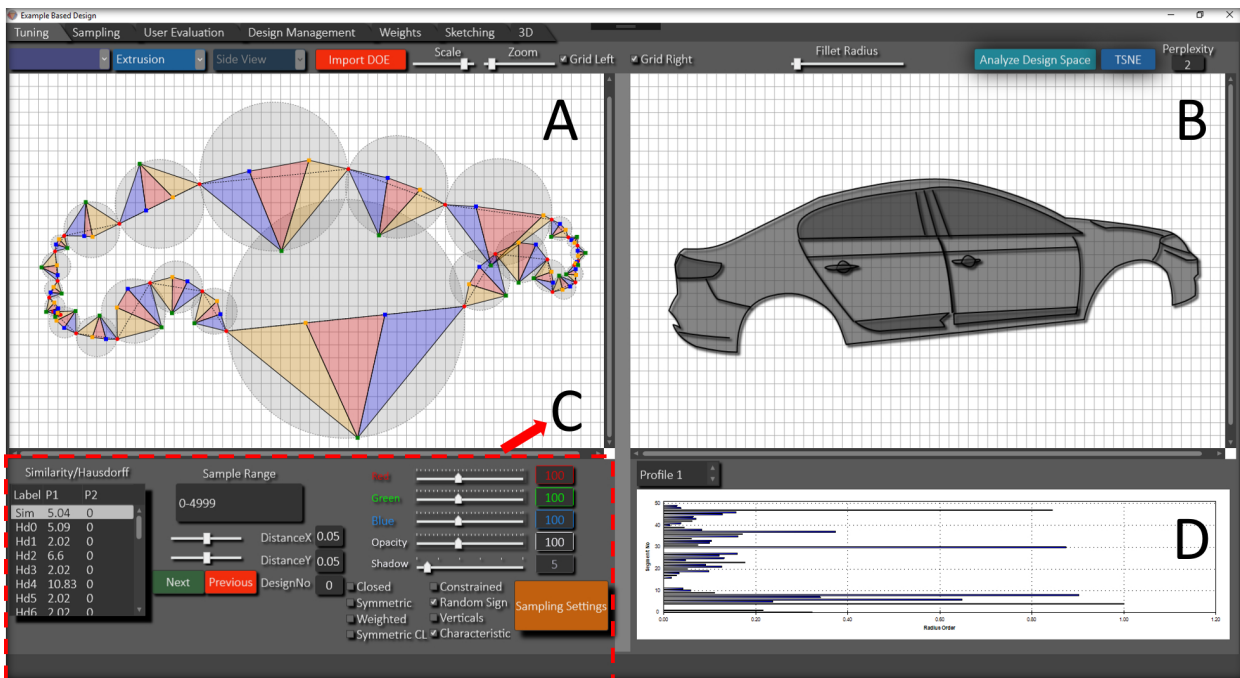

Figure 4.4: Tuning interface to set optimal sample settings observing their impacts on test samples.

Figure 4.5: Approximation using biarcs, which are indicated by red.

4.1.2.2 User evaluation interface

In aesthetic design sampling, it is very important to consider the user's subjective evaluation when exploring creative designs. This interface allows users to evaluate generated samples interactively and to store some while the sampling continues.

Figure 4.6 shows this interface. A single-chain sampling algorithm is used. First, M samples are generated, and the user can evaluate on each of them. Two types of evaluation are used. The first is a binary evaluation, in which they can accept or reject a sample, and the second is a five-point Likert-type [138] evaluation ($1 - 5$ scale) which is used for simple scoring. If a design is accepted or given the highest score, the sample is added to a list. The samples in this selected list, including the control points, can be exported to external statistical software for further analysis. The "update" button generates a new sample set.

The weights ($w = (w_x, w_y)$) (see Section 3.3.3), can be manually changed to guide the sampling process observing how the generated shapes are affected by these values. The design space is $2n$-dimensional in which the dimensions are n-control points and each of the design samples is represented by a landmark in this space. Here the guiding means locating the landmark in a desired location of the space to give desired shape features to the sample. A non-expert can intuitively adjust the weights for relevant control points to preserve ($w = 0$), make modifications prominent ($w > 1$) or slightly modify ($0 < w < 1$) relevant features. To sum up, to reach the desired location in the design space, the landmarks must move along a correct direction, which can be adjusted observing the reaction of the shape to the assigned weights. There is also an additional interface displayed in Fig. 4.7 that simplifies the weight assigning for relevant points. In this interface, the user simply clicks on a point and assigns its weights using text boxes to update relevant weights from a database.

Furthermore, a user can edit a displayed sample slightly by dragging points (see top left design in Fig. 4.6).

Finally, the samples in the selected list are displayed together. They can be exported to external software and used to create CAD models.
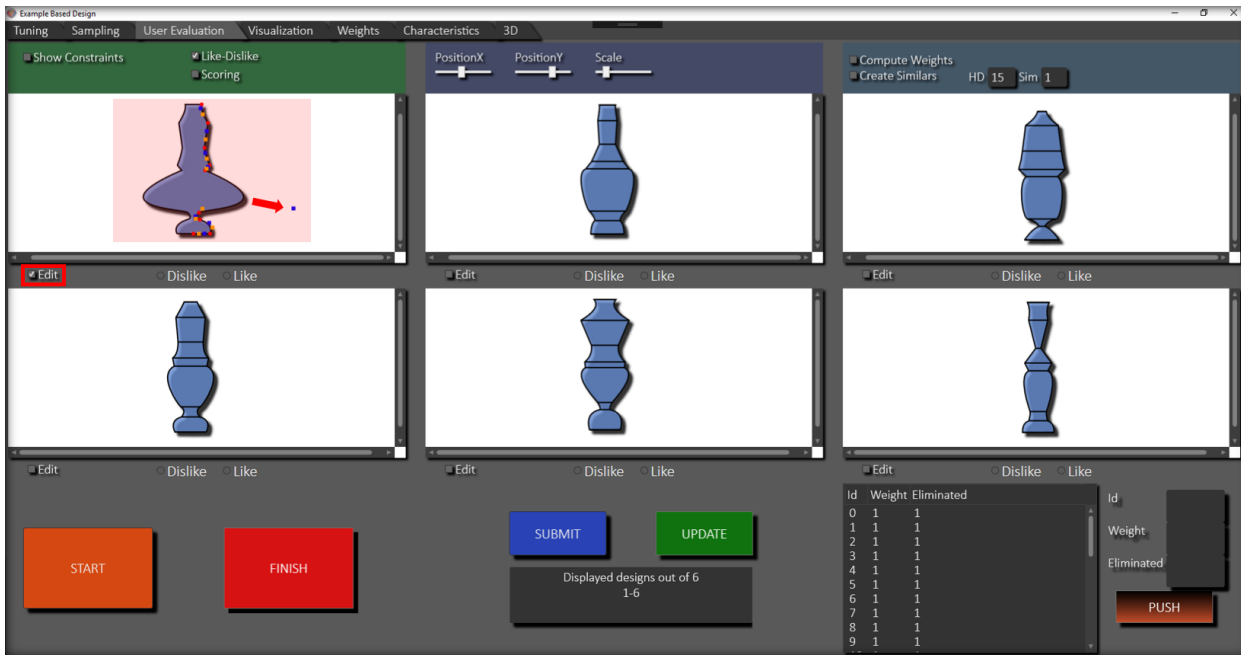
Figure 4.6: User evaluation interface to evaluate the generated samples interactively and assign weights for the control points to guide the sampling process.
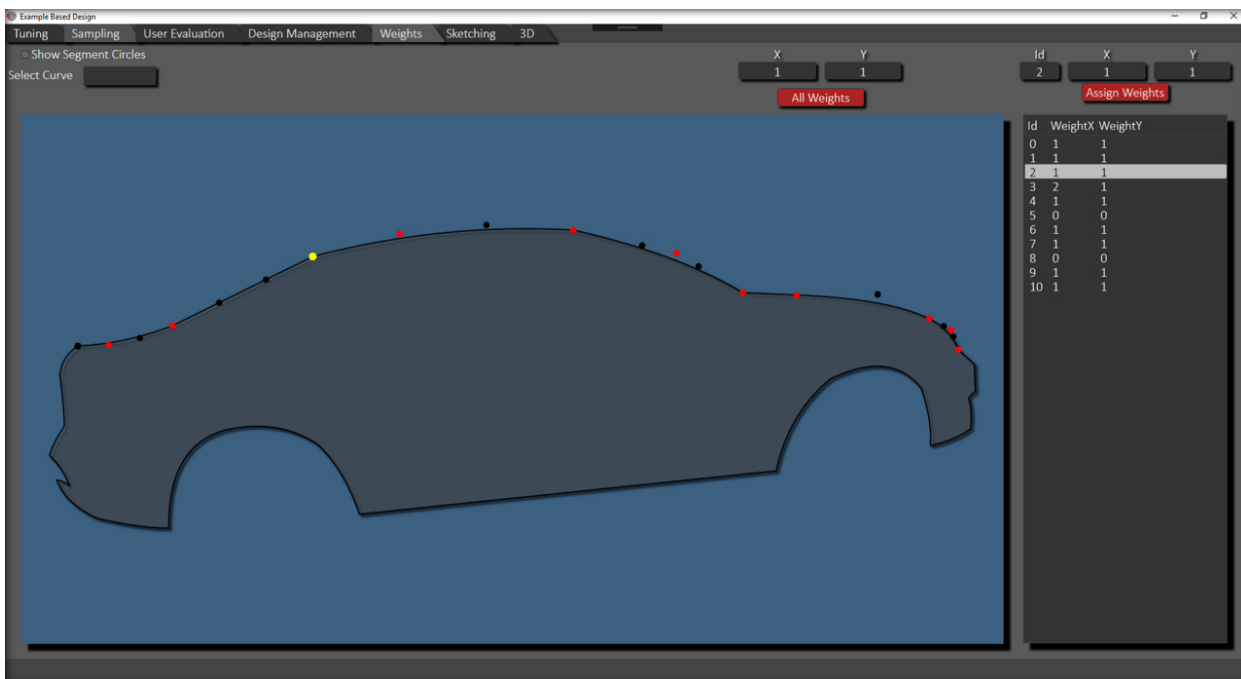
Figure 4.7: Weight assigning interface.

4.1.2.3 Sampling interface

This interface shows the test samples generated in the tuning interface as well as the designs generated by the sampling algorithm (Fig. 4.8). The settings of the sampling algorithm (Section 3.4.2), such as ϕ, M, and N, and the time constraint can be defined here. The sampling run time and the energy $E^{AE}(L_k)$ are shown at the bottom of the interface. This interface also supports recording generated profile samples from different views and displaying all of them together (see Fig. 4.9). The generated profiles from different views are matched to represent each as a single design to be then converted into the 3D models.

There is also additional option for sampling, which uses the chain algorithm in different way. According to this, a small sample set is generated from the exemplar and a random sample is then selected from this set to be used as an exemplar while generating another sample set (see Fig. 4.27a). The process is repeated up to the number of times the user enters. Two example sets are displayed in appendix (Fig. 4.27b).

The profiles can be overlaid to demonstrate the variations (Fig. 3.14). Various visualizations can be realized using combinations of primitives such as the circles, triangles and control points.

In this interface, characteristic lines are not shown due to performance issues; instead, sketching interface displayed in Fig. 4.10 is developed to add the lines if exist. In addition, the profile curve can be projected with different angles to have a perspective view of the shape (see Fig. 4.22 for examples).
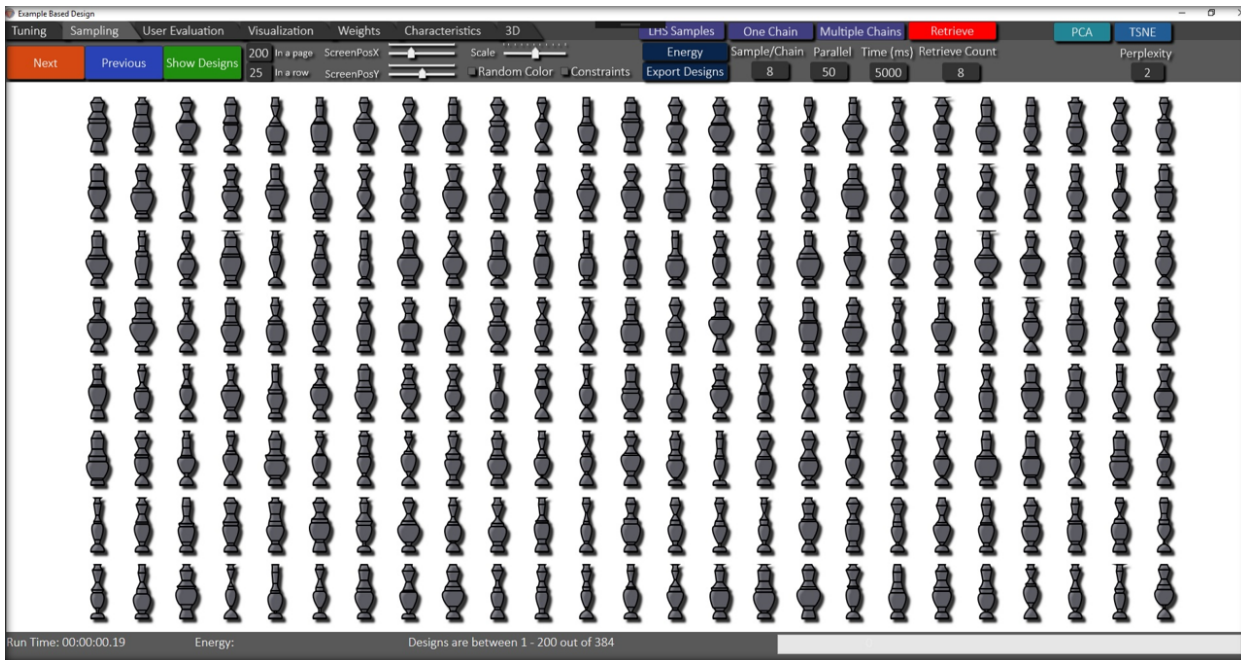
Figure 4.8: Sampling interface to run the sampling algorithm, show the generated samples and visualize the variations overlapping the samples onto each other using position sliders.
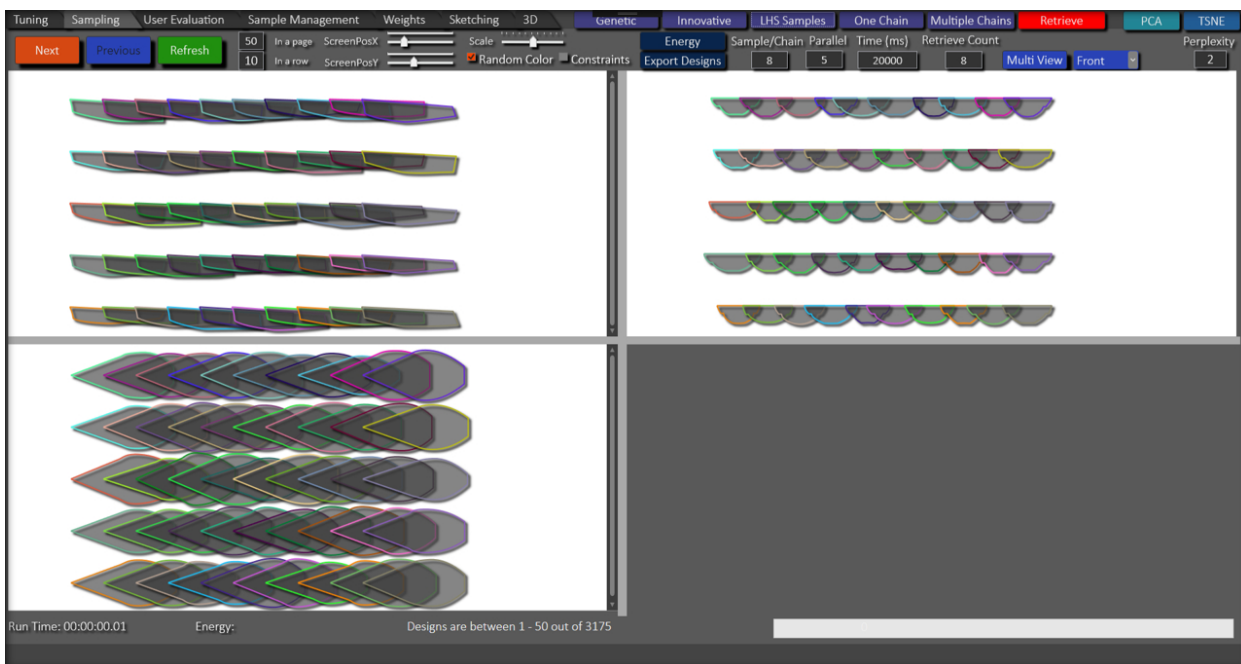
Figure 4.9: Multi-view module of the sampling interface.
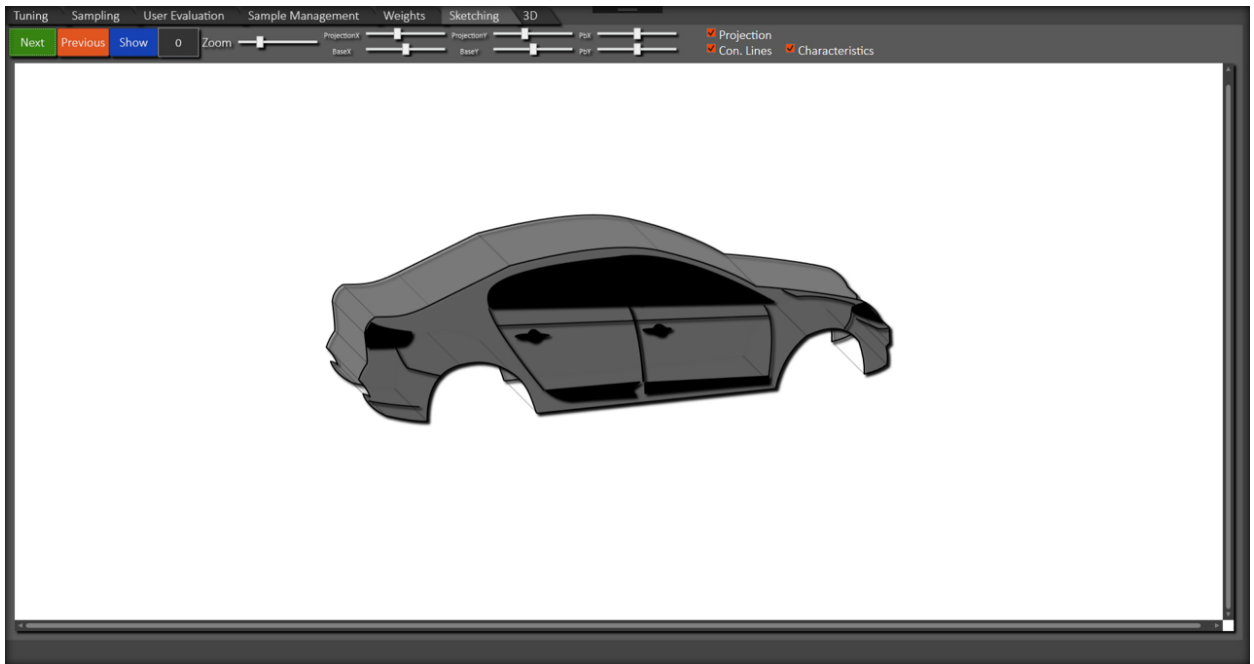
Figure 4.10: Sketching interface adds characteristic lines if exist to the samples displayed in sampling interface.

4.1.2.4   3D visualization with external CAD connection

A generated profile D can be reconstructed in an external CAD tool using its composite Bézier curve. Figure 4.11 shows a system that we prepared with Rhino / Grasshopper [125] to convert profile D into 3D models. This system is quite easy to use. It requires data files of points of the exemplar profile and characteristic lines, and the weights for the points if needed (Fig. 4.11a). After that, a new sample set Ω can be generated using a sampling component that we developed using C# to be used in Grasshopper (Fig. 4.11b), or sharing a real-time updated text file that includes the points of D exported by our software (Fig. 4.11c). Note that, the sampling component is able to conduct all proposed methods including the parallel sampling and sample retrieval by minimizing the potential energy without needing our software. The sampling settings can also be easily changed within the Grasshopper system; however, to learn optimal settings easily and quickly, the tuning interface (Fig. 4.6) might still be needed. Finally, the profile curves are constructed from the points and converted into 3D models as NURBS surfaces by revolution, extrusion, sweep or network surface method using another component displayed in Fig. 4.11d. In addition, the generated models can also be applied textures and assigned materials to enhance the visual experience, as shown in Fig. 4.12.

The sweep method fits a surface through cross-sections guided by two profile curves and the

network surface fits a surface through a curve network created by the intersections of three or four profile curves with cross-sections. In the design system, the cross-sections are defined only to the location where the shape is changed. The component that is used to create a 3D model also can derive user-specified number of cross-sections to be placed with equal intervals. To do this, each of the profile curve into equal pieces and a cross-section is copied and affine transformed to be fitted between the corresponding end points of the pieces (see Fig. 4.13). Figures 4.28 to 4.31 show the example samples created by sweep and network surface methods.
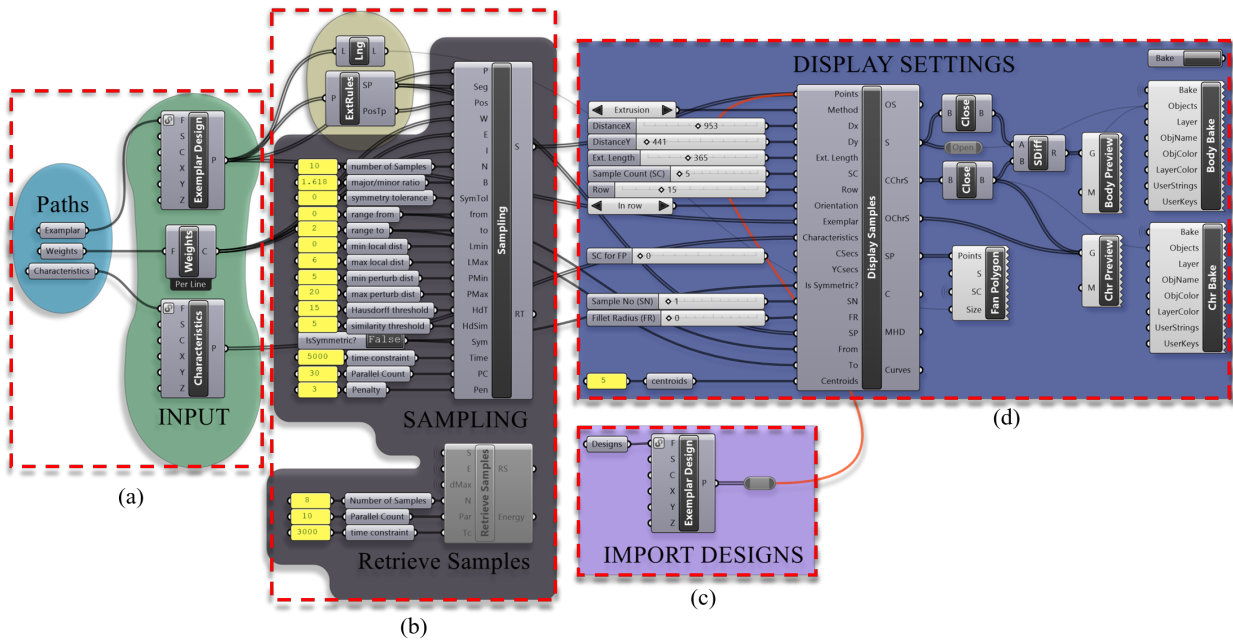
Figure 4.11: Rhino / Grasshopper system. (a) Inputs are imported from the user directories. (b) Samples are generated with the proposed component based on user settings (c) or imported from a text file generated by our tool. (d) The samples are converted into 3D and displayed to the users.

Figure 4.12: The 2D profile of an ewer is varied and converted into 3D. Textures are applied to the 3D models.
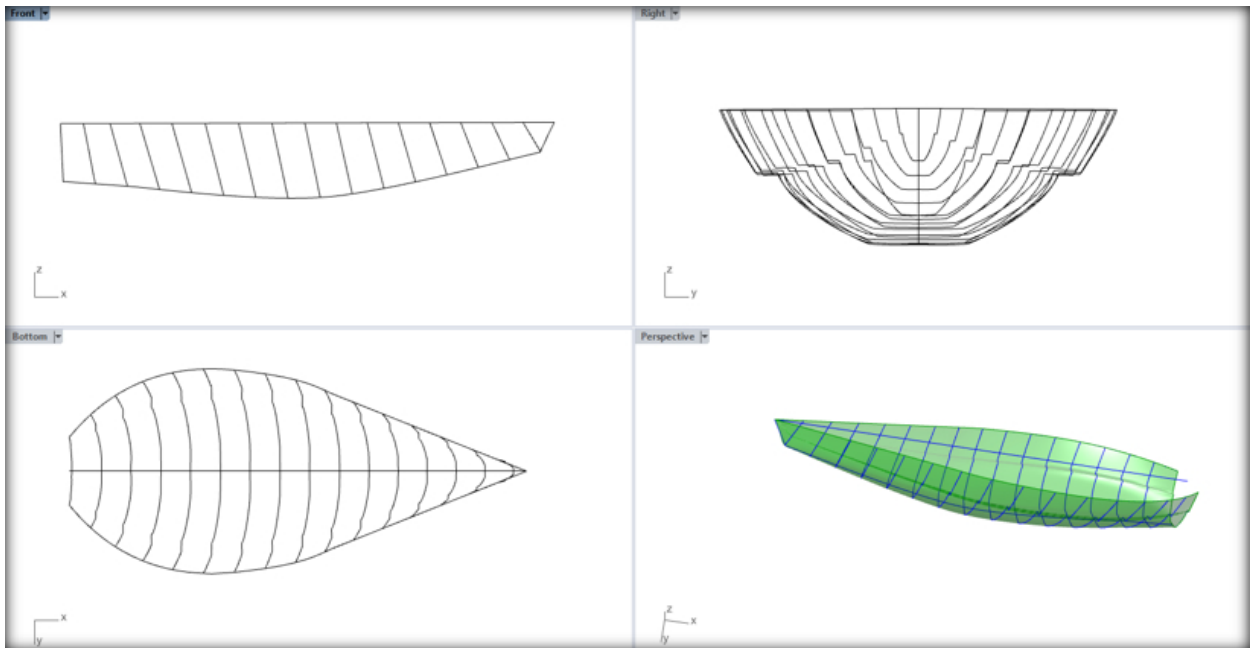
Figure 4.13: Rhino interface, in which a hull cross-section is derived user-specified number of times and fitted along the profile curves.

4.1.3 Sample Management Interface

Sample management interface is designed to manage large number of samples generated in the Section 4.1.2.3 by analyzing and filtering them based on a formula, which is explained in the following section.

First, K-means clustering [139] is used to divide the generated samples into user-specified number of clusters to make managing them easier. The very first displayed samples are the clusters' centroids and the exemplar profile D_{org} that user provided. In Fig. 4.14, the centroids are placed around the D_{org} (in red). When a centroid is clicked, it goes to the center and become D_{org} and its cluster members are placed around it. The surrounding samples are colored between light and dark blue indicating the highest and lowest value computed by a selected formula. Figure 4.16 shows some options to organize samples. The samples can be located at a constant distance to create a circular shape around the center or to be the one with lower computed value closer to the center sample. In addition, the samples can be ordered in a way that their formula values are getting increased in clockwise or counterclockwise direction.

Sample management interface modules are explained below with corresponding regions named by capital letters in Fig. 4.14:

- **A:** Main canvas is where the samples are displayed. The organization and color of the

samples are determined based on similarity or a user-defined formula.

- **B:** A copy of a sample dropped in "B" is stored in a separate list.

- **C:** The samples in "B" are pairwise compared based on a formula.

- **D:** The formulas are defined through *Formula Interface* (Fig. 4.17) and selected here to filter out the samples using sliders. The sliders define upper and lower values such that if formula value of a sample is out of the range, the sample is removed from the canvas temporarily. Moreover, a graph can be created over "A" using two formulas to be one versus another (see Fig. 4.15).

- **E:** Any sample can be dropped here to manipulate its points. The modified sample can be dragged from "E" to any other region, so it can be used to derive new samples in "G", can be exported to Rhino in "F", or can be compared with others in "B". In addition, there is a search button that displays the samples in "A" and organizes based on their similarity to this modified sample.

- **F:** A sample dropped here is exported to a file shared with Rhino so that its 3D model is simultaneously created.

- **G:** Any sample dropped into this region is used as an exemplar profile and single chain algorithm is executed to create new samples from this sample. Through "Accept" and "Delete" buttons, the generated samples can be added to the original list or it can be deleted completely.

- **H:** When the mouse cursor enters inside the boundary of a sample in any region, its large scaled version is displayed here.
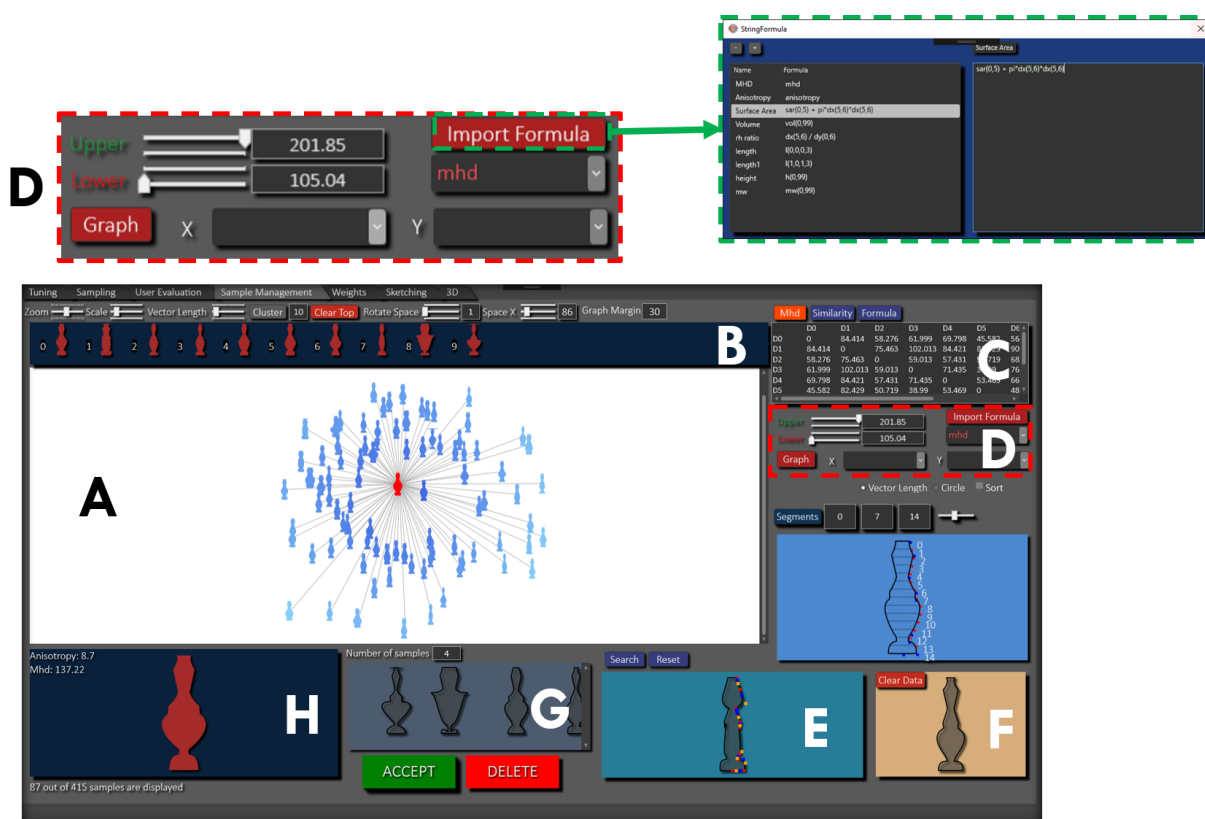
Figure 4.14: Sample management interface that filters and analyzes the samples based on formulas that can be created based on similarities or geometric constraints.
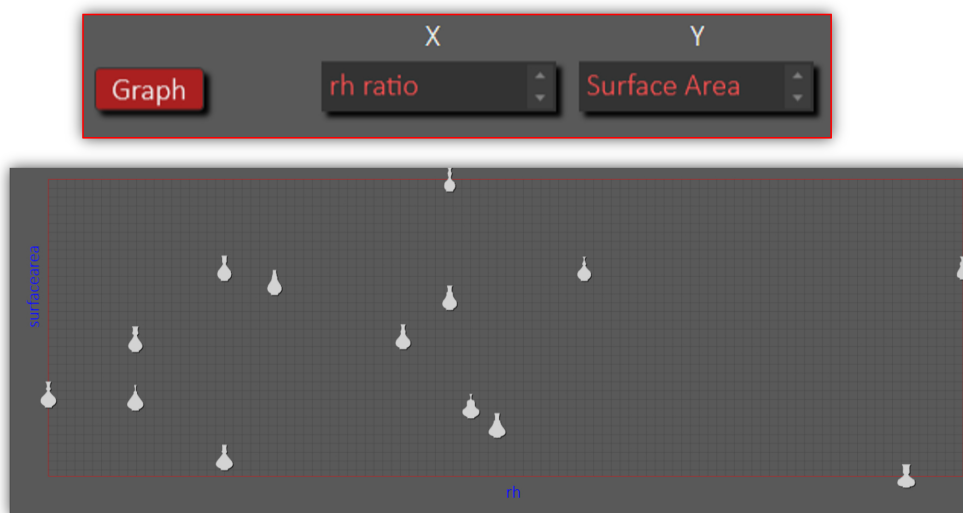
Figure 4.15: A graph of *radius/height* (*r/h*) ratio versus *surface area* is defined through the region **D** and displayed in the region **A** of the sample management interface.

Distance to center

by Formula   Constant

Order

Random

Sorted
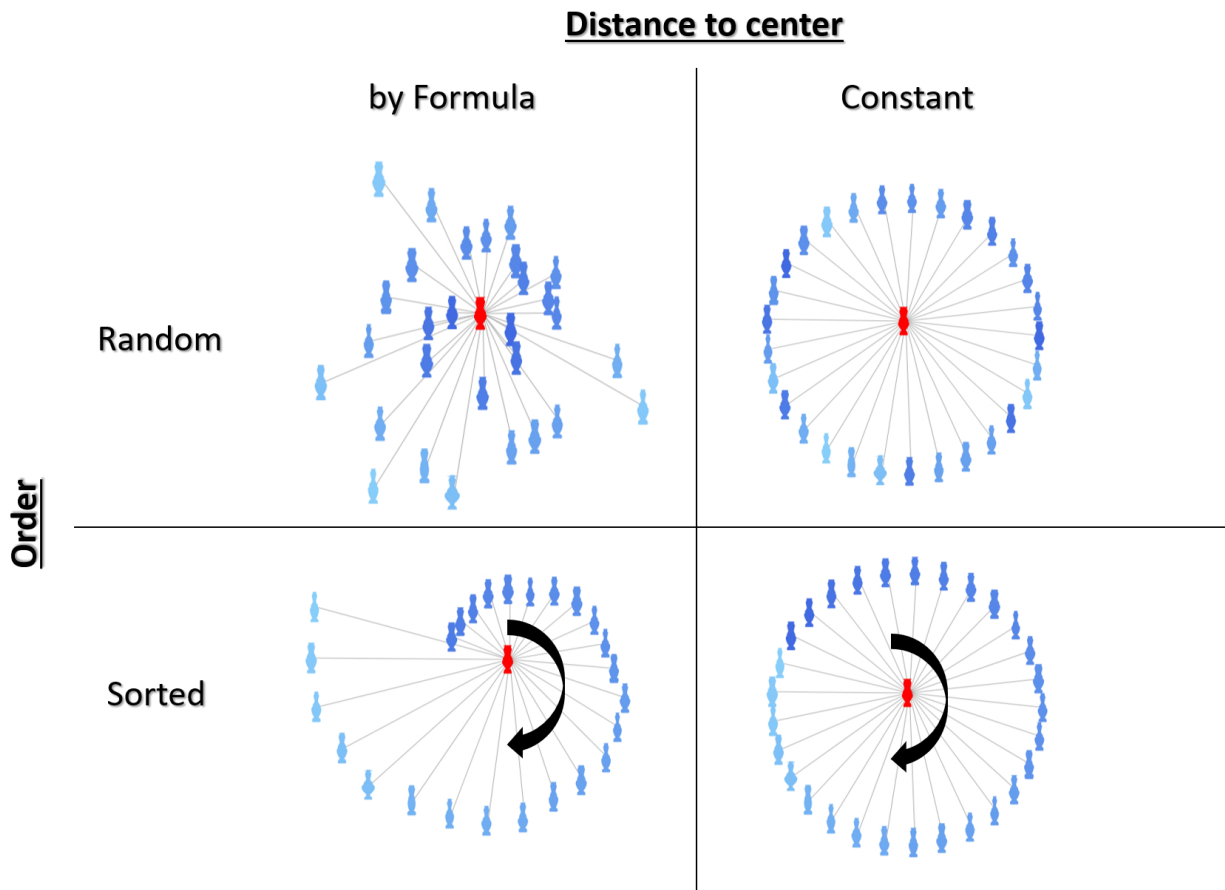
Figure 4.16: Sample organization options.

Formula Definition

In this thesis, the formula is an equation defined using proposed functions given in Table 4.1. Such formula is used to compute a value for a queried property of a sample such as similarity with other samples, width and volume to be evaluated by the users. The variables of the functions are segment numbers, and labels, which are automatically assigned for the control points or the points found on the profile curve with user-specified equal horizontal or vertical intervals. Besides, the cross-sections are located by the intervals along the curve and also labeled to be called by a function. Figure 4.17 shows the interface used for the formula definition, where the points and the cross-sections are also labeled. For an instance, an example formula can be defined using a single function as $dx(s23, s13)$ where dx (Delta X) computes horizontal distance between two points labeled as $s23$ and $s13$ (see Fig. 4.18). The samples out of a range of distances set by the user are then filtered out and the remaining samples are organized to be the distances are getting increased in the clockwise direction as illustrated in Fig. 4.18. Similarly, the function dy (Delta Y) computes vertical distance and l (Length) computes Euclidean distance between two points. w (Width) finds

maximum *dx* and *h* (Height) finds maximum *dy* of the shape. Users can call any points' *x* and *y* coordinates using the functions *px* and *py*. The tangent angle of a line created by three points can be calculated using *an* (Angle). Furthermore, the similarity measures ρ^{total} and *MHD* can be computed for the samples against the sample at the center using *mhd* and *sim* functions. There is also a function *ud* (User Defined) that can call earlier defined formulas by their name, which lets users create modular formulas as a combination of sub formulas. All of these functions can be combined using the basic mathematical operators that are addition, subtraction, multiplication, and division to create more complicated formulas.

Figure 4.19a displays the implementation of function *ar*, which computes areas of the samples. To do that, each sample is approximated to a polygon created by the points on its profile curve (see Fig. 4.19b), and the area of the polygon is then calculated by following Shoelace formula:

$$A = \frac{1}{2} \left| \sum_{i=1}^{n-1} (x_i y_{i+1} + x_n y_1) - \sum_{i=1}^{n-1} (x_{i+1} y_i - x_1 y_n) \right|$$

To compute a volume of a sample, pyramidal frustums are defined between consecutive intervals where top and bottom areas indicate the areas of relevant cross-sections (see Fig. 4.20). The shape volume is then computed as the sum of all volumes of these pyramidal frustums. Therefore, more sensitive volume computation can be achieved by increasing the number of intervals. Note that, the area for non-circle cross-sections is also computed by the Shoelace formula. The volume of a shape composed of *m* pyramidal frustums is calculated as follows:

$$V = \sum_{j=0}^{m-1} \frac{1}{3} \left(A_j + A_{j+1} + \sqrt{A_j A_{j+1}} \right) h_j$$

Note that, some functions such as *vol*, *w* and *h* can be computed only for part of the shape defined by segment numbers (see Fig. 4.21).

Table 4.1: Available functions for formula definition.

Name	Functions	Name	Functions
Math Operators	+,-,*,/	Length	l
MHD	mhd	Angle	an
Anisotropy	sim	Delta X	dx
User Defined	ud	Delta Y	dy
Volume	vol	Point X	px
Block Volume	bvol	Point Y	py
Area	ar	Surface Area	sar
Width	w	Height	h
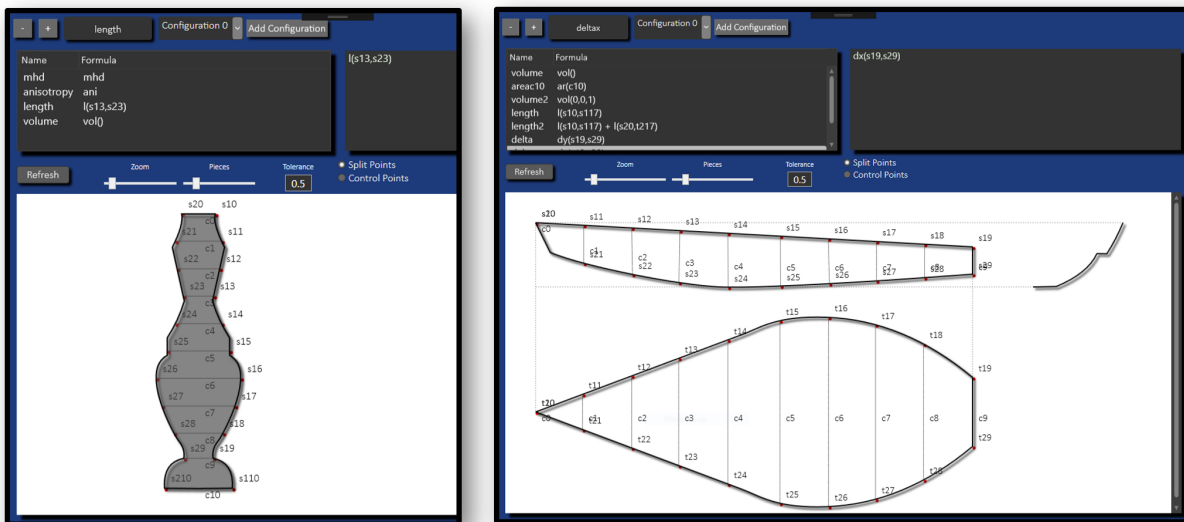
Figure 4.17: Formula definition interface. Example labeling for a sample with single view displayed on the left and multi-view on the right. In this interface, the user first defines the number of intervals and points are found on the curve accordingly. These points and the control points are automatically labeled and displayed to the user to be used as variables for the functions to be used in formula. Besides, the cross-sections are fitted between the the corresponding points and labeled to be called by its label in the functions. For example, a user can compute the area of fifth cross-section with label $C4$ using the formula $ar(C4)$.
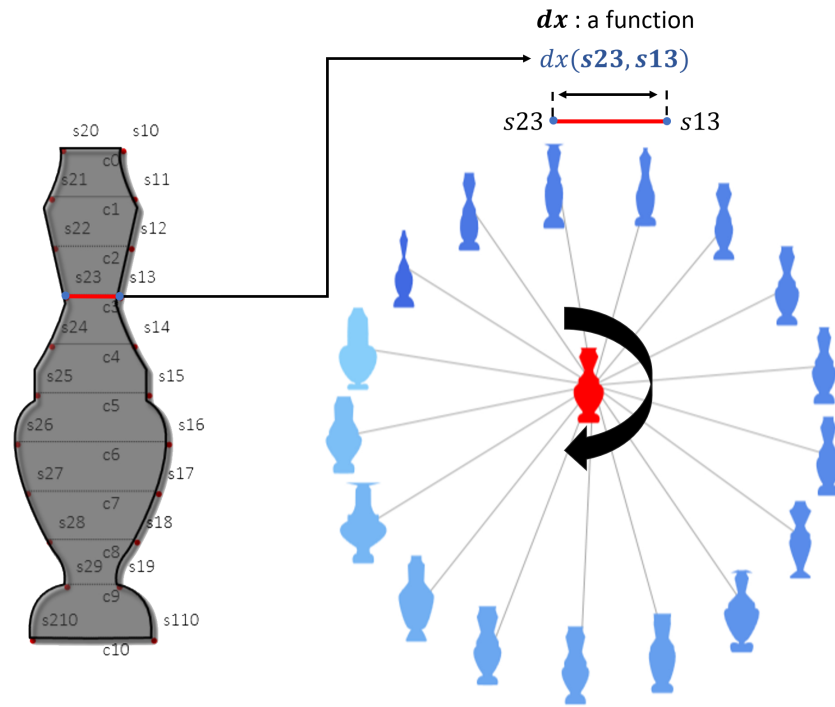
Figure 4.18: Samples are organized based on an example formula $dx(s23, s13)$ where dx is a function to compute horizontal distance between two points on the profile curves that are labeled as $s23$ and $s13$.
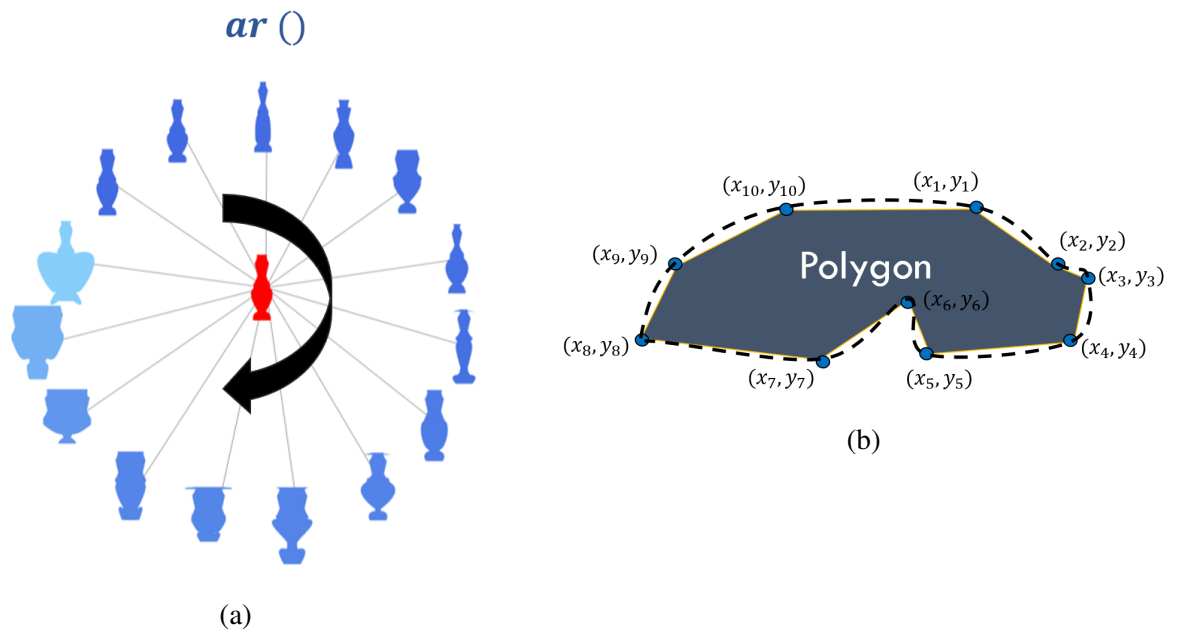
Figure 4.19: (a) Example implementation of *ar* function that computes side view area of ewer samples. (b) A polygon created by the points on a curve to compute the approximated area.
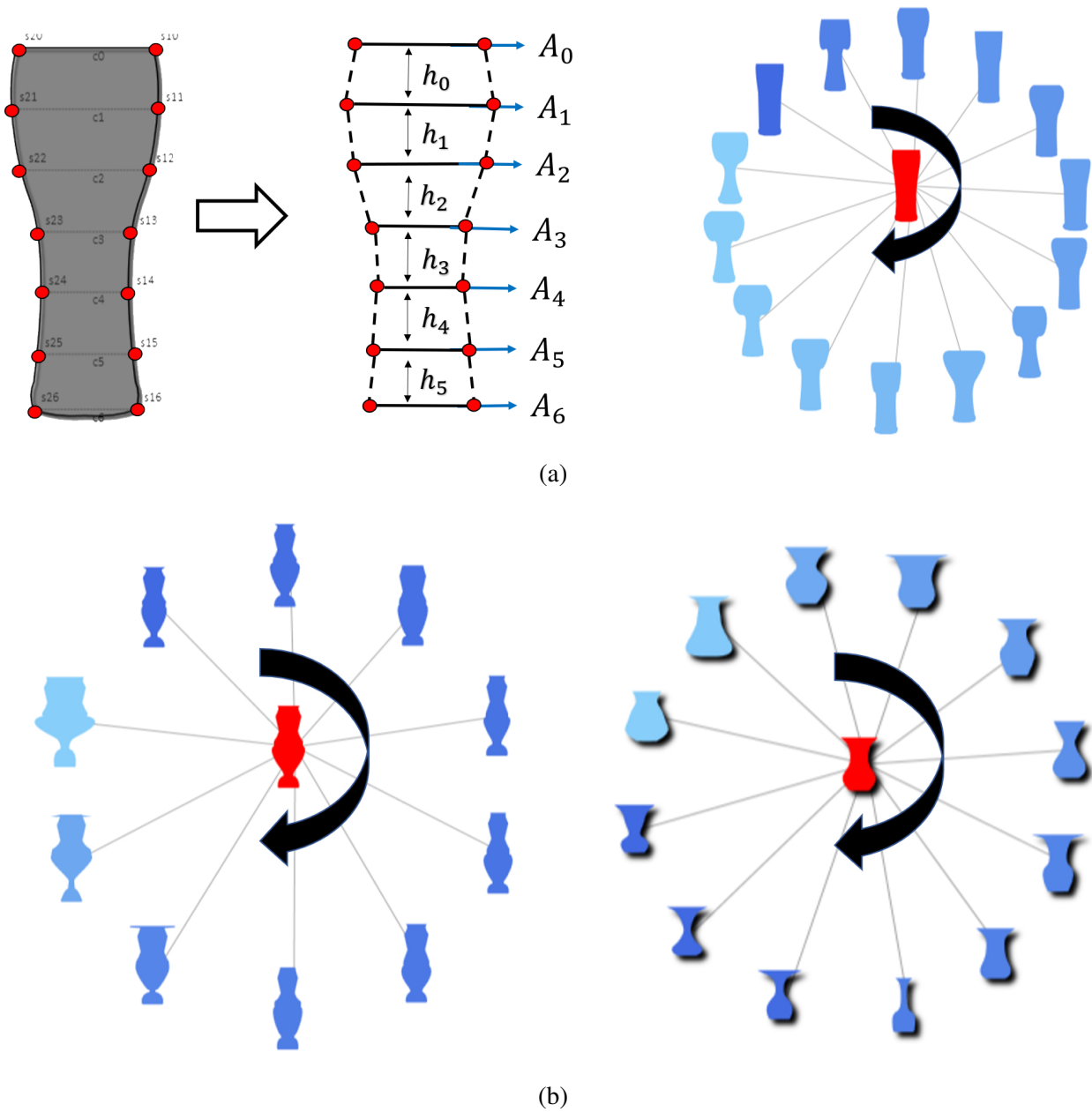
(a)

(b)

Figure 4.20: (a) 6 pyramidal frustums are defined to compute the volume of displayed glass profile using the function *vol*. (b) Ewer and tea glass samples organized by computed volume values.

(a)

(b)
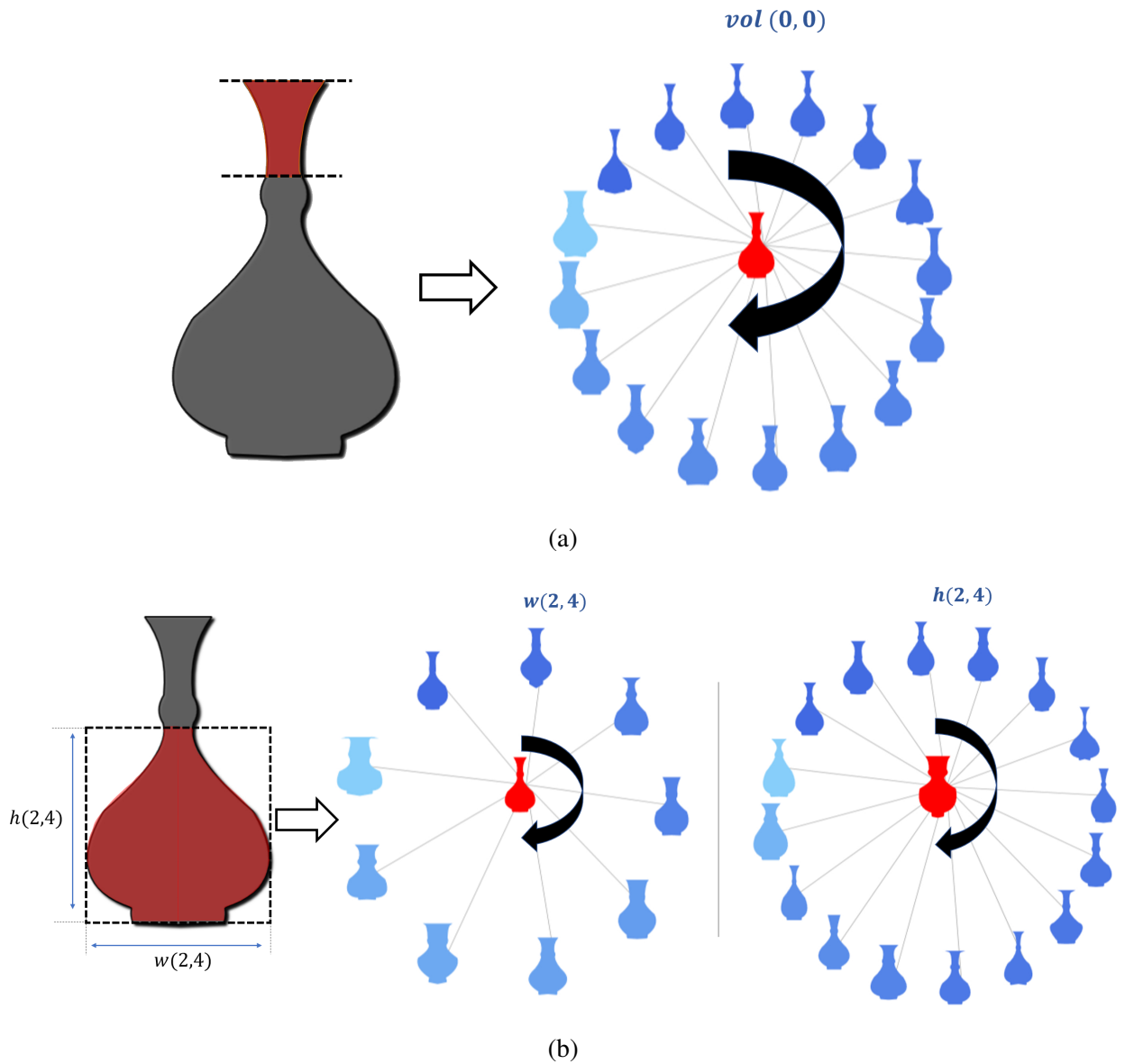
Figure 4.21: The samples are organized with (a) volume computed only for first segment by $vol(0,0)$, (b) and width and height computed for the region between 2nd and 4th segments by $w(2,4)$ and $h(2,4)$.

Appendix
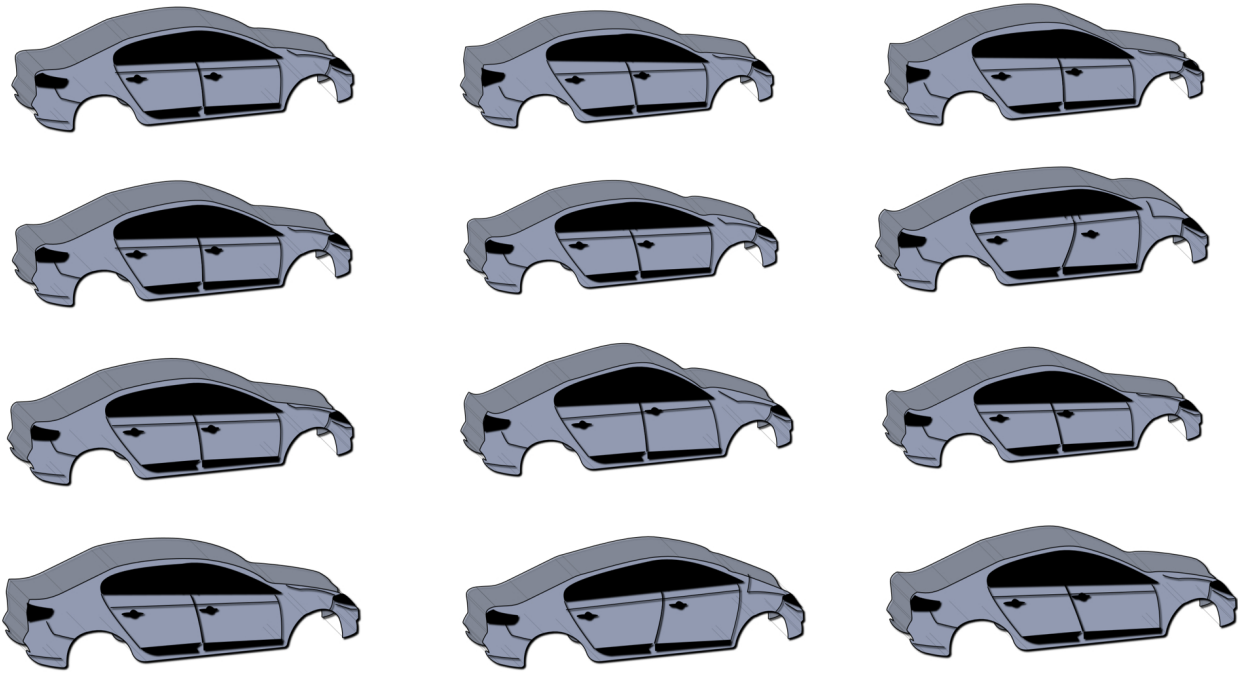
Figure 4.22: 3D perspectives created by projecting the car profile curves.
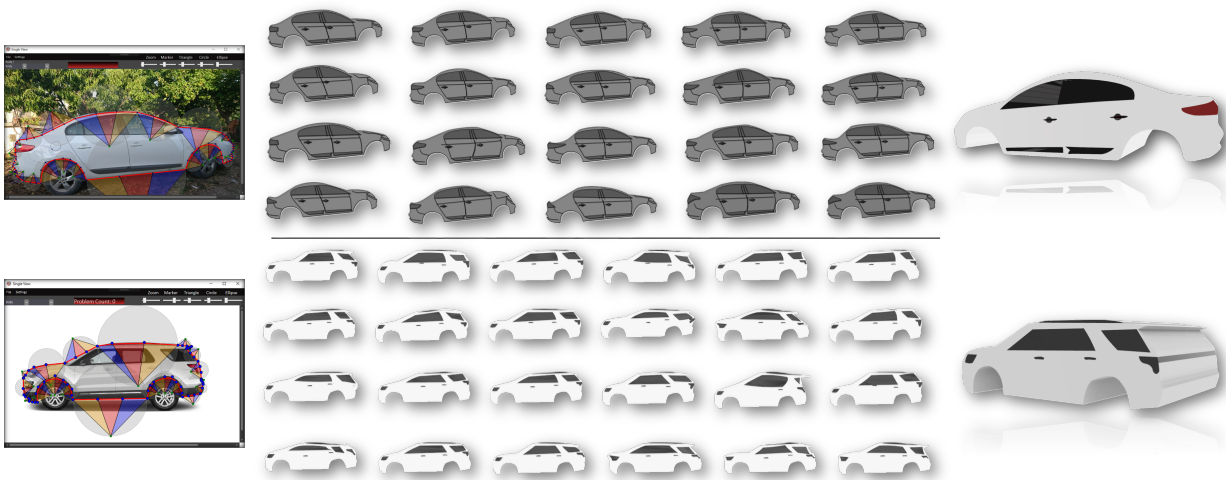
Figure 4.23: 2D sketches and 3D models of car examples with characteristic lines.
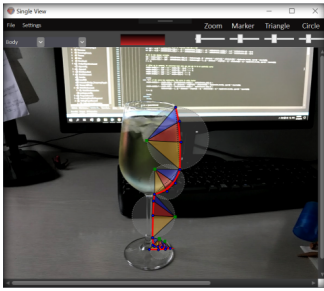
Figure 4.24: A wine glass example.
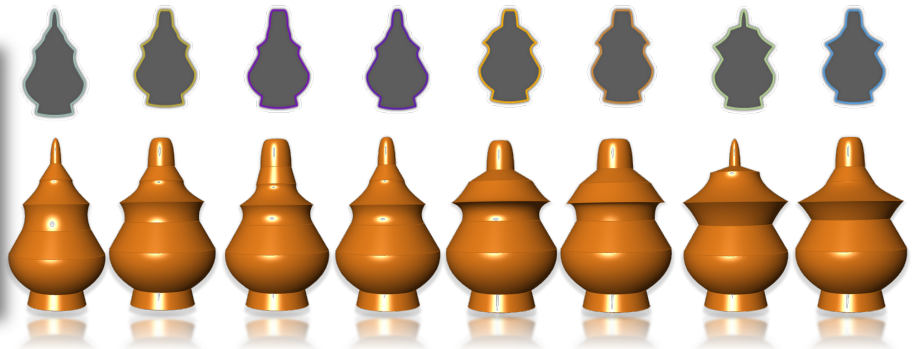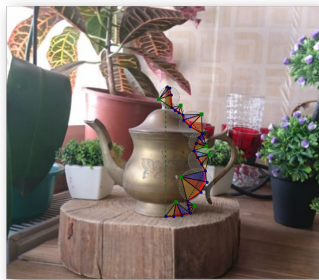
Figure 4.25: An antique teapot example.

Sample/ Variables	V1	V2	V3	V4	V5	V6	V7
S1	1	1	1	1	1	1	1
S2	1	1	1	2	2	2	2
S3	1	2	2	1	1	2	2
S4	1	2	2	2	2	1	1
S5	2	1	2	1	2	1	2
S6	2	1	2	2	1	2	1
S7	2	2	1	1	2	2	1
S8	2	2	1	2	1	1	2

Figure 4.26: Samples generated by uploaded table on the right, which is L8 orthogonal array for 7 variables with two factors.
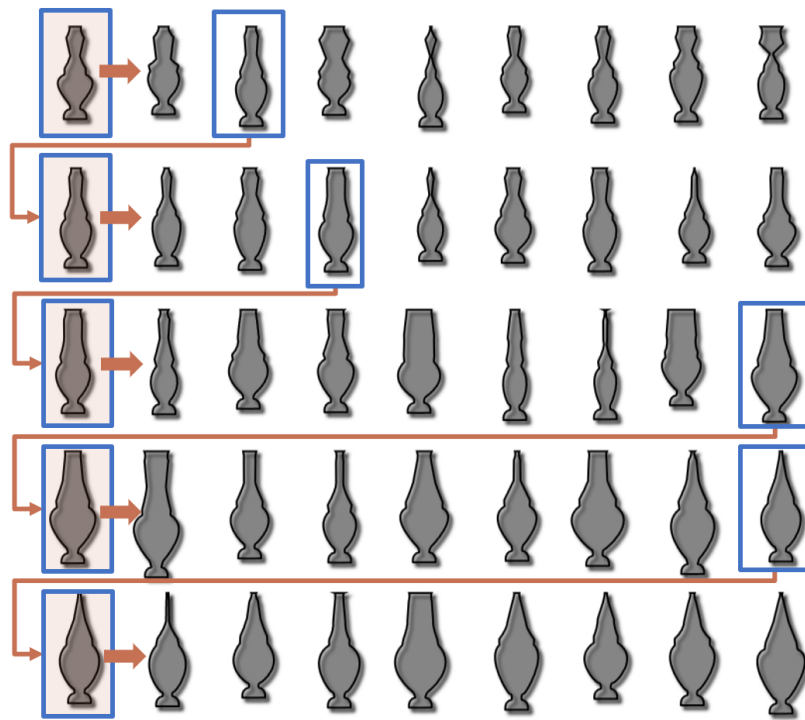
(a)
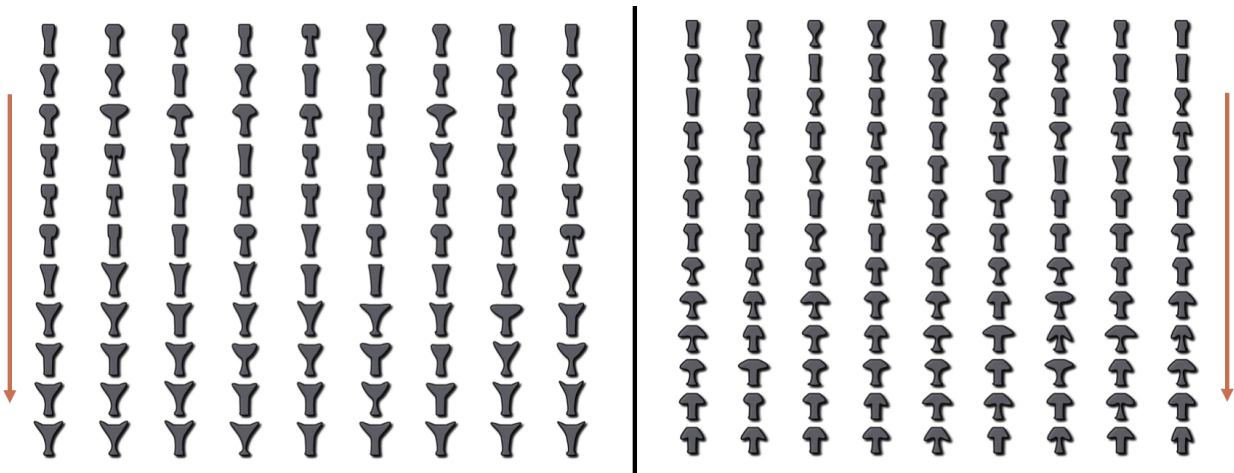
(b)

Figure 4.27: (a) Each row contains a sample set generated using the leftmost model as the exemplar profile. Each sample set was created after another from top to bottom, and using a random sample of previous set as the exemplar profile. (b) Same algorithm applied to the glass profile with more iterations.
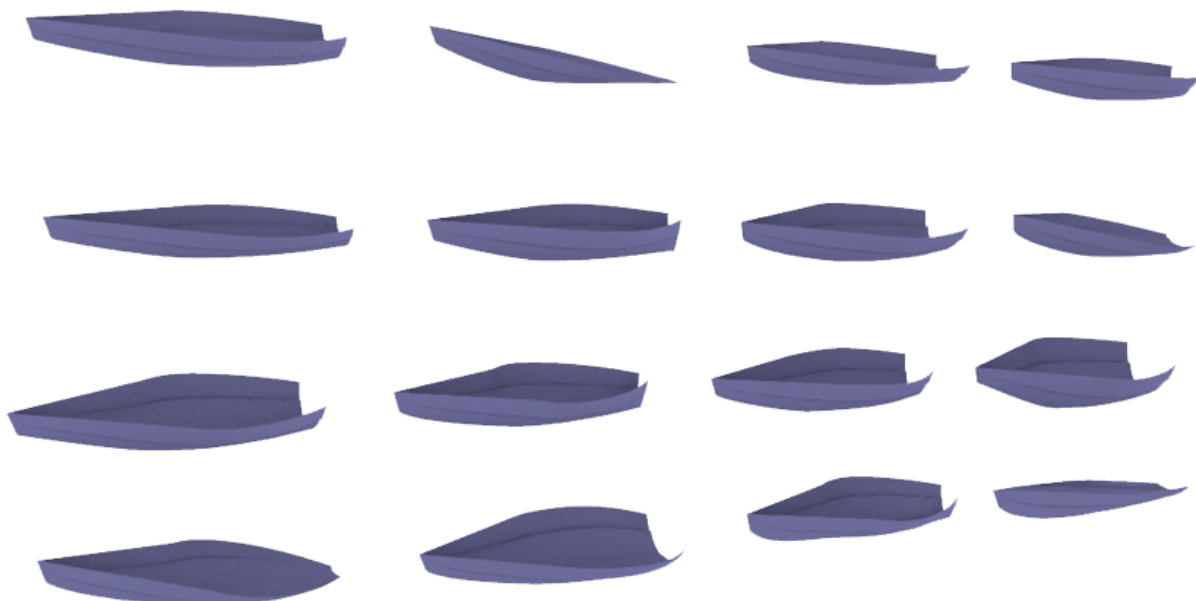
Figure 4.28: Hull samples generated by network surface method using 4 profile curves and a single open cross-section.

Figure 4.29: Hairdryer samples generated by sweeping a single closed cross-section.
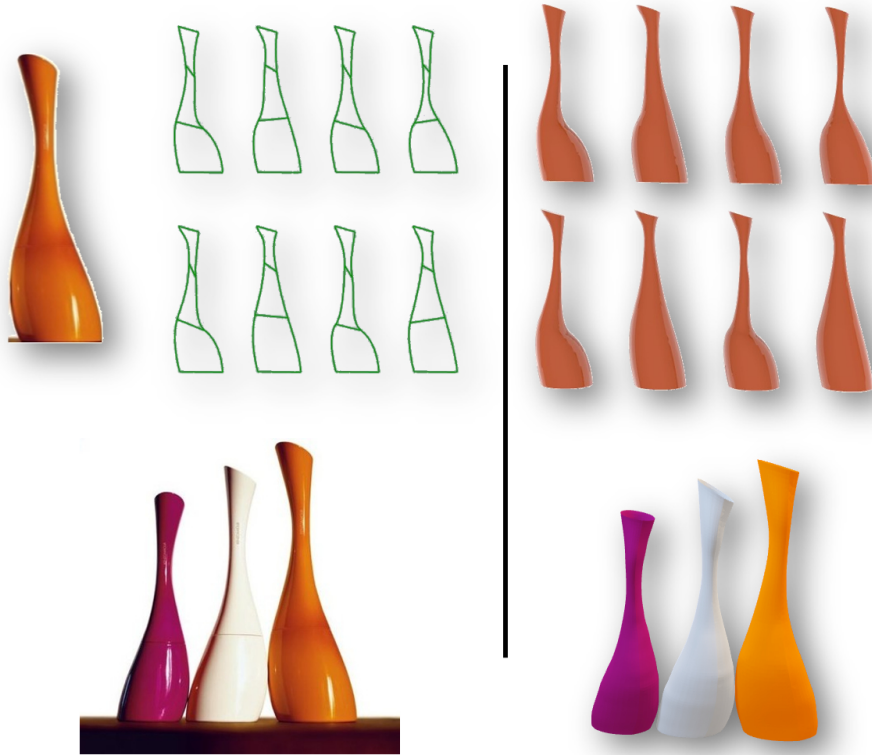
Figure 4.30: Vase samples (on the right) created from the images (on the left) with sweep method using 2 profile curves and a single closed cross-section.

Figure 4.31: Bottle samples created with sweep method using 2 profile curves and multiple closed cross-sections.

Chapter 5

Conclusion

5.1 Thesis Summary

Conceptual design is one of the stages of common design process models in which many solutions are developed in basic forms for a design problem. The solutions are then evaluated and proceeded to the next stages where the selected solutions are detailed and further tested. The aesthetic is an important criterion to satisfy for differentiation of a product. However, there are often many other criteria such as engineering design constraints, cost and time that elevate the difficulty of developing the aesthetic ideas. In this thesis, there are two approaches considered to be helpful for this problem. The first approach is a human-oriented design method that represents customer feelings about the design aesthetic by a set of design parameters. To do this, a survey method was proposed that monitors the eye movements of the participants to figure out the attractive and more relevant parameters to the given set of goals. The second approach is a generative design method, which provides many design alternatives to explore solution candidates among them. The generative method is implemented by software to lower the required efforts for generating the design samples. Also, the users can define their geometric constraints through the proposed software to narrow down the solutions.

In Chapter 2, an eye tracking aided survey (ETAS) method was suggested for collecting data objectively and more accurately than the traditional methods for human-oriented design approaches. The proposed method was applied to an adjective-based design concept, in which adjectives are used to describe parametric hull designs and related to the design parameters in mathematical forms. The research materials were 10 hull adjectives learned via a survey method and 54 parametric hull designs that were generated modifying 26 design parameters according to the Taguchi experimental method. The eye tracking device was used to collect gaze data of the survey participants while they are examining the screen to select appropriate adjectives for the displayed hull design. After that, the gaze data was analyzed using eye tracking tools such as the area of interest (AOI) that encloses an area to be examined, heat map that represents attractive regions of stimuli by a color scale, and gaze plot that displays scan paths of the participants by gaze transitions from one spot to another.

Two gaze metrics were mainly used for quantitative analysis of the gaze data. If locally accumulated gaze fixations can be associated with a design parameter, an AOI is defined for the parameter to compute relative time duration (RTD) metric, which is obtained dividing the time spent in the AOI with total time spent by a participant for the question. On the other hand, if the gaze transitions are observed in large areas and not local accumulation, the relevant parameter is analyzed with transition probability metric that indicates the frequency of gaze transitions between

two AOIs. If a parameter has a local impact on the hull design to be suitable for AOI definition without overlapped by another parameter's impact area in the ETAS question interface, RTD was computed for this parameter. However, some parameters affect large portions of the shape, but how the participants analyze them is unknown. Hence, the search behaviors of the subjects for such parameters were first learned from the template learning survey (TLS), in which subjects are given special tasks for each of these parameters to observe related gaze data individually and decide on appropriate gaze metric. However, if the gaze fixations for a parameter were randomly distributed, the parameter was not analyzed and kept out of the examination. Moreover, the spread areas of the gaze points observed in TLS were also used to set the positions and sizes of the AOIs.

The gaze data collected via ETAS was first roughly analyzed based on RTD values of five important regions enclosed with AOIs in the ETAS interface (Fig. 2.16). The regions are the front view of the hull, the adjectives in, and the hull sections that are the entrance, middle-body and run section. According to the results, the middle-body section took most of the attention having 37% of total RTD, it is followed by the entrance section with 20%, then the adjective region with 19%, the front view with 18% and finally the run section with 6%.

Second, the parameters were analyzed one by one with the RTD and transition probability metrics to determine attractive parameters for the participants. Only the attractive parameters were then used in the regression analysis to learn important parameters for each adjective. The regression models were found using the generalized linear model (GLM) and the best-subset selection methods. The best-subset method simply calculates the residual sum of squares (RSS) for all possible regression models found by GLM and only some models with minimum RSS were determined. These models were then evaluated according to the Akaike information criteria (AIC) and D^2 (explained variance ratio) to select the best subset $\hat{X}$ for each adjective. The design parameters took place in the regression models of adjectives were given in a table (Table 2.3) together with the mean absolute percentage error (MAPE), D^2 and correlation values as performance measures of the models. The D^2 values of the selected regression models are ranged between 0.16 and 0.45 out of 1 and MAPE values are ranged between 0.16 and 0.39. The correlations ranged between 0.37 and 0.67 show the relationships between the gaze data and the participant preferences. The performance measures of the regression outputs are poor to be used in prediction of the adjectives for the hulls, but good enough to verify the existence of relationships between the design parameters and the adjective choices through the gaze data. This is because the gaze data tend to be noisy since the participants' attention is vulnerable and may easily be distracted and shifted to different areas. Furthermore, the participants were not designers, so their decisions mostly unstable as their preferences do not rely on tangible items but subjective opinions, which may be changed

from one question to another. To sum up, important correlations have been found, which verify that the participants' preferences are related to their attention on the displayed designs; thus, the determined important parameters based on the gaze data are valid. The knowledge of the attractive regions and design parameters, and more relevant parameters for the aesthetic objectives is helpful for designers to generate the target designs efficiently avoiding unnecessary modifications of the irrelevant parameters.

In Chapter 3, a generative sampling system was introduced to help designers for gathering many samples with minimum effort. The system starts with the profile curve definition as composite Bézier curve using control points provided by the users. To prevent generating irregular shapes such as those with undulation, loop and cusp during the sampling process; a circle, three triangles, and an ellipse are constructed for each segment of the profile curve to be used as constraints such that the triangles are not allowed to be flipped onto each other, the internal points cannot be inverted respect to the circle diameter and cross border of the ellipse. A sampling region in the design space can be defined by a few settings such as the maximum perturbation value $d_{max}^{perturbation}$, and the similarity thresholds θ_{sim} and θ_{MHD} of anisotropy ρ^{total} and modified Hausdorff distance MHD. θ_{sim} and θ_{MHD} let the users decide how far and how close the generated samples to the example profile can be. A customized iterative local search algorithm called chain sampling was utilized to fulfill the requirements of both segment constraints and similarity goals effectively. The chain sampling algorithm generates the samples one by one, where a newly generated sample that is not more dissimilar from the exemplar than θ_{sim} allows must satisfy all segment constraints and be at least θ_{MHD} far away from previously generated samples. As it is displayed in Fig. 3.18, the generated ewer, glass, and car profile samples are regular and far enough from each other. A parallel sampling algorithm was also used that several times executes the chain sampling to create a design pool. Besides, there is an option provided to retrieve a sub-sample set from the pool minimizing the Audze-Eglais potential energy E^{AE} to make sure the samples in the set are different from each other.

The proposed generative method in Chapter 3 was implemented by a software introduced in Chapter 4, which presents optional features, alternative sampling methods and a sample management system through several interfaces. There is a design system interface in which the profile curves are defined using control points imported from text files or provided by mouse clicks over a design image. Besides, it supports profile definitions up to three views of an object, which is then going to be converted into 3D by either sweep or network surface method.

The software includes a tuning interface in which test samples created using Latin hypercube sampling (LHS) method are used to find optimum values for sampling settings such as $d_{max}^{perturbation}$,

θ_{MHD} and θ_{sim}. The fan polygons and the ellipses are also visualized in this interface so that users can observe the constraining failures of the test samples while the settings are tuned. Furthermore, it is possible to import a design table to create samples to be used as test samples or for a controlled experiment like needed in the human-oriented design methods explained in Chapter 2.

A sampling interface was utilized to generate and visualize samples using different methods. First, users can derive samples from a single exemplary design using the chain sampling algorithm. The chain algorithm has the potential to be used with different strategies. One of them has already been explained as a parallel sampling method that synchronously executes the algorithm user-specified number of times, which all uses the same exemplary profile to create a large sample set. In another sampling method, the chain algorithm is executed several times to be one after another, but each one uses a random or user-selected sample from the previous chain's output as an exemplar to generate a new sample set. Such an algorithm can extend the sampling region to explore more creative samples. The test samples created by the default *LHS* method or a design table can also be displayed in this interface. The designs here are shown by rows and columns with intervals controlled via sliders. Setting the intervals as "0" the samples can be overlapped at a fixed point to observe the variation of the samplings. Finally, all the samples can be exported appropriately to be converted in 3D models using any external CAD software, which is preferred as Rhino/Grasshopper for this thesis. A system is created in Grasshopper using components developed by C# programming language. The system automatically reads the exported text files from the proposed software and creates the 3D models as NURBS surfaces with a method the user selects.

A user evaluation interface was also proposed, which creates samples using a chain sampling algorithm and immediately displays to the users. There are radio buttons under each of the design to collect and record user responses as Likert-type scores or like/dislike options depending on the user choice. The samples are generated as long as the user hits the update button and the responses are kept recorded. The high scored samples are stored and visualized in the sampling interface, and all samples with the responses can be exported to analyze using external statistical software. Moreover, the users can assign weights for modification of each control point to guide the sampling process.

Finally, a sample management interface was offered in which a formula can be created by either similarity measures (*MHD* or *anisotropy*) or geometric constraints defined by users using functions such as horizontal, vertical and Euclidean distances between points; and width, height, volume and area of the shape. The sample management starts with clustering the samples using the K-means method and each cluster is then organized individually according to the defined formula.

The users can set a range with desired maximum and minimum values to filter out the samples whose formula results are out of the range. The samples can also be analyzed with a graph of one formula versus another. Besides, the interface consists of several areas with various purposes such as generating new samples from a selected sample, editing sample and searching similar samples to this edited sample, exporting the selected samples to be converted into 3D in Rhino simultaneously, and pairwise comparison of the selected samples based on a formula.

5.2   Discussion

Overall, the proposed methods are suggested to create aesthetic designs efficiently and effectively in the conceptual design stage.

The outcome of Chapter 2 is the knowledge of a set of attractive and important parameters for an aesthetic objective. For this purpose, eye tracking is used during the surveys and a group of parameters is said to be important for an adjective if the participants looked at them while they select that specific adjective. Such a claim is proved by finding correlations between gaze data of the parameters and the adjective selections; thus, the parameters are related to the adjectives based on the participants' attention. The knowledge of important parameters in an aesthetic objective lets designers narrow down the design space to the relatively smaller regions that cover more promising solutions for customer satisfaction as the regions are defined based on their impressions. Moreover, when industrial designers have to work on a form constrained by engineering design requirements that increase the difficulty for finding the desired solution, such knowledge lets designers effectively create the ideas modifying only relevant shape features that most likely took attention of the customers.

The proposed eye tracking method was applied to a yacht hull because it is easy to parametrize thanks to existing common hull design frameworks. The parameters must be good enough to obtain desired design samples and suitable to be used by designers in their design framework. Also, the adjectives must clearly identify the relevant design without leading confusions for the subjects that might cause a noisy data. For example, car and mobile phone designs are suitable for the proposed method since there are already common design parameters defined and accepted by many designers, and appropriate adjectives can easily be learned from people already familiar with these designs.

Chapter 3 suggests an example based design method where the design alternatives are derived from a central idea. The integration of this approach with Chapter 4 provides easiness automatizing the constraint definition, defining the sampling region based on the similarity that can be set by users intuitively, and determining the size of the design space as simple as setting the $d_{max}^{perturbation}$. The constraint definitions are usually problem specific and require designer expertise. In the proposed method, primitive shapes like circle and triangle that can be defined for any cubic curve are used to generalize the constraint definition for various product profiles composed of such curves. Also, these shapes can be visualized that makes easier to comprehend the constraining method for inexperienced users. Different values of similarity thresholds allow users to generate designs either sticking to the example design or more creative versions of it. Moreover, the system also

automatically recognizes some conditions on profile curves such as continuity between the segments, concavity and curve degree of each segment. These conditions are then conveyed in the generated samples to build them from an initial user idea that may contain key properties to be maintained. In this way, users could improve or replace their initial ideas analyzing similar alternatives. Note that although each segment is initially defined as a cubic curve, the segments' degree may be reduced to quadratic or linear based on the conditions. The conditions can also be disabled slightly dragging the control points of the profile curve. For example, if the control points of a segment are collinear, the segment is conditioned to be linear; however, breaking the collinearity in the exemplar profile such condition is disabled easily. To extend the sample set with different ideas, the similarity thresholds can be set accordingly and the defined profile curve can be modified through the interface easily before generating new samples. Furthermore, the generated samples can be used as an example design to generate new designs from it; therefore, beyond the very first sampling region can be explored.

The main advantage of the system is that a user without any experience can generate sample sets quickly only providing control points by mouse clicks on an image. This is useful for designers who do not want to spend time with the CAD during the conceptual stage. The system is also suitable for partial modifications such that the segments of the profile are declared by the users so that only those segments are modified while the shape is maintained for the rest. It is believed that the partial modifications are useful to upgrade an existing design focusing only specific portions, which is a more usual case in the industry to use existing production lines as much as possible.

There are usually a set of geometrical requirements defined right in the beginning that product must satisfy aside the aesthetics. The generated samples can be narrowed down by user-defined geometric constraints satisfying some of these requirements. For example, a wide bottleneck can be desirable for bottle designs in large volume; therefore, the width of relevant segments can be constrained through the sample management interface. Volume, area and surface area functions can also be used to coarsely estimate the capacity or the required material amount for a product from its design sample. As another example, the ratio length to width and length to height can be used in design when proportions are important. On the other hand, the proposed system is not suitable for constraints that cannot be defined through the profile curves such as surface fairness, the durability of the shape or manufacturability constraints (i.e., the suitability of a design for injection molding).

The proposed generative method can be used for various shapes as long as they can be represented by composite Bézier curves with up to 3 views. Extrusion, revolution, sweeping and network surface methods are available to produce 3D models of the profile samples such as hairdryer,

yacht hull, ewer, bottle, and glass. For more complicated shapes like car design, the proposed system can be used for a profile from a single view at a time. On the other hand, since each segment of the profile curve is defined as cubic Bézier curve, high quality aesthetic shapes such as those with curvature continuous curves cannot be created by the proposed design scheme. Furthermore, the proposed example based generative design concept can be applied for different shape representation schemes if the shape is represented by parameters, constraining methods are provided to prevent generating irregular shapes, similarity measures are defined, and functions are available to extract some essential conditions from the example design to be conveyed in the generated samples.

The proposed software was also evaluated by two product designers and found useful for industrial design. They suggested constraining the samples based on geometry and sampling ideas such as the proposed innovative sampling. We are specifically encouraged by them to work on the sample management interface that is considered one of the most essential parts of the system to be useful for the designers.

5.3 Future Works

There are several possible improvements and extensions of the proposed methods:

- In Chapter 2, a yacht hull was used, in which the hydrodynamic and hydrostatic performances are crucial. As such performance properties in addition to aesthetic properties are important, the aesthetics are handled first to be then combined with a performance based system. The current version of the sample management system is now under development to handle such hull performance requirements.

- We find it valuable to propose a technique that parametrizes designs and evaluates the parameters with automatically defined AOIs based on the parametrization. Doing that, we would like to encourage industrial design area to use our method to get prominent designs with even less labor, time, and costs.

- In Chapter 3, we have started with 2D profile curves to be converted into 3D models later on so that users without CAD skills are able to use the provided tool. However, the proposed method is also possible to be used directly for 3D models with some updates. A 3D model can be represented with multiple views, and what we do in this study is to pick a view and modify it to find new appearances from that viewpoint. Such modification of single view can be directly reflected without any difference to 3D models of various shapes; specifically, for the revolvable ones, in which only a single profile curve is revolved, and some free-form shapes that can be created sweeping shape constant cross sections along a profile curve.

- In case there are more than one profile curves from different viewpoints need to be modified, each view can be handled one by one to generate its new samples as usual. Hereafter, these new samples of multiple views can be synthesized to reconstruct a 3D model using the network surface or the sweeping method. However, to generate feasible 3D models modifying all profile curves at the same time and combined them successfully, extra constraints are needed at the joints of these combined curves. One of the main objectives of this study is to generalize the method so that it can work on various profiles without requiring additional effort from users. Therefore, it is required to define the extra constraints that can be applied to the various problems. Moreover, the new constraint must be able to consider three-dimensional interactions to ensure continuity of 3D curves throughout the synthesized model if the proposed generative method is going to be implemented directly on 3D models. As for now, our method is able to generate network surfaces from 2D profile curves from

different viewpoints; however, it cannot be applied to directly in 3D shapes, which will be handled in the future.

- To fully automatize the proposed system in Chapter 4, an image processing method (such as [140]) will also be embedded in the future to extract the required points from a given image instead of mouse clicks. This feature can also be extended to be a search engine, similar to the sketch based shape retrieval methods [141, 142, 143]. In these methods, a given input sketch is analyzed to learn its local and global shape features to be matched with 3D models in a data set with the highest feature similarity. Similarly, once the proposed system is augmented with the point extraction ability, it can be applied to the collection of 2D images or appropriate views of 3D models to find similar designs to the given exemplar evaluating the corresponding shape features.

- The proposed method in Chapter 3 is an example based design that aims to preserve initial idea to find its alternatives to improve the idea. Therefore, although interesting designs can be found by setting larger similarity thresholds or using the innovative sampling algorithm that extends the sampling region, they are still connected to the example profile since the conditions of this profile are used throughout the sampling procedures. One of the future works is letting users import several exemplars to be used together in generating new samples by interpolation [144] or mutation [83] among them.

- Finally, in the current version of the user evaluation interface (Section 3.2.1.4), the users have to enter the weights manually or according to parameters' importance that is figured out statistically analyzing the samples respect to collected user responses. This interface can be improved in the future to compute the weights automatically using an evolutionary algorithm to make it fully interactive.

Acknowledgments

I would like to express my deepest gratitude to my supervisor Professor Hiromasa Suzuki for his support, encouragement, and suggestions throughout my time as his student at the University of Tokyo. Without his guidance and persistent help, this dissertation would not have been possible.

I am indebted to thank Associate Professor Erkan Gunpinar, Department of Mechanical Engineering, Istanbul Technical University, for his collaboration and advices. I also thankfully acknowledge the contribution of Professor Myung-Soo Kim, Department of Computer Science and Engineering, Seoul National University, to my study through his valuable recommendations.

I gratefully thank to my committee members: Professor Kenjiro Takai Miura, Department of Mechanical Engineering, Shizuoka University; Professor Yasushi Umeda, Department of Precision Engineering, The University of Tokyo; Associate Professor Yuki Igarashi, Department of Frontier Media Science, Meiji University; and Associate Professor Yutaka Ohtake, Department of Precision Engineering, The University of Tokyo, for their time, effort and valuable suggestions to make this thesis better.

I would like to thank Dr. Koichi Ohtomi for his technical discussions and Mr. Hiroyuki Katayama for his help on the experimental setup. I also thank Associate Professor Yukie Nagai from Tokyo Metropolitan University for her help to conduct the eye tracking surveys with Japanese students and discussions about my studies.

Special thanks to Mr. Adem Tas, software developer, for his technical advises and collaboration on the tool development, to Mr. Sangjun Han, Seoul National University, Korea, for his help on biarc approximation, and to Mr. Shahroz Khan, Research Assistant at the University of Strathclyde, for sharing his knowledge about yacht hull design. I appreciate the feedback offered by designers Mr. Kazuhiro Nihei and Mr. Shinichi Sumikawa for the developed tools and thank them for advice and illuminating discussions on product design.

I gratefully acknowledge the financial support received for my doctorate through The University of Tokyo Fellowship. I also acknowledge that this dissertation is partially based on results obtained from a project commissioned by the New Energy and Industrial Technology Development Organization (NEDO).

I would like to send my thank to my close friends Yasemin Yesil Tas, Ali Akca, Ozge Toprak and Ilyas Geyik, who are always beside me with their unconditional supports. I owe a very important debt to Mr. Katsutoshi Muramatsu, who was my tutor during my freshman year, and dear friend Yoko Watanabe for making my life in Japan enormously easy. I also thank lab secretary Ms. Rumi Tsujiguchi and Ms. Junko Ono from the department office for their immense kindness

Bibliography

[1] Booz, A. . Hamilton, Management of new products, Booz, Allen & Hamilton, 1968.

[2] L. B. Archer, The structure of design processes, 1968.

[3] N. L. Svensson, Introduction to engineering design, Pitman, 1974.

[4] F. Barron, D. M. Harrington, Creativity, intelligence, and personality, Annual review of psychology 32 (1) (1981) 439–476.

[5] M. J. French, J. Gravdahl, M. French, Conceptual design for engineers, Springer, 1985.

[6] N. Cross, Engineering design methods, Vol. 4, 1989.

[7] K. T. Ulrich, S. D. Eppinger, Product design and development, McGraw-Hill New York, 1995.

[8] M. Basadur, P. Pringle, G. Speranzini, M. Bacot, Collaborative problem solving through creativity in problem definition: Expanding the pie, Creativity and Innovation Management 9 (1) (2000) 54–76.

[9] V. V. Kryssanov, H. Tamaki, S. Kitamura, Understanding design fundamentals: how synthesis and analysis drive creativity, resulting in emergence, Artificial Intelligence in engineering 15 (4) (2001) 329–342.

[10] G. Pahl, W. Beitz, Engineering design: a systematic approach, Springer Science & Business Media, 2013.

[11] K. Gericke, L. Blessing, Comparisons of design methodologies and process models across domains: a literature review, in: DS 68-1: Proceedings of the 18th International Conference on Engineering Design (ICED 11), Impacting Society through Engineering Design, Vol. 1: Design Processes, Lyngby/Copenhagen, Denmark, 15.-19.08. 2011, 2011.

[12] K. Gericke, L. Blessing, An analysis of design process models across disciplines, in: DS 70: Proceedings of DESIGN 2012, the 12th International Design Conference, Dubrovnik, Croatia, 2012.

[13] J. Figueiredo, N. C. Correia, I. Secca Ruivo, J. L. Alves, Transdisciplinarity and design: Comparative review and synthesis for the design process, in: Radical Designist-(ThRAD) A Design Culture Journal, 2016.

[14] T. J. Howard, S. J. Culley, E. Dekoninck, Describing the creative design process by the integration of engineering design and cognitive psychology literature, Design studies 29 (2) (2008) 160–180.

[15] P. H. Bloch, Seeking the ideal form: Product design and consumer response, Journal of marketing 59 (3) (1995) 16–29.

[16] N. Crilly, J. Moultrie, P. J. Clarkson, Seeing things: consumer response to the visual domain in product design, Design studies 25 (6) (2004) 547–577.

[17] M. Kumar, C. H. Noble, Beyond form and function: Why do consumers value product design?, Journal of Business Research 69 (2) (2016) 613–620.

[18] C. Ranscombe, B. Hicks, G. Mullineux, A method for exploring similarities and visual references to brand in the appearance of mature mass-market products, Design Studies 33 (5) (2012) 496–520.

[19] H.-Y. CHEN, J.-C. TU, K.-C. WANG, Research into the application of kansei engineering to the modeling aesthetic design of a numerical control machine tool, International Journal of Affective Engineering 16 (3) (2017) 191–202.

[20] K. Kim, K.-p. Lee, Collaborative product design processes of industrial design and engineering design in consumer product companies, Design Studies 46 (2016) 226–260.

[21] W. E. Eder, Engineering design vs. artistic design: Some educational consequences., Online Submission 3 (4) (2013) 259–280.

[22] D. H. Abelow, Customer-based product design module, uS Patent 5,999,908 (Dec. 1999).

[23] S. Chaudhuri, E. Kalogerakis, S. Giguere, T. Funkhouser, Attribit: content creation with semantic attributes, in: Proceedings of the 26th annual ACM symposium on User interface software and technology, ACM, 2013, pp. 193–202.

[24] S. R. Gangurde, M. M. Akarte, Customer preference oriented product design using ahp-modified topsis approach, Benchmarking: An International Journal 20 (4) (2013) 549–564.

[25] M. Heinz, Intelligent product design, Ph.D. thesis, Leuphana University of Lüneburg (2012).
URL http://opus.uni-lueneburg.de/opus/volltexte/2016/14391

[26] M. Nagamachi, Kansei engineering: a new ergonomic consumer-oriented technology for product development, International Journal of industrial ergonomics 15 (1) (1995) 3–11.

[27] K. M. Dogan, E. Gunpinar, Learning yacht hull adjectives and their relationship with hull surface geometry using gmdh-type neural networks for human oriented smart design, Ocean Engineering 145 (2017) 215–229.

[28] S. Khan, E. Gunpinar, K. M. Dogan, A novel design framework for generation and parametric modification of yacht hull surfaces, Ocean Engineering 136 (2017) 243–259.

[29] J. McCormack, A. Dorin, T. Innocent, et al., Generative design: a paradigm for design research, Proceedings of Futureground, Design Research Society, Melbourne, 2004.

[30] E. Gunpinar, S. Gunpinar, A shape sampling technique via particle tracing for cad models, Graphical Models 96 (2018) 11–29.

[31] S. Krish, A practical generative design method, Computer-Aided Design 43 (1) (2011) 88–100.

[32] S. Khan, M. J. Awan, A generative design technique for exploring shape variations, Advanced Engineering Informatics 38 (2018) 712–724.

[33] E. Kalogerakis, S. Chaudhuri, D. Koller, V. Koltun, A probabilistic model for component-based shape synthesis, ACM Transactions on Graphics (TOG) 31 (4) (2012) 55.

[34] Q. Tan, L. Gao, Y.-K. Lai, S. Xia, Variational autoencoders for deforming 3d mesh models, in: IEEE Conf. on Computer Vision and Pattern Recognition (CVPR), 2018, pp. 5841–5850.

[35] F. L. Bookstein, Size and shape spaces for landmark data in two dimensions, Statistical science (1986) 181–222.

[36] M.-P. Dubuisson, A. K. Jain, A modified hausdorff distance for object matching, in: Pattern Recognition, 1994. Vol. 1-Conference A: Computer Vision & Image Processing., Proceedings of the 12th IAPR International Conference on, Vol. 1, IEEE, 1994, pp. 566–568.

[37] G. D. Taylor, J. R. English, R. J. Graves, Designing new products:: Compatibility with existing production facilities and anticipated product mix, Integrated Manufacturing Systems 5 (4/5) (1994) 13–21.

[38] M. Liefvendahl, R. Stocki, A study on algorithms for optimization of latin hypercubes, Journal of Statistical Planning and Inference 136 (9) (2006) 3231–3247.

[39] Tobii pro software (2016).
URL https://www.tobiipro.com/product-listing/tobii-pro-studio/

[40] M. E. H. Creusen, J. P. L. Schoormans, The different roles of product appearance in consumer choice, Journal of product innovation management 22 (1) (2005) 63–81.

[41] M. Yamamoto, D. R. Lambert, The impact of product aesthetics on the evaluation of industrial products, Journal of Product Innovation Management 11 (4) (1994) 309–324.

[42] J. Blijlevens, M. E. Creusen, J. P. Schoormans, How consumers perceive product appearance: The identification of three product appearance attributes, International Journal of design 3 (3) (2009) 27–35.

[43] A. T. Duchowski, A breadth-first survey of eye-tracking applications, Behavior Research Methods, Instruments, & Computers 34 (4) (2002) 455–470.

[44] D. Noton, L. Stark, Scanpaths in eye movements during pattern perception, Science 171 (3968) (1971) 308–311.

[45] T. Blascheck, K. Kurzhals, M. Raschke, M. Burch, D. Weiskopf, T. Ertl, State-of-the-art of visualization for eye tracking data, in: Proceedings of EuroVis, Vol. 2014, 2014.

[46] M. Nagamachi, Kansei engineering as a powerful consumer-oriented technology for product development, Applied ergonomics 33 (3) (2002) 289–294.

[47] H. Yanagisawa, S. Nakano, T. Murakami, A Proposal of Kansei Database Framework and Kansei Modelling Methodology for the Delight Design Platform, Journal of Integrated Design and Process Science 20 (2) (2016) 73–84.

[48] H. Y. Chen, Y. M. Chang, Extraction of product form features critical to determining consumers' perceptions of product image using a numerical definition-based systematic approach, International Journal of Industrial Ergonomics 39 (1) (2009) 133–145.

[49] M. Alshehri, S. Alghowinem, An exploratory study of detecting emotion states using eye-tracking technology, in: Science and Information Conference (SAI), 2013, IEEE, 2013, pp. 428–433.

[50] M. V. Yousefi, E. Karan, A. Mohammadpour, S. Asadi, Implementing eye tracking technology in the construction process, in: 51st ASC Annual International Conference Proceedings, 2015, pp. 752–759.

[51] A. Mohammadpour, E. Karan, S. Asadi, L. Rothrock, Measuring end-user satisfaction in the design of building projects using eye-tracking technology, in: Computing in Civil Engineering 2015, 2015, pp. 564–571.

[52] M. Kim, Y. Kang, S. A. Bakar, A Nightscape Preference Study Using Eye Movement Analysis, ALAM CIPTA, International Journal of Sustainable Tropical Design Research and Practice 6 (2) (2013) 85–99.

[53] R. B. Noland, M. D. Weiner, D. Gao, M. P. Cook, A. Nelessen, Eye-tracking technology, visual preference surveys, and urban design: preliminary evidence of an effective methodology, Journal of Urbanism: International Research on Placemaking and Urban Sustainability 10 (1) (2017) 98–110.

[54] S. Kukkonen, Exploring eye tracking in design evaluation, Joining Forces (2005) 119–126.

[55] M. Köhler, B. Falk, R. Schmitt, Applying Eye-Tracking in Kansei Engineering Method for Design Evaluations in Product Development, International Journal of Affective Engineering 14 (3) (2015) 241–251.

[56] K. Koivunen, S. Kukkonen, S. Lahtinen, H. Rantala, S. Sharmin, Towards deeper understanding of how people perceive design in products, CADE2004 Web Proceedings of Computers in Art and Design Education Conference, MA Eriksen, L. Malmborg, and J. Nielsen, eds., Sweden, 2004.

[57] P. Du, E. F. MacDonald, Eye-tracking data predict importance of product features and saliency of size change, Journal of Mechanical Design 136 (8) (2014) 81005.

[58] S. Khalighy, G. Green, C. Scheepers, C. Whittet, Quantifying the qualities of aesthetics in product design using eye-tracking technology, International Journal of Industrial Ergonomics 49 (2015) 31–43.

[59] A. Hyrskykari, S. Ovaska, P. Majaranta, K.-J. Räihä, M. Lehtinen, Gaze path stimulation in retrospective think-aloud, Vol. 2, Journal of Eye Movement Research, 2008.

[60] G. Taguchi, System of experimental design; engineering methods to optimize quality and minimize costs, 1988.

[61] A. A. Bojko, Informative or misleading? Heatmaps deconstructed, in: International Conference on Human-Computer Interaction, Springer, 2009, pp. 30–39.

[62] A. Olsen, The Tobii I-VT fixation filter, Tobii Technology, 2012.

[63] A. VOßKÜHLER, V. Nordmeier, L. Kuchinke, A. M. Jacobs, OGAMA (Open Gaze and Mouse Analyzer): open-source software designed to analyze eye and mouse movements in slideshow study designs, Behavior research methods 40 (4) (2008) 1150–1162.

[64] G. Barequet, S. Har-Peled, Efficiently approximating the minimum-volume bounding box of a point set in three dimensions, Journal of Algorithms 38 (1) (2001) 91–109.

[65] K. Holmqvist, M. Nyström, R. Andersson, R. Dewhurst, H. Jarodzka, J. de Weijer, Eye tracking: A comprehensive guide to methods and measures, OUP Oxford, 2011.

[66] V. Ponsoda, D. Scott, J. M. Findlay, A probability vector and transition matrix analysis of eye movements during visual search, Acta psychologica 88 (2) (1995) 167–185.

[67] M. Frigge, D. C. Hoaglin, B. Iglewicz, Some implementations of the boxplot, The American Statistician 43 (1) (1989) 50–54.

[68] P. McCullagh, Generalized linear models, European Journal of Operational Research 16 (3) (1984) 285–292.

[69] A. Miller, Subset selection in regression, CRC Press, 2002.

[70] H. Akaike, Information theory and an extension of the maximum likelihood principle, in: Selected Papers of Hirotugu Akaike, Springer, 1998, pp. 199–213.

[71] E. J. Wagenmakers, S. Farrell, AIC model selection using Akaike weights, Psychonomic bulletin & review 11 (1) (2004) 192–196.

[72] A. Guisan, N. E. Zimmermann, Predictive habitat distribution models in ecology, Ecological modelling 135 (2) (2000) 147–186.

[73] W. N. Venables, B. D. Ripley, Modern applied statistics with S-PLUS, Springer Science & Business Media, 2013.

[74] J. A. Morgan, J. F. Tatar, Calculation of the residual sum of squares for all possible regressions, Technometrics 14 (2) (1972) 317–325.

[75] K. P. Burnham, D. R. Anderson, Model selection and multimodel inference: a practical information-theoretic approach, Springer Science & Business Media, 2003.

[76] A. McLeod, C. Xu, bestglm: Best subset GLM, URL http://CRAN. R-project. org/package= bestglm, 2010.

[77] R. Team, RStudio: integrated development for R, RStudio, Inc., Boston, MA URL http://www.rstudio.com, 2015.

[78] J. Fox, G. Monette, Generalized collinearity diagnostics, Journal of the American Statistical Association 87 (417) (1992) 178–183.

[79] J. F. Hair, C. M. Ringle, M. Sarstedt, PLS-SEM: Indeed a silver bullet, Journal of Marketing theory and Practice 19 (2) (2011) 139–152.

[80] B. J. Chalmer, Understanding Statistics, Taylor & Francis, 1986.

[81] K. Pearson, Mathematical contributions to the theory of evolution.–on a form of spurious correlation which may arise when indices are used in the measurement of organs, Proceedings of the royal society of london 60 (359-367) (1896) 489–498.

[82] J. Frazer, Creative design and the generative evolutionary paradigm, in: Creative evolutionary systems, Elsevier, 2002, pp. 253–274.

[83] P. Balakrishnan, V. S. Jacob, Genetic algorithms for product design, Management Science 42 (1996) 1105–1117.

[84] C. M. Herr, T. Kvan, Adapting cellular automata to support the architectural design process, Automation in Construction 16 (1) (2007) 61–69.

[85] G. Stiny, Introduction to shape and shape grammars, Environment and planning B: planning and design 7 (3) (1980) 343–351.

[86] G. S. Hornby, J. B. Pollack, The advantages of generative grammatical encodings for physical design, in: Evolutionary Computation, 2001. Proceedings of the 2001 Congress on, Vol. 1, IEEE, 2001, pp. 600–607.

[87] S. Khan, E. Gunpinar, Sampling cad models via an extended teaching–learning-based optimization technique, Computer-Aided Design 100 (2018) 52–67.

[88] T. Fischer, C. M. Herr, Teaching generative design, in: 2001): Proceedings of the 4th Conference on Generative Art, 2001.

[89] Generative design (2018).
URL https://www.autodesk.com/solutions/generative-design

[90] Generative design for additive manufacturing (2018).
URL https://www.frustum.com/

[91] Introducing inspire 2018 (2018).
URL https://solidthinking.com/inspire2018.html

[92] R. H. Kazi, T. Grossman, H. Cheong, A. Hashemi, G. W. Fitzmaurice, Dreamsketch: Early stage 3d design explorations with sketching and generative design, in: UIST, 2017, pp. 401–414.

[93] V. Dhokia, W. P. Essink, J. M. Flynn, A generative multi-agent design methodology for additively manufactured parts inspired by termite nest building, CIRP Annals 66 (1) (2017) 153–156.

[94] K. Shea, R. Aish, M. Gourtovaia, Towards integrated performance-driven generative design tools, Automation in Construction 14 (2) (2005) 253–264.

[95] M. J. Pugliese, J. Cagan, Capturing a rebel: modeling the harley-davidson brand through a motorcycle shape grammar, Research in Engineering Design 13 (3) (2002) 139–156.

[96] S. Orsborn, J. Cagan, R. Pawlicki, R. C. Smith, Creating cross-over vehicles: Defining and combining vehicle classes using shape grammars, Ai Edam 20 (3) (2006) 217–246.

[97] S.-W. Hsiao, C.-H. Chen, A semantic and shape grammar based approach for product design, Design studies 18 (3) (1997) 275–296.

[98] M. Agarwal, J. Cagan, A blend of different tastes: the language of coffeemakers, Environment and Planning B: Planning and Design 25 (2) (1998) 205–226.

[99] M. Agarwal, J. Cagan, K. G. Constantine, Influencing generative design through continuous evaluation: Associating costs with the coffeemaker shape grammar, AI EDAM 13 (4) (1999) 253–275.

[100] K. Xu, H. Zhang, D. Cohen-Or, B. Chen, Fit and diverse: Set evolution for inspiring 3d shape galleries, ACM Transactions on Graphics, (Proc. of SIGGRAPH 2012) 31 (4) (2012) 57:1–57:10.

[101] H. C. Lee, T. Herawan, A. Noraziah, Evolutionary grammars based design framework for product innovation, Procedia Technology 1 (2012) 132–136.

[102] M. O'Neill, J. McDermott, J. M. Swafford, J. Byrne, E. Hemberg, A. Brabazon, E. Shotton, C. McNally, M. Hemberg, Evolutionary design using grammatical evolution and shape grammars: Designing a shelter, International Journal of Design Engineering 3 (1) (2010) 4–24.

[103] S. W. Kielarova, P. Pradujphongphet, E. L. Bohez, New interactive-generative design system: hybrid of shape grammar and evolutionary design-an application of jewelry design, in: International Conference in Swarm Intelligence, Springer, 2015, pp. 302–313.

[104] Y. guoyan, W. Xiaozhen, L. peng, A constraint based evolutionary decision support system for product design, in: Control and Decision Conference, 2009. CCDC'09. Chinese, IEEE, 2009, pp. 2585–2590.

[105] B. Yannou, F. Cluzel, M. Dihlmann, Evolutionary and interactive sketching tool for innovative car shape design, Mechanics & Industry 14 (1) (2013) 1–22.

[106] F. Cluzel, B. Yannou, M. Dihlmann, Using evolutionary design to interactively sketch car silhouettes and stimulate designer's creativity, Engineering Applications of Artificial Intelligence 25 (7) (2012) 1413–1424.

[107] J. Kelly, P. Y. Papalambros, C. M. Seifert, Interactive genetic algorithms for use as creativity enhancement tools., in: AAAI Spring Symposium: Creative Intelligent Systems, 2008, pp. 34–39.

[108] W. Chen, M. Fuge, Beyond the known: detecting novel feasible domains over an unbounded design space, Journal of Mechanical Design 139 (11) (2017) 111405.

[109] X. Xie, K. Xu, N. J. Mitra, D. Cohen-Or, W. Gong, Q. Su, B. Chen, Sketch-to-design: Context-based part assembly, Vol. 32, 2013, pp. 233–245.

[110] M. Averkiou, V. G. Kim, Y. Zheng, N. J. Mitra, Shapesynth: Parameterizing model collections for coupled shape exploration and synthesis, in: Computer Graphics Forum, Vol. 33, Wiley Online Library, 2014, pp. 125–134.

[111] I. Alhashim, H. Li, K. Xu, J. Cao, R. Ma, H. Zhang, Topology-varying 3d shape creation via structural blending, ACM Transactions on Graphics (TOG) 33 (4) (2014) 158.

[112] M. E. Yumer, S. Chaudhuri, J. K. Hodgins, L. B. Kara, Semantic shape editing using deformation handles, ACM Transactions on Graphics (TOG) 34 (4) (2015) 86.

[113] M. Dang, S. Lienhard, D. Ceylan, B. Neubert, P. Wonka, M. Pauly, Interactive design of probability density functions for shape grammars, ACM Transactions on Graphics (TOG) 34 (6) (2015) 206.

[114] K. Wang, M. Savva, A. X. Chang, D. Ritchie, Deep convolutional priors for indoor scene synthesis, ACM Transactions on Graphics (TOG) 37 (4) (2018) 70.

[115] C. Lassner, G. Pons-Moll, P. V. Gehler, A generative model of people in clothing, in: Computer Vision (ICCV), 2017 IEEE International Conference on, IEEE, 2017, pp. 853–862.

[116] O. Sbai, M. Elhoseiny, A. Bordes, Y. LeCun, C. Couprie, DeSIGN: Design Inspiration from Generative Networks, CoRR, 2018.

[117] G. Nishida, I. Garcia-Dorado, D. G. Aliaga, B. Benes, A. Bousseau, Interactive sketching of urban procedural models, ACM Trans. Graph. 35 (4) (2016) 130:1–130:11.

[118] J. Li, K. Xu, S. Chaudhuri, E. Yumer, H. Zhang, L. Guibas, Grass: Generative recursive autoencoders for shape structures, ACM Trans. Graph. 36 (4) (2017) 52:1–52:14.

[119] C. Zhu, K. Xu, S. Chaudhuri, R. Yi, H. Zhang, Scores: Shape composition with recursive substructure priors, ACM Trans. Graph. 37 (6) (2018) 211:1–211:14.

[120] A. Sinha, A. Unmesh, Q. Huang, K. Ramani, Surfnet: Generating 3d shape surfaces using deep residual networks, in: Computer Vision and Pattern Recognition (CVPR), 2017 IEEE Conference on, IEEE, 2017, pp. 791–800.

[121] C. Nash, C. K. Williams, The shape variational autoencoder: A deep generative model of part-segmented 3d objects, in: Computer Graphics Forum, Vol. 36, Wiley Online Library, 2017, pp. 1–12.

[122] H. Huang, E. Kalogerakis, B. Marlin, Analysis and synthesis of 3d shape families via deep-learned generative models of surfaces, in: Computer Graphics Forum, Vol. 34, Wiley Online Library, 2015, pp. 25–38.

[123] J. Liu, F. Yu, T. Funkhouser, Interactive 3d modeling with a generative adversarial network, in: 3D Vision (3DV), 2017 International Conference on, IEEE, 2017, pp. 126–134.

[124] E. Smith, D. Meger, Improved adversarial systems for 3d object generation and reconstruction, arXiv preprint arXiv:1707.09557, 2017.

[125] R. McNeel, Grasshopper-generative modeling with rhino, mcneel north america, seattle, usa (2010).

[126] R. Kamalian, E. Yeh, Y. Zhang, A. M. Agogino, H. Takagi, Reducing human fatigue in interactive evolutionary computation through fuzzy systems and machine learning systems, in: Fuzzy Systems, 2006 IEEE International Conference on, IEEE, 2006, pp. 678–684.

[127] H. Takagi, D. Pallez, Paired comparison-based interactive differential evolution, in: Nature & Biologically Inspired Computing, 2009. NaBIC 2009. World Congress on, IEEE, 2009, pp. 475–480.

[128] Y. Zhang, et al., Reduced human fatigue interactive evolutionary computation for micromachine design, in: Machine Learning and Cybernetics, 2005. Proceedings of 2005 International Conference on, Vol. 9, IEEE, 2005, pp. 5666–5671.

[129] L. B. Kara, K. Shimada, Supporting early styling design of automobiles using sketch-based 3d shape construction, Computer-Aided Design and Applications 5 (6) (2008) 867–876.

[130] C. G. Small, The statistical theory of shape, Springer Science & Business Media, 2012.

[131] H. R. Lourenço, O. C. Martin, T. Stützle, Iterated local search, in: Handbook of metaheuristics, Springer, 2003, pp. 320–353.

[132] M. L. Zelditch, D. L. Swiderski, H. D. Sheets, Geometric morphometrics for biologists: a primer, Academic Press, 2012.

[133] L. v. d. Maaten, G. Hinton, Visualizing data using t-sne, Journal of machine learning research 9 (Nov) (2008) 2579–2605.

[134] C. R. De Souza, Accord. net framework, A framework for scientific computing. Available in: http://accord-framework. net, 2014.

[135] P. F. Felzenszwalb, Representation and detection of deformable shapes, IEEE Transactions on Pattern Analysis and Machine Intelligence 27 (2) (2005) 208–220.

[136] B. G. Husslage, G. Rennen, E. R. Van Dam, D. Den Hertog, Space-filling latin hypercube designs for computer experiments, Optimization and Engineering 12 (4) (2011) 611–630.

[137] Z. Šír, R. Feichtinger, B. Jüttler, Approximating curves and their offsets using biarcs and pythagorean hodograph quintics, Computer-Aided Design 38 (6) (2006) 608–618.

[138] R. Likert, A technique for the measurement of attitudes., Archives of psychology, 1932.

[139] J. A. Hartigan, M. A. Wong, Algorithm as 136: A k-means clustering algorithm, Journal of the Royal Statistical Society. Series C (Applied Statistics) 28 (1) (1979) 100–108.

[140] J. Canny, A computational approach to edge detection (1987) 184–203.

[141] M. Eitz, R. Richter, T. Boubekeur, K. Hildebrand, M. Alexa, Sketch-based shape retrieval., ACM Trans. Graph. 31 (4) (2012) 31–1.

[142] B. Li, Y. Lu, C. Li, A. Godil, T. Schreck, M. Aono, M. Burtscher, H. Fu, T. Furuya, H. Johan, Shrec'14 track: Extended large scale sketch-based 3d shape retrieval, Vol. 2014, 2014, pp. 121–130.

[143] F. Wang, L. Kang, Y. Li, Sketch-based 3d shape retrieval using convolutional neural networks, in: Proceedings of the IEEE Conference on Computer Vision and Pattern Recognition, 2015, pp. 1875–1883.

[144] H. Johan, Y. Koiso, T. Nishita, Morphing using curves and shape interpolation techniques, in: Proceedings the Eighth Pacific Conference on Computer Graphics and Applications, IEEE, 2000, pp. 348–454.

Publications

List of publications related to this thesis:

- **International Journal Papers.**

    1. Dogan, K. M., Suzuki, H., & Gunpinar, E. (2018). Eye tracking for screening design parameters in adjective-based design of yacht hull. Ocean Engineering, 166, 262-277.

    2. Dogan, K. M., Suzuki, H., Gunpinar, E., & Kim, M. S. (2019). A generative sampling system for profile designs with shape constraints and user evaluation. Computer-Aided Design, 111, 93-112.

- **International Conference Papers with Review.**

    1. Dogan, K. M., Suzuki, H., Gunpinar, E., & Katayama (2017), H. Eye Tracking Aided Survey (ETAS) for Evaluation of Yacht Hull Design Parameters. In International Conference on Design and Concurrent Engineering 2017 & Manufacturing Systems Conference (iDECON/MS 2017). Osaka, JAPAN.

    2. Dogan, K. M., Suzuki, H., Gunpinar, E., & Kim, M. S. (2018). Example Based Sampling of Design Space for Facilitating Diverse Product Designs. In Proceedings of the 4th International Conference on Industrial and Business Engineering (ICIBE' 18). ACM, New York, NY, USA, 276-281.

- **Domestic Conference Papers without Review.**

    1. Dogan, K. M., Suzuki, H., Gunpinar, E., Katayama, H. A Study on Method for Visual Evaluation of Geometric Design Parameters, Proceedings of JSPE Semestrial Meeting, 2017, Volume 2017S, 2017 JSPE Spring Conference, Session ID H62, Pages 605-606, Released September 01, 2017.

List of publications not related to this thesis:

- **International Journal Papers.**

  1. Khan, S., Gunpinar, E., & Dogan, K. M. (2017). A novel design framework for generation and parametric modification of yacht hull surfaces. Ocean Engineering, 136, 243-259.

  2. Dogan, K. M., & Gunpinar, E. (2017). Learning yacht hull adjectives and their relationship with hull surface geometry using GMDH-type neural networks for human oriented smart design. Ocean Engineering, 145, 215-229.